GEOPHYSICS, VOL. 42, NO. 5 (AUGUST 1977); P. 995–1005, 10 FIGS., 2 TABLES

RIDGE REGRESSION INVERSION APPLIED TO CRUSTAL RESISTIVITY SOUNDING DATA FROM SOUTH AFRICA

W. R. PETRICK*, W. H. PELTON*, AND S. H. WARD*

Ridge regression inversion has been used to test the applicability of various one-dimensional crustal models to the interpretation of deep Schlumberger sounding data from southern Africa (Van Zijl and Joubert, 1975). Four main models were investigated: a simple three-layered earth, a layered earth with a transition zone exhibiting a linear decrease in log resistivity with depth, a similar earth with the transition zone determined by cubic splines, and a model having exponential resistivity behavior at depth. The last model corresponds to temperature-dependent semiconduction through solid mineral grains (Brace, 1971). It was found that all of these models are capable of fitting the sounding data from southwestern Africa, while all except the semiconduction model fit the data from southeastern Africa. One is, thereby, immediately alerted to the problem of lack of resolution in Schlumberger sounding data where geologic control is not available.

A major problem with the inversion of Schlumberger data alone is that accurate information is obtainable only for the resistivity-thickness product of the resistive portion of the crust. On the other hand, magnetotelluric data, when available, tends to provide information on the thickness, but very little information on the true resistivity of the section. In order to resolve both resistivity and thickness it is possible to invert simultaneously Schlumberger and magnetotelluric (MT) data. Results obtained from the combined inversion of the African resistivity data and hypothetical MT data show that a considerable improvement in model resolution can be achieved using MT amplitude data even of poor accuracy from a relatively limited frequency range (0.1 to 100 Hz), whereas inclusion of MT phase information is of negligible additional benefit.

Unfortunately, no significant test can be made, from data available at the time of our analysis, of the applicability of one-dimensional inversion in a geologic circumstance which probably demands more dimension.

INTRODUCTION

Deep crustal sounding data from various areas of the world usually indicate three main zones of differing conductivity. The surface zone is composed of porous, weathered material or sedimentary rocks with resistivity usually less than 500 Ω-m. Below this layer, the basement rocks typically have a much higher resistivity, between 10^4 and 10^5 Ω-m, corresponding to much lower porosities. These high resistivities persist for several kilometers, usually followed by a decrease in resistivity of at least an order of magnitude (Keller, 1971). The exact depth at which this decrease occurs is usually not well known, nor is the mechanism which causes it.

Recently some very deep Schlumberger soundings (VES for vertical electric sounding) were conducted in southern Africa (Van Zijl and Joubert, 1975). Although their paper suggests a relatively detailed model for the resistivity of the crust, little information is given concerning the uncertainty of the model or whether other models may equally well fit the data. Accordingly, we have attempted a further analysis of the soundings using ridge regression inversion. We are attempting only the next obvious

Manuscript received by the Editor August 2, 1976; revised manuscript received January 14, 1977.
*University of Utah, Salt Lake City, UT 84112.

step in improvement of data analysis, and we are not attempting to extract nor evaluate the maximum amount of information from the available data sets. Therefore, the objectives of our analysis are limited to the following. We wished to ascertain (1) if the linear decrease in log resistivity at depth, indicated by Van Zijl and Joubert, was truly well-determined by the data, (2) if other crustal models such as that proposed by Brace (1971) could be safely excluded from consideration, and (3) what additional benefit magnetotelluric (MT) data would provide in resolving the resistivity of the crust.

INVERSION THEORY

We shall present only a brief summary of the least-squares inversion method used in this study. More detailed discussions regarding geophysical applications have been given by Glenn et al (1973) and Inman (1975). A description of the statistical estimates may be found in Glenn and Ward (1976). We will follow their notation as closely as is practical.

Least-squares method

Our geophysical problem may be linearized as follows:

$$\mathbf{\Delta G} = \mathbf{A}\mathbf{\Delta P} + \boldsymbol{\epsilon}, \tag{1}$$

where the $n \times m$ matrix of derivatives $\mathbf{A}$ relates a small change in model parameters $\mathbf{\Delta P}$ to a small change in data $\mathbf{\Delta G}$. When the departure from linearity $\boldsymbol{\epsilon}$ is small, we may obtain $\mathbf{\Delta P}$ from

$$\mathbf{\Delta P} = (\mathbf{A}^T\mathbf{A})^{-1}\mathbf{A}^T\mathbf{\Delta G}, \tag{2}$$

where we have merely multiplied both sides of (1) by the generalized inverse operator,

$$\mathbf{H} = (\mathbf{A}^T\mathbf{A})^{-1}\mathbf{A}^T. \tag{3}$$

By premultiplying $\mathbf{H}$ by $\mathbf{A}$ we may define $\mathbf{S}$, the information density matrix. The diagonal of $\mathbf{S}$ contains large values at positions corresponding to data points which are contributing significant information to the total model determination. The derivative matrix $\mathbf{A}$, on the other hand, gives an approximate breakdown as to which data points contribute to the determination of each parameter. Therefore, through the use of either the information density matrix or the derivative matrix, it is possible to deduce the range of data required to resolve a particular model.

Once a model is selected and the data obtained, the object of least-squares inversion is to minimize the square error between the calculated model and the observed data, given by

$$\xi^2 = \mathbf{\Delta G}^T\mathbf{\Delta G}. \tag{4}$$

If the problem is exactly linear, only one determination of $\mathbf{\Delta P}$ will be necessary. All geophysical sounding problems, however, are nonlinear and usually several iterations are required to obtain a satisfactory solution from a given initial guess.

Weighted least-squares

Thus far, our least-squares inversion technique assumes uniform data error. This may be a rather poor assumption when considering several data sets simultaneously. To overcome this difficulty, we must resort to weighted least-squares in which the various data sets (or data points) are appropriately weighted in such a way that very noisy data do not contribute the same degree of influence over the inversion as relatively precise data.

We accomplish this by multiplying (1) by a weight matrix $\mathbf{W}$, so that the expression for parameter change becomes,

$$\mathbf{\Delta P} = (\mathbf{A}^T\mathbf{W}^T\mathbf{W}\mathbf{A})^{-1}(\mathbf{A}^T\mathbf{W}^T\mathbf{W})\,\mathbf{\Delta G}, \tag{5}$$

and the weighted square error, which we minimize is,

$$\xi_w^2 = \mathbf{\Delta G}^T\mathbf{W}^T\mathbf{W}\,\mathbf{\Delta G}. \tag{6}$$

When the usual assumption is made that the error at each data point is independent of the error at all other data points, $\mathbf{W}$ reduces to a diagonal matrix. Thus if we know the standard deviation σ_i of each of the data points, it is natural to determine the elements of the weight matrix as follows (Lawson and Hanson, 1974):

$$W_{ii} = \frac{1}{\sigma_i}\ i = 1, n. \tag{7}$$

Often, however, we have a better idea of the *relative* error between data sets than of the true error at each point. In such situations, we may use weights equal to 1.0 for the first data set and relative weights for each subsequent set. An estimate for the true variance of the data in the first set may then be obtained from the reduced chi-square,

$$\chi_\nu^2 = \frac{\xi_w^2}{\nu}, \tag{8}$$

where ξ_w^2 is defined by (6) and ν is the degrees of freedom $n - m$.

Ridge regression

There is still one other difficulty with which we must contend before obtaining an efficient inversion

routine. Should one or more of the parameters be very poorly determined, the matrix $\mathbf{A}^T\mathbf{A}$ will be nearly singular and an eigenvalue decomposition of this matrix would reveal one or more near-zero eigenvalues. To overcome this difficulty, we could reduce the rank of the matrix by reparameterizing the problem. A similar result may more easily be achieved, however, by simply weighting out the very small eigenvalues through the addition of a small positive constant λ to the diagonal elements of $\mathbf{A}^T\mathbf{A}$ before inversion. This technique is known as Marquardt's method or damped least-squares (Lawson and Hanson, 1974). The equation for determining parameter change then becomes,

$$\Delta\mathbf{P} = (\mathbf{A}^T\mathbf{W}^T\mathbf{W}\mathbf{A} + \lambda\mathbf{I})^{-1}(\mathbf{A}^T\mathbf{W}^T\mathbf{W})\,\Delta\mathbf{G}. \quad (9)$$

A large value of λ results in an algorithm which is slow to converge, but which is very stable. On the other hand, a value of λ which is smaller leads to an algorithm which is faster, but which may diverge. Routines which carefully select an appropriate value for λ at each step in the inversion process are called ridge regression algorithms, and it is this type of algorithm which we have used in our inversion approach (Levenberg, 1944; Foster, 1961; Marquardt, 1963; Bevington, 1969). Note that all parameter statistics must be calculated with $\lambda = 0$.

Parameter statistics

Once the inversion process produces a model which best fits the observed data, the question of fundamental importance is: how accurately are the model parameters known?

We may obtain some feeling for how well our model is determined from the data by examining the parameter covariance matrix, which for the weighted least-squares technique is given by,

$$\text{cov}\,(\mathbf{P}) = \chi_\nu^2(\mathbf{A}^T\mathbf{W}^T\mathbf{W}\mathbf{A})^{-1}. \quad (10)$$

An estimate for the standard deviation of each parameter may be derived from the square root of the appropriate diagonal element of cov (**P**) and the parameter correlation coefficients may be obtained by normalizing the parameter covariance matrix in the following manner:

$$\text{cor}\,P_{ij} = \frac{\text{cov}\,P_{ij}}{(\text{cov}\,P_{ii}\cdot\text{cov}\,P_{jj})^{1/2}}. \quad (11)$$

A linear relationship between two parameters is implied by a correlation coefficient with an absolute value near 1.0. If the correlation coefficient is near -1.0, only the product between two parameters (e.g., $T = \rho t$) is well determined. Conversely, if the correlation coefficient is near $+1.0$, only the ratio between two parameters (e.g., $S = t/\rho$) is resolved. In order to estimate how well S or T is determined, we effectively reparameterize the problem by holding either the resistivity or the thickness constant and obtain statistics on the remaining parameter. Another approach, aimed at individual parameter definition, is to include additional data containing more information concerning one of the parameters.

PARAMETERIZATION OF PROBLEMS

There are perhaps three main considerations involved in parameterizing problems. The first of these is the choice of dimensions for the data. Since Schlumberger apparent resistivity data usually have an error which is a fixed percentage of each measurement, it is very convenient to parameterize the VES problem in terms of log apparent resistivity. In this way we avoid the requirement of a weight matrix with elements inversely proportional to the magnitude of each measurement.

The next important consideration is to try to choose as parameters only those truly important variables which have some hope of being resolved by the data. Of course, there are situations where the relative importance of a variable is not at all well-known beforehand. In these situations it is necessary to include the variable as a parameter and then to analyze the resulting statistics. Usually, however, the interpreter will have some feeling, perhaps from prior curve-matching experience, as to which simple models might be determined from inversion, and will thus be able to avoid selection of grossly insignificant variables as parameters.

The last consideration involves the choice of dimensions for the parameters. It is important that we choose an appropriately dimensioned parameter space such that our inversion problem is reasonably linear. This requirement is met for the layered earth model, if we invert with respect to log resistivities and log thicknesses. The logarithmic transformation has the effect of completely excluding negative resistivities and negative thicknesses from consideration. As a result, parameter confidence regions are approximately ellipsoidal and are accurately described by the parameter correlation matrix and percentage parameter standard deviations.

CALCULATION OF THE FORWARD PROBLEM

Since first derivatives with respect to any parameter of any model may be readily approximated by

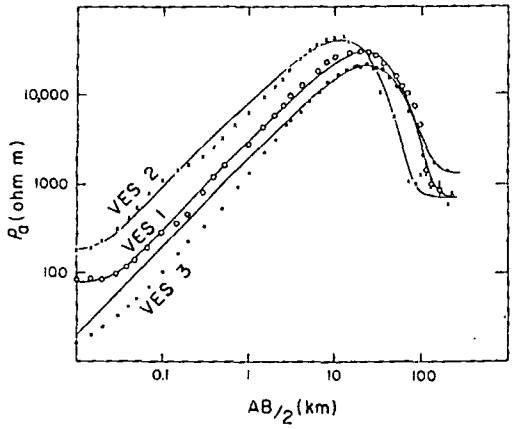

FIG. 1. South African deep resistivity sounding data and theoretical curves presented by Van Zijl and Joubert (1975). Associated models are shown in Figure 3b.

taking the first forward difference, the main requirement of the ridge regression inversion technique is that a fast algorithm be available for the calculation of each model. The approach we used in our study was to segment our crustal models into thin layers and then use the fast algorithms already available for the layered earth MT and resistivity sounding problems (Ward, 1967; Rijo et al, 1976).

RESISTIVITY INVERSION

Shown in Figure 1 are the data from the three deep crustal Schlumberger soundings conducted in southern Africa. The reader is referred to the article by Van Zijl and Joubert (1975) for a discussion of the data acquisition and accuracy. The sounding locations are shown in Figure 2. Prior to inversion, the sounding data corresponding to AB/2 less than 3 km were deleted. This was necessary since the shorter AB/2 portion of the sounding data exhibits considerable error due to lateral variation of the S_1 value associated with the surface weathered layer. This effect is particularly noticeable for VES 2 and VES 3 in Figure 1. Since a correct fit to the remainder of the data depends upon the choice of S_1, we chose a nominal 100 Ω-m resistivity value for the thin overburden and allowed the inversion process to vary t_1. In this way we were guaranteed an optimum S_1 value compatible with the larger spacing data. Subsequent examination of the derivative matrices for all models confirmed that as long as S_1 was determined, the deletion of the shorter spacing data had negligible effect on the determination of the main crustal parameters of interest in our study.

Layered earth model

Our first approach was to invert each sounding separately in order to determine the best three-layer model fitting each data set. Although the data fits were just as good as those obtained by Van Zijl and Joubert in Figure 1, the parameter statistics were not very satisfactory, as shown in column IA of Table 1. Evidently VES 1 is the only sounding which provides information on both the resistivity ρ_2 and thickness t_2 of the resistive portion of the crust. This layer is apparently very thin under southeastern Africa so that VES 2 and VES 3 merely indicated $\rho_2 t_2$ products of 4.85×10^8 Ω-m^2 and 4.77×10^8 Ω-m^2, respectively.

Since ρ_2 is not at all well-determined by the latter two soundings alone, we wished to incorporate information somehow from the eastern part of the continent in order to arrive at a best estimate for ρ_2 compatible with all three sets of sounding data. To do this, we inverted the three VES simultaneously, thus coupling together information on ρ_2 from all three soundings into one derivative matrix. The results of the inversion are shown in columns II and IIA of Table 1 and in Figure 3a. The best estimate for ρ_2 common to all three soundings is 67,600 Ω-m, and since the data fit for the simultaneous inversion is approximately the same as that for each separate inversion, it appears that the hypothesis of a common ρ_2 is not totally unreasonable, considering the VES data alone.

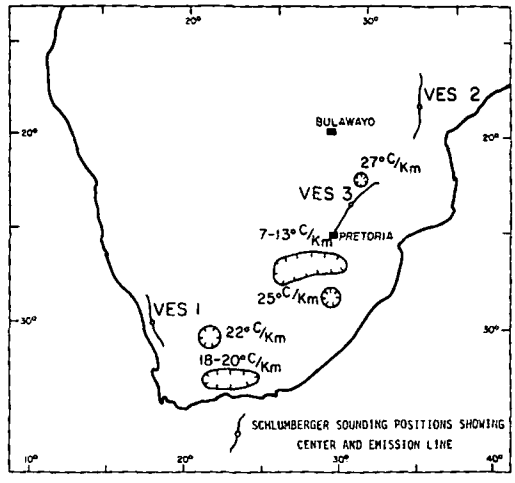

FIG. 2. Location of three Schlumberger sounding sites (Van Zijl and Joubert, 1975) and geothermal gradient values from Lee and Uyeda (1965).

Table 1. Summary of percent parameter standard deviations associated with the three-layered earth model for various data set combinations.

		I	IA	II	IIA	IIB	IIC	IID	IIE
MODEL	PARAMETER	PARAMETER VALUE	EACH VES. SEPARATELY	PARAMETER VALUE	ALL VES. COMBINED	VES. and MT ($\lvert\rho_a\rvert$)	VES. and MT ($\lvert\rho_a\rvert$ & ϕ)	MT ALONE ($\lvert\rho_a\rvert$)	MT ALONE ($\lvert\rho_a\rvert$ & ϕ)
VES 1 KAMIESKROON	ρ_1	100 Ω-m	CONSTRAINED	100 Ω-m	CONSTRAINED	CONSTRAINED	CONSTRAINED	>1000%	>1000%
	ρ_2	41900 Ω-m	22%	67600 Ω-m	COUPLED 48%	18%	16%	>1000%	>1000%
	ρ_3	539 Ω-m	21%	588 Ω-m	18%	16%	15%	130%	70%
	t_1	25.0 m	16%	30.8 m	13%	7%	7%	>1000%	>1000%
	t_2	18073 m	20%	11500 m	46%	17%	15%	>1000%	55%
VES 2 MAVONDE	ρ_1	100 Ω-m	CONSTRAINED	100 Ω-m	CONSTRAINED	CONSTRAINED	CONSTRAINED	>1000%	>1000%
	ρ_2	128×10^5 Ω-m	592%	67600 Ω-m	COUPLED 48%	19%	17%	>1000%	>1000%
	ρ_3	755 Ω-m	12%	743 Ω-m	8%	10%	10%	130%	50%
	t_1	13.7 m	66%	11.3 m	24%	13%	12%	>1000%	>1000%
	t_2	3840 m	578%	7180 m	46%	16%	15%	>1000%	430%
VES 3 PIETERSBURG	ρ_1	100 Ω-m	CONSTRAINED	100 Ω-m	CONSTRAINED	CONSTRAINED	CONSTRAINED	>1000%	>1000%
	ρ_2	1.35×10^5 Ω-m	>1000%	67600 Ω-m	COUPLED 48%	25%	21%	>1000%	>1000%
	ρ_3	1230 Ω-m	6%	1230 Ω-m	12%	6%	5%	90%	53%
	t_1	56.2 m	24%	53.9 m	7%	4%	3%	>1000%	>1000%
	t_2	3520 m	>1000%	7050 m	49%	25%	21%	>1000%	>1000%

If we assume, then, a relatively constant ρ_2, it would appear that the thickness t_2 of the resistive portion of the crust may decrease across southern Africa from about 11.5 km in the west to 7 km in the east. This decrease in thickness, however, is dependent upon the assumption of a relatively homogeneous crust. As the gravity data shown by Hales and Gough (1962) indicate, this assumption may not be a particularly good one. The obvious next step in analyzing deep resistivity data in South

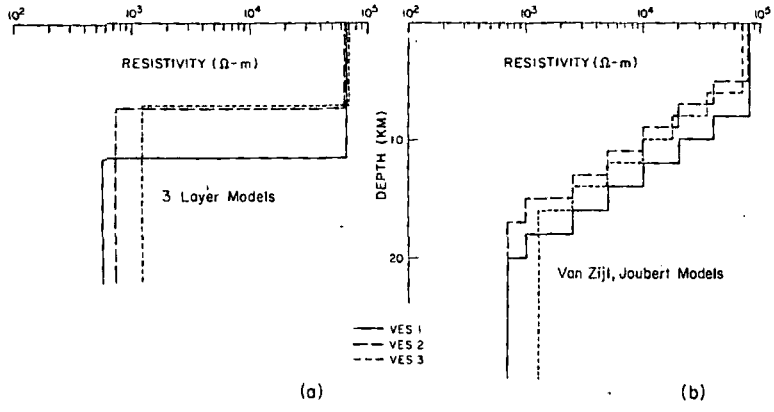

FIG. 3. Crustal conductivity models derived from the South African resistivity sounding data. (a) Our three-layered models. (b) Models proposed by Van Zijl and Joubert (1975).

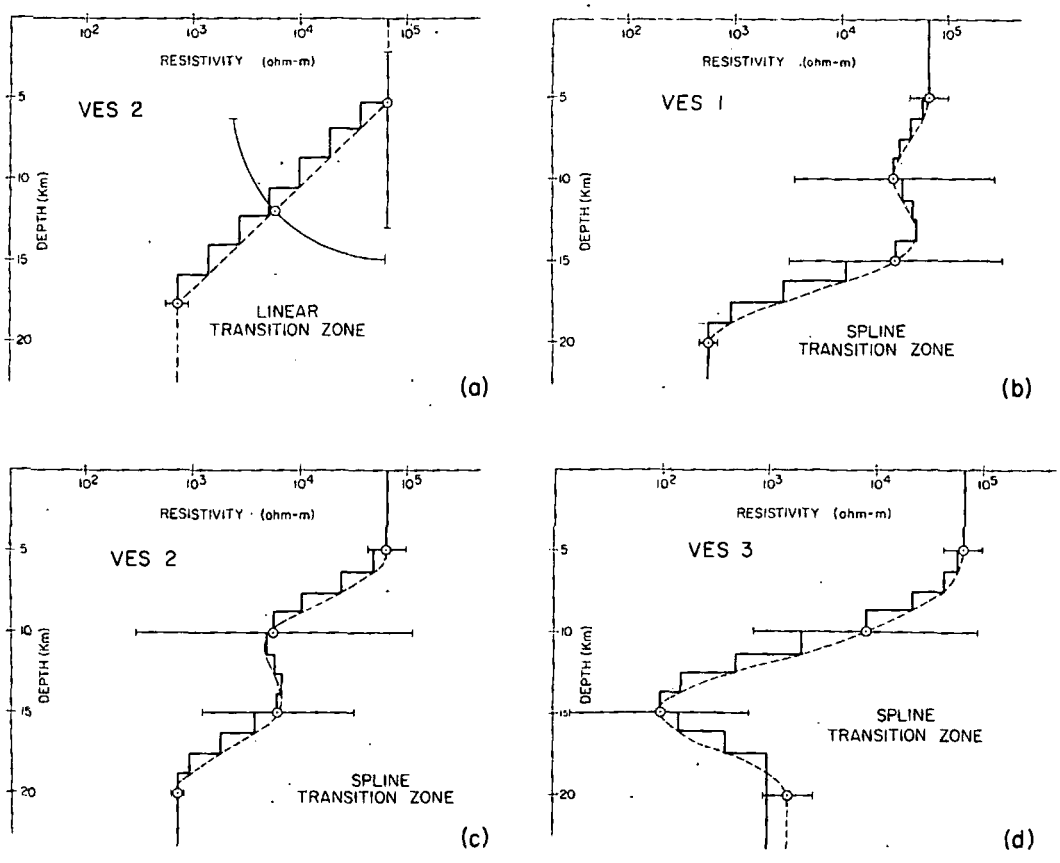

FIG. 4. Reparameterized models using linear and spline functions to approximate the transition zone. Error bars show parameter standard deviations associated with various components of the models.

Africa is modeling of two- or three-dimensional structures by either forward or inverse algorithms. Unfortunately, the available electrical data do not warrant or even permit this degree of sophistication.

Linear transition zone model

The next one-dimensional crustal model which we chose to investigate was the one suggested by Van Zijl and Joubert (1975). As illustrated in Figure 3b, they propose a linear decrease in log resistivity with depth between the resistive and underlying conductive region of the crust. Since the authors neglected to mention evidence substantiating this feature, we wished to find out if the transition zone was truly well-determined by their data.

To parameterize the model, we chose the normal parameters for a three-layered earth and added one additional parameter, slope, which was responsible for specifying the resistivity and thickness of six or seven additional layers which defined the transition zone. As shown in Figure 4a, this slope parameter is extremely poorly determined by the data from VES 2, and yet this sounding provided the best estimate for slope among the three VES. The main difficulty in determining the slope is that it is extremely highly correlated with the thickness t_2 of the second layer. Thus, there are many parameter combinations ranging from small t_2 and near-zero slope to large t_2 and near perpendicular slope which equally well fit the data.

Spline transition zone model

In order to explore further the transition zone postulated by Van Zijl and Joubert, we investigated a model having a very flexible cubic spline dependence for log resistivity as a function of depth. Although the transition zone is characterized by only two parameters, corresponding to the base points of

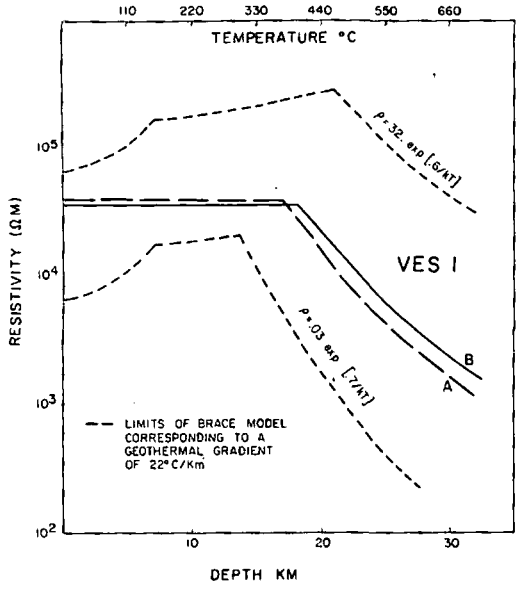

FIG. 5. Mineral semiconduction models determined for sounding location 1. A: Model for which E_0, and ρ_0 were empirically determined. B: Model for which E_0, ρ_0 and dT/dz were variables.

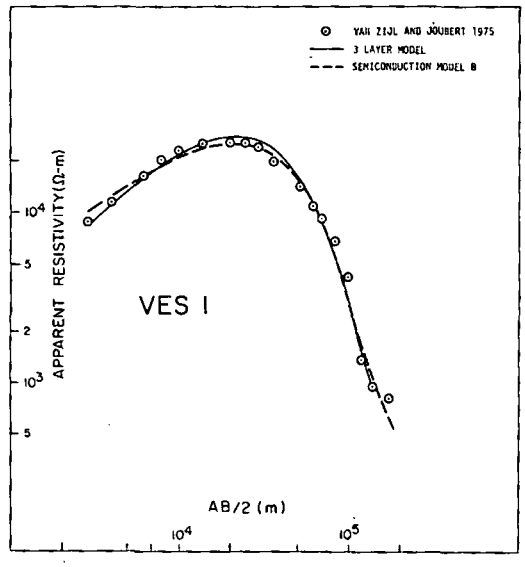

FIG. 6. VES 1 data fit for the mineral semiconduction model B. The data fit obtained using the three-layered model is included for comparison.

the spline, the model is free to simulate virtually any smooth functional behavior in the depth range 5 to 20 km. Beyond this range, the model again has all the standard three-layer earth parameters except for t_2.

The results of the inversions with respect to the spline transition zone are shown in Figure 4b, c, and d. It is evident that the two base points specifying the functional behavior of the transition zone are very poorly determined. It is not really possible to ascertain if the transition is indeed abrupt as suggested by VES 1 or is slowly gradational, as perhaps indicated by VES 2. The only parameters which are reasonably well determined are the resistivities of the resistive zone and of the underlying conductive layer.

Semiconduction model

The last model which we wished to investigate was one which includes semiconduction through mineral grains as the major conduction mechanism at depth in the crust. For this model the rock resistivity depends upon absolute temperature T, as

$$\rho = \rho_0 e^{+\frac{E_0}{kT}},$$

where E_0 is the activation energy, k is Boltzmann's constant, and ρ_0 is an empirically determined constant (Parkhomenko, 1967; Hermance, 1973).

Brace (1971) has presented bounds for rock resistivity assuming crack and pore-dominated conduction in the upper few kilometers of the earth's crust and semiconduction at greater depth. His bounds for observable dry semiconduction behavior correspond to $E_0 = 0.6$eV, $\rho_0 = 30$ Ω-m (upper bound), and $E_0 = 0.7$eV and $\rho_0 = 0.03$ Ω-m (lower bound). Accordingly, our first attempt at inversion of the semiconduction model was to choose median semiconduction behavior corresponding to

$$\rho = 1.0\, e^{+\frac{.65}{kT}},$$

where T was specified in terms of the geothermal gradient s and depth z by

$$T^0K = sz + 300.$$

Inversion of VES 1 to a two-layered model modified by semiconduction behavior at depth, gave an estimate of 23°C/km for the geothermal gradient in southeastern Africa. This model is plotted as curve A in Figure 5. Also shown in the figure are the upper and lower Brace bounds, assuming a geothermal gradient of 22°C/km.

Our next step was to invert with respect to activa-

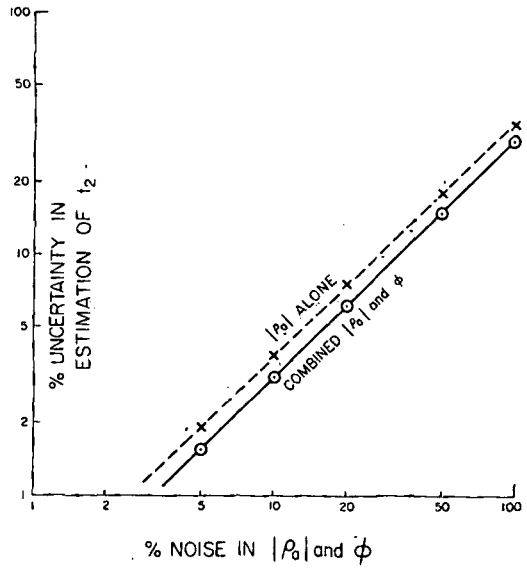

FIG. 7. Uncertainty in the estimation of the thickness of the resistive zone for various percent noise in MT data over the frequency range from 10^{-4} to 10^{4} Hz.

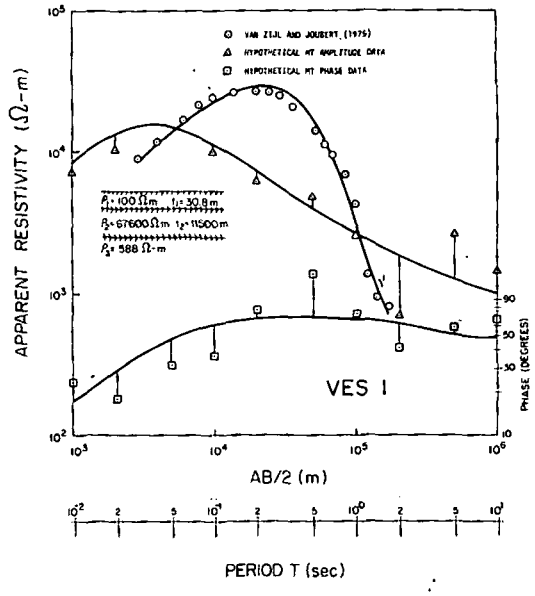

FIG. 8. VES 1. Experimental Schlumberger and hypothetical MT sounding data with best fitting theoretical three-layer sounding curves. Associated model is shown in Figure 3b.

tion energy E_0 and ρ_0, as well as geothermal gradient s, in an attempt to obtain the optimum set of parameters fitting the data from VES 1. The resulting model is shown as curve B in Figure 5. There was relatively minor change in E_0 and ρ_0, indicating that the average semiconduction behavior was a reasonable assumption. The estimate for geothermal gradient decreased slightly from 23°C/km to 21°C/km.

Shown in Figure 6 is the resulting data fit for model B compared with the best-fitting 3 layered earth model for VES 1. The fit is about the same for both models. The results concerning the data from VES 2 and VES 3 are considerably different, however. There is no combination of semiconduction parameters which can provide a good fit to the latter two soundings.

MT INVERSION

In order to determine what role MT data might play in the resolution of a crustal conductivity model, we generated hypothetical MT amplitude and phase data using the models obtained from the simultaneous resistivity inversion. The MT data were then contaminated with prescribed amounts of log normal error to simulate the effect of real field data.

MT data were generated over two frequency ranges. One set covers the frequency range from 0.1 to 100 Hz while the other covers the extended range from 10^{-4} to 10^{4} Hz. The narrow range contains only information concerning those parameters found to be poorly determined by the inversion of individual resistivity data sets, whereas the extended range represents the complete spectrum of useful frequencies concerning all of the three-layered model parameters. The appropriate frequency ranges were determined from an analysis of all columns of the derivative matrix **A**.

As illustrated in columns IID and IIE of Table 1, inversion of the narrow range amplitude data containing 50 percent noise was incapable of defining any of the model parameters. The inclusion of phase information at the same error level improved only the estimate of ρ_3 and t_2.

Somewhat similar results were obtained when the extended data set was inverted. As shown in Figure 7, the addition of phase information had relatively minor influence on the resolution of the most important crustal parameter t_2. This was not the case for all parameters of the three-layered model, however. When only MT amplitude data were available, the addition of phase information was useful in the total model determination.

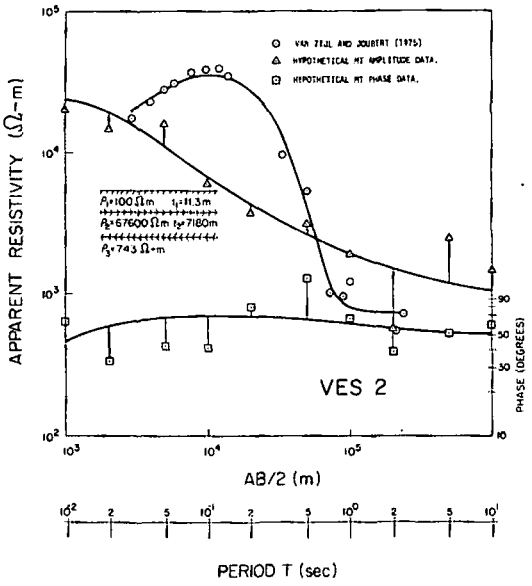

FIG. 9. VES 2. Experimental Schlumberger and hypothetical MT sounding data with best fitting theoretical three-layer sounding curves. Associated model is shown in Figure 3b.

SIMULTANEOUS RESISTIVITY AND MT INVERSION

Although it is possible to invert resistivity and MT data separately, thus obtaining independent estimates for $\rho_2 t_2$ and t_2, one of the major objectives of our study was to investigate the *simultaneous inversion* of resistivity and MT data. We particularly wished to determine whether noisy MT amplitude data from the narrow frequency range 0.1 to 100 Hz could substantially improve resolution of ρ_2 and t_2.

To carry out the simultaneous inversion, we combined derivatives with respect to both VES data and MT amplitude data into a single **A** matrix. However, since the error in the MT data was much greater than that for the VES data, it was necessary to use a weight matrix **W** in order to adjust appropriately the contribution to parameter determination from each data set. For the elements in **W**, we chose the value 1.0 corresponding to the VES data and the ratio of logarithmic VES error to logarithmic MT error for the elements of **W** corresponding to the MT data.

Layered earth model

The results of the simultaneous inversion of log resistivity data and log MT amplitude data to a layered earth model are shown in column IIB of Table 1. The data fits are shown in Figures 8 through 10. It is evident that the addition of MT amplitude information results in increased resolution of all parameters, particularly ρ_2 and t_2 for VES 2 and VES 3 (compare columns IA and IIB). The addition of *both* MT amplitude and phase information to the VES data, however, results in only relatively minor improvement over the addition of MT amplitude data alone, as shown in column IIC of Table 1.

Linear transition zone model

Since the addition of MT data significantly aided the resolution of poorly determined layered earth parameters, we chose as our last study in this paper to investigate the benefit of simultaneous VES and MT inversion on the resolution of the linear transition zone model proposed by Van Zijl and Joubert. We specifically wished to determine what accuracy of data would be required in order to resolve independently the highly correlated slope and t_2 parameters.

To investigate the effect of noise on both the VES data as well as the MT data, we generated theoretical data sets for both, using the models given by Van Zijl and Joubert in Figure 3b. The range of

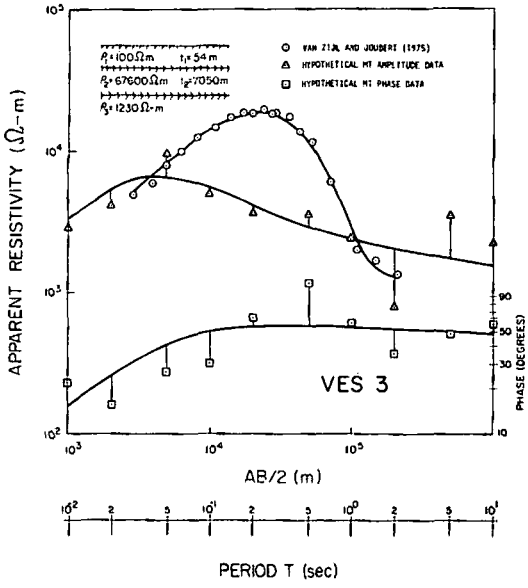

FIG. 10. VES 3. Experimental Schlumberger and hypothetical MT sounding data with best fitting theoretical three-layer sounding curves. Associated model is shown in Figure 3b.

frequencies and AB/2 was the same as that shown in Figures 8 through 10.

Table 2 presents the results of the simultaneous inversions for various combinations of data noise. It is apparent that a data accuracy better than 10 percent for VES and better than 20 percent for MT amplitude data is required in order to resolve the model. The addition of MT phase information results in only minor improvement in resolution.

Table 2. Summary of percent parameter standard deviations for parameters associated with a linear transition zone for simultaneous resistivity-MT inversion with various combinations of data noise.

RES PCT DATA ERROR	5%	5%	10%	20%	10%
MT $\lvert\rho_0\rvert$ PCT DATA ERROR	5%	5%	20%	20%	50%
MT ρ PCT DATA ERROR	5%	—	—	—	—
PCT STD DEV SLOPE	11%	14%	50%	70%	UNDET
PCT ST DEV THICKNESS t_2	13%	17%	55%	79%	UNDET

DISCUSSION AND CONCLUSIONS

Our analysis of the African sounding data was mainly intended to illustrate the application of ridge regression inversion to a difficult problem in geophysical interpretation. We have by no means exhausted all possibilities for useful data combinations or for one-dimensional models that will fit the data. Of those models investigated, three provide reasonable, if admittedly simplistic, views of the crustal conductivity profile.

The first acceptable model is that of a simple three-layered earth. Assuming a relatively constant resistivity of about 68,000 Ω-m for the resistive section of the crust, this layer appears to decrease in thickness from approximately 11.5 km in southwestern Africa to 7 km in southeastern Africa. Below this resistive zone, there is perhaps a two order of magnitude increase in conductivity.

One geologic section which is compatible with this three-layered model is that of a granitic upper crust underlain by basalt (Keller, 1971). The boundary between these two rock types may account for the increase in conductivity and for the increase in shear wave velocity to 3.75 km/sec at a depth of 8 km obtained by Bloch et al (1969) from surface wave dispersion analysis.

The second acceptable model for the crust is one which has a linear decrease in log resistivity with depth. Although Van Zijl and Joubert appear to favor this model, our analysis of their data indicates that the linear transition feature is very poorly resolved.

This poor resolution for the transition zone became very evident when the third model, exhibiting cubic spline functional behavior, was used to fit the data. Since the spline base points are highly correlated with one another, there are a great number of possible functional dependencies for the transition region, all of which fit the data equally well.

The only *unsuccessful* attempt at fitting the data occurred when we tried to fit the results from VES 2 and VES 3 to the semiconduction model. While the last data points from these soundings are relatively noisy, they do appear to indicate a reasonably constant resistivity of perhaps 700 Ω-m below the resistive zone. Assuming that these data are reliable, it is difficult to attribute the resistivity decrease under southeastern Africa to purely temperature-dependent semiconduction behavior and a relatively constant geothermal gradient.

There is no similar difficulty, however, with the data from VES 1 in southwestern Africa. Using average rock semiconduction properties, we were able to obtain a good fit to the data by inverting to an unknown geothermal gradient. As shown in Figure 2, the values of 21°C/km and 23°C/km obtained from the inversion compare very favorably with the nearest published value of 22°C/km obtained by Lee and Uyeda (1965).

Carte and van Rooyen (1971) have published geothermal gradient values of 18°C/km very close to VES 1, but a slight change in ρ_0 to .527 Ω-m and E_0 to .608 eV is sufficient to counter the effect of a lower geothermal gradient, and give essentially the same resistivity section as that of model B shown in Figure 5.

One of the main deficiencies with inverting VES data alone is that usually only a resistivity-thickness product may be determined when a thin resistive layer is encountered. We partially overcame this problem by simultaneously inverting VES 1 with VES 2 and VES 3 in order to obtain a value for ρ_2 which was compatible with all three soundings. The result, however, is only as good as the assumption that ρ_2 is reasonably constant from VES 1 to VES 2 and VES 3.

Much better results may be obtained when MT data are simultaneously inverted with VES data. Our analysis indicates that a substantial increase in parameter resolution can be obtained from inclusion of MT amplitude data, with as much as 50 percent noise, over the relatively narrow frequency range 0.1 Hz to 100 Hz.

Models more complex than a layered earth, however, will require more precise data in order to be truly well-resolved. For example, the detection of the linear transition zone postulated by Van Zijl and Joubert will probably require simultaneous inversion of resistivity data with less than 10 percent noise and MT amplitude data with less than 20 percent noise. This "noise level" includes all effects of 2-D inhomogeneities as well as measurement inaccuracies.

One somewhat surprising result indicated by our simultaneous inversion studies was the relatively minor benefit achieved by the addition of MT phase information. Although phase data are a useful addition to MT amplitude data alone, the constraints provided by phase appear very similar to those provided by VES data. Thus, when deep VES measurements are available as they are in southern Africa, it appears necessary only to collect MT amplitude information in order to provide increased parameter resolution.

The reader should be cautioned that we have not attempted to find a total suite of one-dimensional models which fit the data. As far as we have studied the problem, a simple three-layered model fits the data as well as the more complex models. Of even more importance, we have not evaluated 2-D nor 3-D models. The data do tend to be dominated by one-dimensional effects; much more data are required before a significant attempt at 2-D and 3-D modeling can be made.

ACKNOWLEDGMENTS

We would like to thank Dr. J. S. V. Van Zijl for friendly, constructive criticism of this paper after submission for publication, and for providing us with a preprint of a paper on his further crustal investigations presented at the ONR Symposium on the Nature and Physical Properties of the Earth's Crust, Vail, Colorado, August 2–6, 1976. We also wish to thank Bruce Smith at the U.S.G.S. in Denver and David Chapman for help in obtaining information useful in this presentation. This research was sponsored by the Energy Research and Development Agency (ERDA) under contract EY-76-S-07-1601, and by the National Science Foundation (NSF) under grant GA-24421.

REFERENCES

Bevington, P. R., 1969, Data reduction and error analysis for the physical sciences: New York, McGraw-Hill Book Co., Inc.

Bloch, S., Hales, A. L., and Landisman, M., 1969, Velocities in the crust and upper mantle of southern Africa from multi-mode surface wave dispersion: Bull. SSA, v. 59, p. 1599–1629.

Brace, W. F., 1971, Resistivity of saturated crustal rocks to 40 km based on laboratory studies, *in* The structure and physical properties of the earth's crust: AGU Geophys. Monogr. no. 14, p. 243–256.

Carte, A. E., and van Rooyen, A.I.M., 1971, Further measurements of heat flow in South Africa: J. Mine Ventilation Soc. of So. Africa, July, p. 94–98.

Foster, M., 1961, An application of the Wiener-Kolmogorov smoothing theory to matrix inversion: J. Soc. Indust. Appl. Math., v. 9, p. 387–392.

Glenn, W. E., Ryu, J., Ward, S. H., Peeples, W. J., and Phillips, R. J., 1973, The inversion of vertical magnetic sounding data: Geophysics, v. 38, p. 1109–1129.

Glenn, W. E., and Ward, S. H., 1976, Statistical evaluation of electrical sounding methods. Part I: Experiment Design: Geophysics, v. 41, p. 1207–1221.

Hales, A. L., and Gough, D. I., 1962, The gravity survey of the Republic of South Africa, Handbook 3, Part II: Isostatic anomalies and crustal structure: Geological Survey of South Africa.

Hermance, J. F., 1973, An electrical model for the sub-Icelandic crust: Geophysics, v. 38, p. 3–13.

Inman, J. R., 1975, Resistivity inversion with ridge regression: Geophysics, v. 40, p. 798–817.

Keller, G. V., 1971, Electrical studies of the crust and upper mantle: AGU Geophys. Monogr. no. 14, p. 107–125.

Lawson, C. L., and Hanson, R. J., 1974, Solving least-squares problems: New York, Prentice-Hall, Inc.

Lee, W. H. K., and Uyeda, S., 1965, Review of heat flow data: AGU Geophys. Monogr. no. 8, p. 87–190.

Levenberg, K., 1944, A method for the solution of certain non-linear problems in least squares: Quart. Appl. Math., v. 2, p. 164–168.

Marquardt, D. W., 1963, An algorithm for least squares estimation of nonlinear parameters: J. Soc. Indust. Appl. Math., no. 2, p. 431–441.

Parkhomenko, E. I., 1967, Electrical properties of rocks: New York, Plenum Press.

Rijo, L., Pelton, W. H., Feitosa, E. C., and Ward, S. H., 1977, Interpretation of apparent resistivity data from Apodi Valley, Rio Grande do Norte, Brazil: Geophysics, v. 42, p. 811–822.

Van Zijl, J. S. V., and Joubert, S. J., 1975, A crustal geoelectrical model for South African Precambrian granitic terrain based on deep Schlumberger soundings: Geophysics, v. 40, p. 657–663.

Ward, S. H., 1967, Electromagnetic theory for geophysical applications, *in* Mining geophysics: Vol. 2, SEG, Tulsa.

Phil. Trans. R. Soc. Lond. A. **286**, 549–565 (1977) [549]
Printed in Great Britain

AREA
S. Africa
Wit wat
Fluid

Fluid inclusion study of the Witwatersrand gold–uranium ores

By T. J. Shepherd
Institute of Geological Sciences, Geochemical Division, 64–78 Gray's Inn Road, London WC1X 8NG

[Plate 1]

Fluid inclusions, preserved in quartz pebbles of the uraniferous and auriferous Precambrian oligomictic conglomerates of the Witwatersrand Basin, provide a unique insight into the genesis of the ores. Using differences in inclusion characteristics in conjunction with intra- and inter-deformational textures for adjacent pebbles, a distinction is made between pre- and post-depositional inclusions. Excluding those related to subsequent brittle fracture, the former comprise five principal types; two of which are distinguished by the development of liquid carbon dioxide. Collectively they indicate a moderate to high pressure–temperature environment of vein quartz formation. Systematic variation in the relative abundance of these inclusion assemblages for different sections of the orefield demonstrates the importance of well-defined provenance areas or multiple entry points into the basins. A marked sympathetic relationship between uraniferous banket ores and the presence of vein quartz rich in liquid carbon dioxide inclusions, together with a corresponding antipathetic relationship for gold, strongly suggests separate sources for the metals. The temporal and spatial aspects of the association 'U-CO_2' also imply a uranium influx into the basin from disrete areas of the hinterland contemporaneous with the sediments. Post-depositional inclusions are subordinate and offer no support for the alternative epigenetic model and show only a later interaction of relatively cool circulating groundwaters. A discussion is given of the probable nature and origin of uranium in the source rocks and its mode of transportation. In conclusion, a proposal is made for the use of applied fluid inclusion research in the evaluation of and exploration for similar deposits.

Introduction

In the southern part of the African Shield, thick sequences of relatively undisturbed Precambrian sediments are well preserved in a series of intercratonic basins. The sequence in the Witwatersrand Basin, considered to be the world's principal source of gold and uranium, comprises four Proterozoic super-groups; the Transvaal, Ventersdorp, Witwatersrand and Dominion Reef Systems (figure 1). Together they rest unconformably upon an extensive Archaean basement complex of granites and high-grade metamorphics. Economic concentrations of gold and uranium are characteristically, though not exclusively, confined to thin oligomictic quartz conglomerate beds which occur throughout the succession, particularly within the Upper Witwatersrand and Lower Dominion Reef formations.

The application of fluid inclusion studies to the genesis of these ores depends on the ability to differentiate between pre- and post-depositional inclusions. The latter refer to fluids active after the deposition of the enclosing sediments and are relevant to the epigenetic 'hydrothermal' model of mineralization, whereas the former refer exclusively to fluids which were circulating in the source area before erosion and thus relate more closely to the alternative syngenetic 'modified-placer' model.

Apart from a brief reference to South African uranium and gold-bearing conglomerates by Krendelev, Zozulenko & Orlova (1973) fluid inclusion data for the Witwatersrand ores is non-existent. In their paper they establish a distinction between pre- and post-depositional inclusions but are unable to apply it with any certainty. From an examination of only three samples they conclude 'The sulphide mineralization in the Witwatersrand conglomerates was formed by the reaction of rocks with solutions at temperatures from 220°–400°C'.

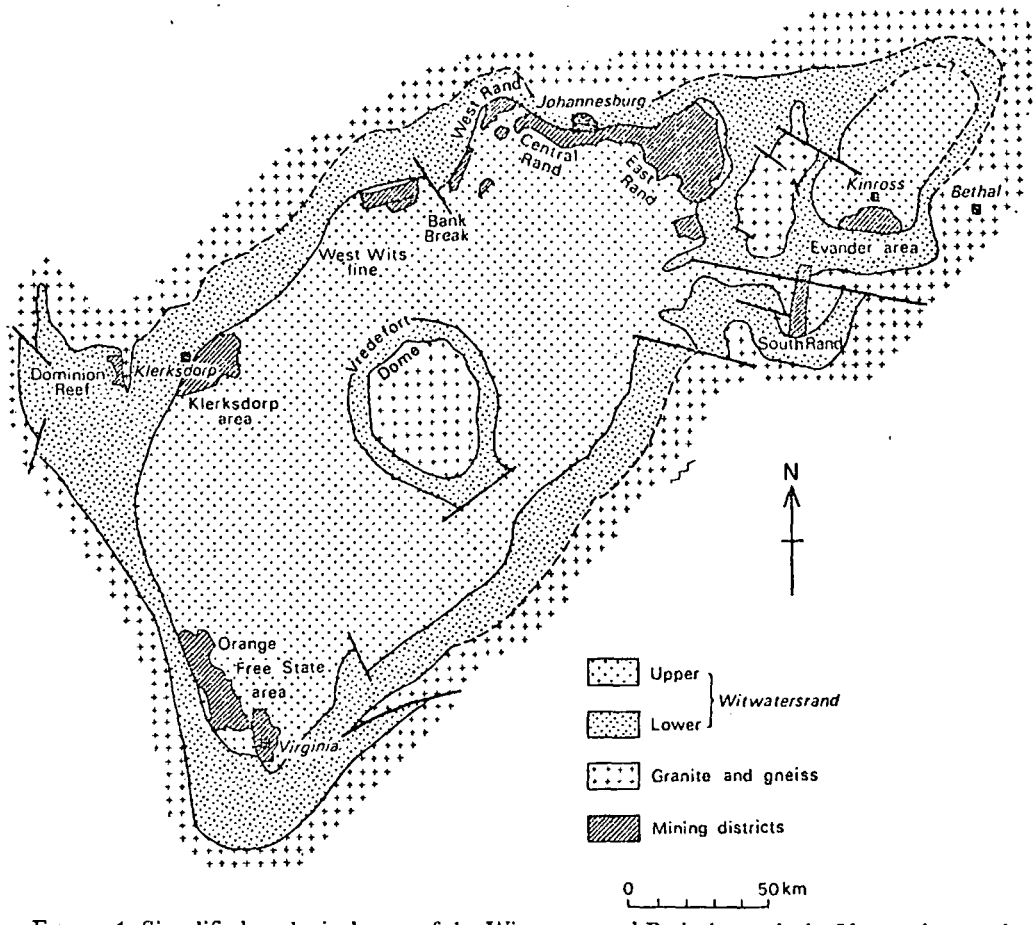

FIGURE 1. Simplified geological map of the Witwatersrand Basin beneath the Ventersdorp and younger cover (after R. Borchers 1961).

Preliminary work on the banket ores suggested that the ubiquitous pebbles of vein quartz provided the most suitable material for preserving the various generations of inclusions. Consequently a special study was made of the type and distribution of inclusions in vein quartz from 23 major mineralized conglomerate horizons in the Witwatersrand Basin.

INCLUSION CHRONOLOGY AND THE EFFECTS OF METAMORPHIC DEFORMATION

In conventional studies one is concerned with the distinction between primary, pseudo-secondary and secondary inclusions in minerals which are *in situ* and have undergone little or no deformation. As defined by Ermakov (1965), primary inclusions are those formed during the growth of the enclosing mineral due to irregularities in crystal growth or fluid inhomogeneity.

Pseudosecondaries occupy fractures formed during crystal growth, while secondaries occur along fractures formed at some subsequent time. For the Witwatersrand pebbles this sequence, where preserved, represents only the first stage of their more complex history. Unlike the pre-depositional inclusions, formation of the post-depositional inclusions was due to the healing of fractures in the pebbles caused by later deformation. Morphologically such inclusions are not easily distinguishable from secondaries *sensu stricto*.

Excluding samples which exhibit localized post-depositional tectonism, the quartz shows a wide range of deformational textures. This is most readily explained by its derivation from a variety of metamorphic and deformational environments equivalent to or of higher grade than the host sediments. Confirmation is provided by the coexistence of strongly contrasting deformational textures in pebbles from the same sample (see figure 3*a*, plate 1). According to White & Treagus (1975) quartz veins deform naturally by a dislocation creep mechanism analogous to that produced in metals and ceramics. The associated optical strain features are continuous and discontinuous undulatory extinction, deformation bands, deformation lamellae, narrow sub-grains and Boehm lamellae. With increasing strain the intercrystalline dislocation structures are replaced by misorientated sub-grains, leading ultimately to a complete recrystallization of the quartz. Without exception, the Witwatersrand pebbles display varying degrees of the above features making it necessary to allow for the effects of later deformation on the pre-depositional inclusions. No systematic study of inclusions during progressive deformation has yet been carried out but the present observations agree closely with those recorded by R. Kerrich (personal communication 1975). The development of undulatory extinction and deformational bands appears to have had little effect on pre-existing inclusions and caused only a 'necking' of the more irregular shaped inclusions. With the establishment of advanced sub-grain development the smaller inclusions (< 10 μm) become disrupted and driven to sub-grain boundaries. The current consensus of opinion is that inclusions in deformed crystals are unreliable geothermometers and give anomalous homogenization temperatures. Synmetamorphic intercrystalline deformation is often succeeded by a period of brittle fracture, accompanying tectonic uplift, and capable of generating further sets of secondary inclusions. However, the task of differentiating between pre- and post-deformational secondaries is beyond the scope of the present work. For the Witwatersrand quartz pebbles the chronology of events may be summarized as follows:

Stage I: Crystal growth in the source area.
1. Formation of primary, pseudosecondary and secondary inclusions.

Stage II: Metamorphic and tectonic deformation in the source area.
1. Intercrystalline deformation and modification of pre-existing inclusions.
2. Brittle fracture and the formation of a second generation of secondary inclusions.

Stage III: Post-depositional tectonic deformation.
1. Minor modifications due to inter-pebble pressure solution phenomena for conglomerates with a high packing index.
2. Brittle fracture and the formation of a third generation of secondary inclusions.

Stage IV: Post-depositional contact thermal metamorphism (probably overlaps with stage III)
1. Thermal rupture of inclusions adjacent to minor intrusives.

Had the Witwatersrand and Dominion Reef Systems suffered a higher grade of regional metamorphism it is doubtful whether many source area inclusions would have survived.

Because of the difficulty in distinguishing between stage I and II secondaries, only the primary and pseudosecondary inclusions were selected for study. Even so the data probably still contains a small component of secondaries.

The comb texture produced by nucleation at a surface followed by growth perpendicular to the surface with mutual impingement is notably lacking in the quartz pebbles. This arrangement is generally taken to imply low-temperature deposition. Instead, the quartz consists of single crystals or interlocking anhedra, typical of higher temperature hydrothermal or syn-metamorphic veins, greisens and pegmatite zones. The apparent granular appearance is considered therefore to be a primary growth texture unrelated to the strain mosaics produced by later deformation.

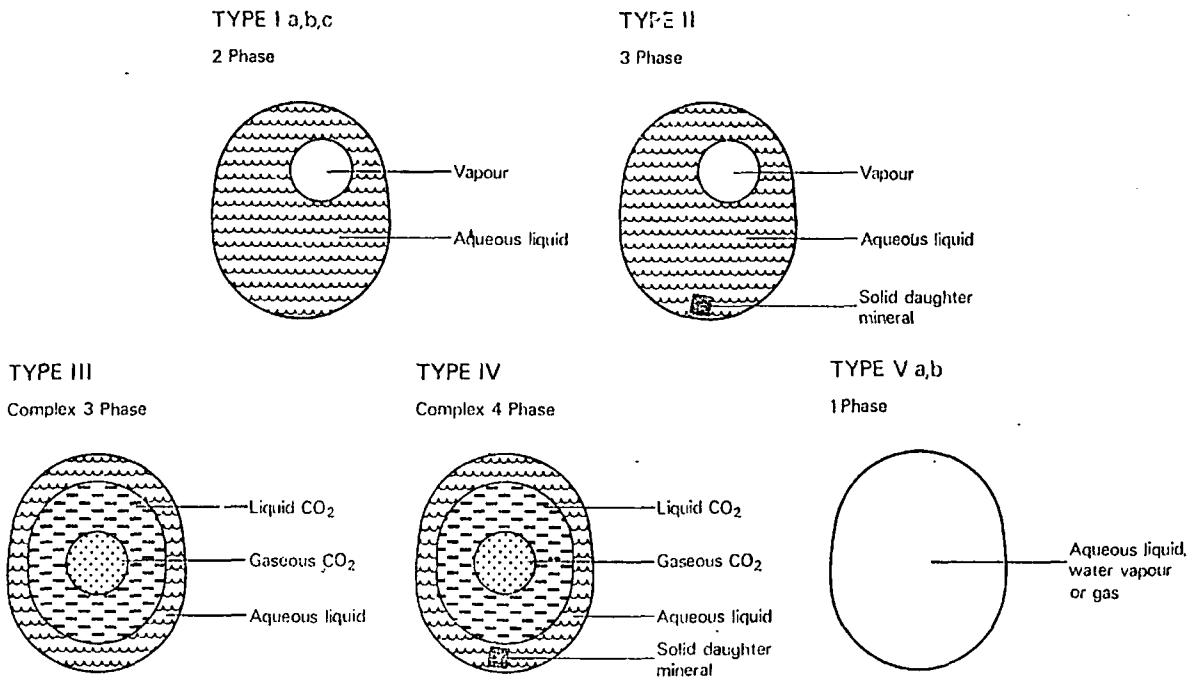

FIGURE 2. Diagrammatic representation of the principal types of fluid inclusion.

DESCRIPTION OF PLATE 1

FIGURE 3. (*a*) Photomicrograph of typical uranium–gold banket ore showing contrasting deformational textures in adjacent vein quartz pebbles (p.t.s. 1940, transmitted light, crossed nicols, bar = 0.25 cm). *Locality:* Main Reef, West Driefontein, West Wits area.

(*b*)–(*f*)Photomicrographs of selected inclusions in pebbles of vein quartz.

(*b*) Group of pre-depositional type I two-phase inclusions (p.t.s. 2006, bar = 50 μm). *Locality:* Dominion Reef, Dominion Reefs, Dominion Reef area.

(*c*) Large pre-depositional type II three-phase inclusion showing rhombic anisotropic daughter mineral (p.t.s. 2050, bar = 100 μm). *Locality:* Vaal Reef, Vaal Reefs, Klerksdorp area.

(*d*) Multifaceted pre-depositional type III three-phase inclusion containing liquid and gaseous carbon dioxide; as arrowed (p.t.s. 2006, 18°C, bar = 50 μm). *Locality:* Dominion Reef, Dominion Reefs, Dominion Reef area.

(*e*) Plane of pre-depositional type I inclusions growing onto and enveloping solid rutile needles; as arrowed. (p.t.s. 1969, bar = 50 μm). *Locality:* Main Reef, Daggafontein, East Rand area.

(*f*) Planar arrays of post-depositional type I inclusions along fractures having a common orientation with respect to adjacent pebbles (p.t.s. 2011, bar = 20 μm). *Locality:* Dominion Reef, Dominion Reefs, Dominion Reef area.

(*g*) Photomicrograph of flame-like Boehm lamellae in vein quartz pebble. (p.t.s. 1969, bar = 50 μm). *Locality:* Main Reef, Daggafontein, East Rand area.

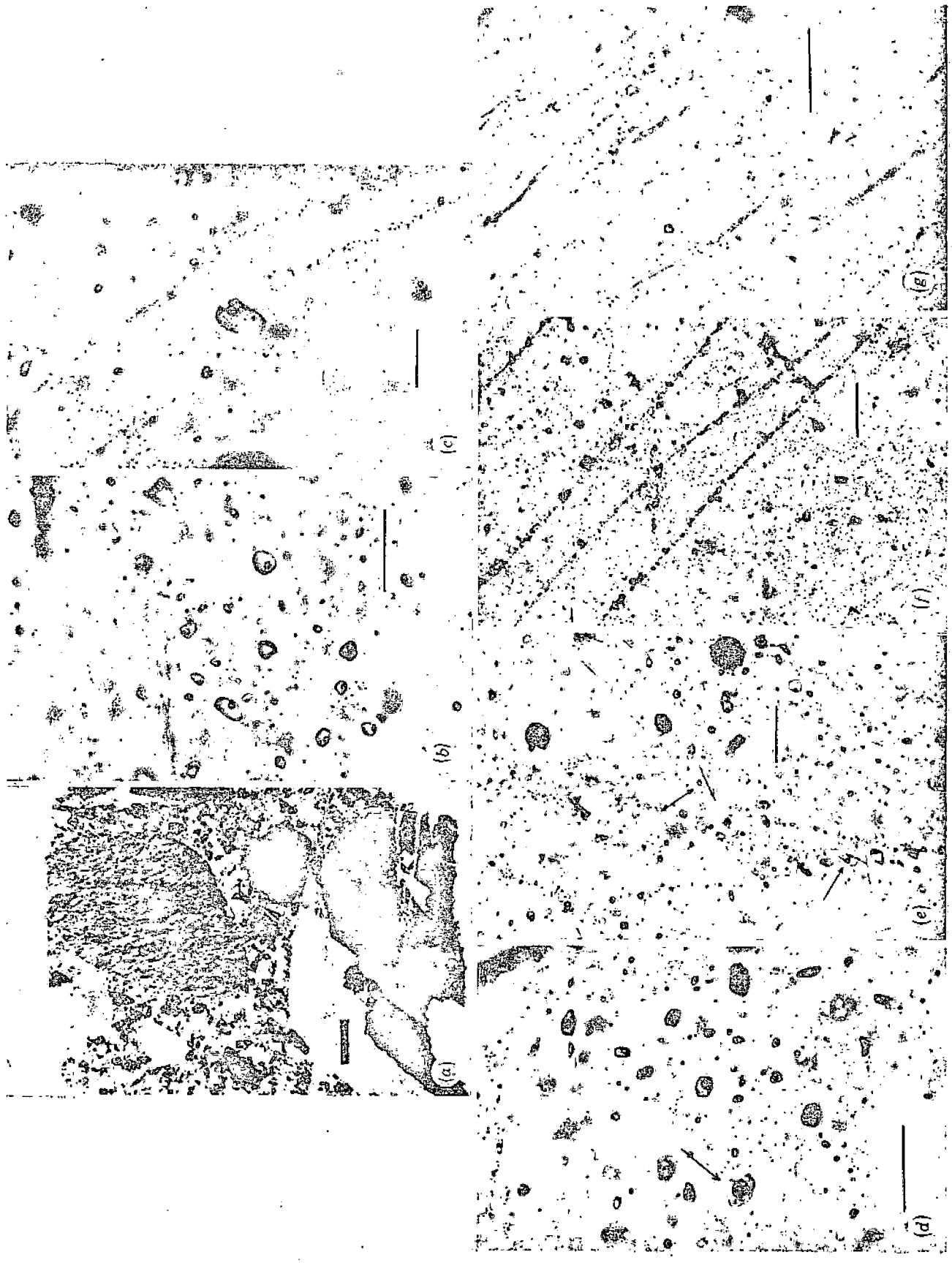

FIGURE 3. For description see opposite.

Types of inclusion

The quartz pebbles contain five principal types of inclusion, varying from < 1 μm to 80 μm in diameter but normally < 20 μm (figure 2).

Type I: Simple two-phase inclusions (aqueous liquid + vapour) (figure 3*b*). These are by far the most abundant and may be divided into three sub-groups according to their vapour/total volume ratio: (*a*) < 0.05, (*b*) ~ 0.1 to 0.15, (*c*) ~ 0.2 to 0.4. For a 10 % (by mass) NaCl solution this is equivalent to homogenization temperatures of (*a*) < 110 °C, (*b*) ~ 170–225 °C, (*c*) ~ 275–400 °C.

Type II: Simple three-phase inclusions (aqueous liquid, vapour + solid daughter minerals) (figure 3*c*). Though less abundant they show considerable variation in daughter mineral content, suggesting a wide range of fluid compositions. Isotropic, anisotropic, euhedral, anhedral, cubic and rhombic phases are well developed. The vapour/total volume ratio for this group ranges from 0.05 to 0.2 but never less than 0.05.

Type III: Complex three-phase inclusions (aqueous liquid, liquid CO_2 + gaseous CO_2) (figure 3*d*).

Type IV: Complex four-phase inclusions (aqueous liquid, liquid CO_2, gaseous CO_2 + solid daughter minerals).

Types III and IV are highly distinctive and contain appreciable quantities of liquid CO_2. Depending upon the temperature at which the CO_2-rich phase homogenizes to the liquid state they contain either liquid CO_2 or liquid CO_2 + gaseous CO_2 at room temperature. The ratio of aqueous liquid/liquid CO_2 varies from about 1.5 to 5.0 for the type III inclusions but generally < 2.5 for the type IV group. Numerically the complex four-phase inclusions are the least important and show little variation in daughter minerals. Inclusions containing liquid CO_2 respond violently to thermal overprinting and frequently explode due to a massive build-up in internal pressure. The black inclusions surrounded by haloes of tiny satellite inclusions commonly associated with the type III inclusions are thought to be the remains of disrupted inclusions with a high initial liquid CO_2 content.

Type V: Single phase inclusions (*a*) aqueous liquid or (*b*) wholly gaseous. The sub-types V*a* and V*b* are mutually exclusive and correspond to different conditions of formation. The aqueous variety is interpreted as a metastable low temperature type I inclusion which has failed to nucleate a small vapour bubble (Roedder 1967). By contrast the gaseous variety though superficially similar to the disrupted type III inclusion is without a debris halo. Where proved coeval with type II, III or IV inclusions it is considered to be diagnostic of fluid boiling; representing the vapour phase of a heterogeneous two-phase liquid–vapour system.

In addition to fluid inclusions, some of the quartz crystals contain solid rutile inclusions, especially in pebbles < 4 mm diameter. The degree of rutilation, shape, dimension and orientation of the needles is variable. An unusual association noted in certain grains is the growth of secondary inclusions on contact with or enveloping the rutile (figure 3*e*).

Pre-depositional inclusions 'primaries'

With the exception of type V*a*, the 'primaries' are represented by all five inclusion types. For any one pebble the number of different types rarely exceeds three, but in a normal specimen of banket ore there may be several pebbles with different assemblages of inclusions.

Theoretically this allows a large number of permissible combinations. The fact that this is not observed demonstrates a restricted P–T–X environment for the veins, which limits the range of possible source areas for the quartz pebbles. The occurrence of different inclusion assemblages and deformational textures in adjacent pebbles provides a useful guide to the recognition of pre- and post-depositional inclusions and supplements the general recognition of primary, pseudosecondary and secondary inclusions. While types I and II generally conform to the Ermakov criteria, types III and IV often occur in curving zones or discontinuous irregular planar arrays. This is quite distinct from the more continuous regular arrays of unequivocal secondaries decorating well-defined healed fractures. Unlike a large euhedral crystal which records the whole P–T–X history of a mineralizing event, an interlocking aggregate of anhedral crystals cannot be expected to respond in the same manner. Thus within the context of a smaller crystal, fundamental changes in fluid chemistry during the main phase of quartz deposition may only be recorded in the secondaries. The CO_2-rich inclusions are therefore regarded as pseudosecondaries with secondary inclusion characteristics. This relationship is probably equivalent to the complex refilling mechanism and development of secondary inclusions described by Kalyuzhnyy & Voznyak (1969) for Zanorysh-type pegmatites. The correct recognition of 'primaries' related to quartz deposition is confirmed by the relative exclusion from the data of incompatible combinations of inclusions as might be expected by superimposing pre-depositional secondaries unrelated to vein formation.

Since dissolved salts are known to suppress the onset of critical phenomena in the system H_2O–CO_2 (Takenouchi & Kennedy 1965) type IV inclusions represent the trapping of supercritical fluids at temperatures higher than those for the corresponding type III variety. Where the liquid CO_2 content of the latter inclusions is greatest they are sometimes accompanied by coexisting type II inclusions suggesting sub-critical immiscibility and the simultaneous trapping of two-fluid phases (a CO_2-rich phase and a H_2O-rich phase). Many intermediate conditions exist, as shown by the range of H_2O/liquid CO_2 ratios, but all suggesting elevated P–T conditions.

Post-depositional inclusions 'secondaries'

The only unambiguous 'secondaries' are those occurring along fractures traversing both pebble and matrix, or as planar arrays with a common orientation in pebbles of different crystallographic orientation (figure 3*f*). For specimens showing no apparent fracture fabric, the occurrence of 'secondaries' along planes of weakness due to crystal anisotropy can not be discounted. Even so, compared to the 'primaries', the post-depositional inclusions are poorly developed and represented almost exclusively by types I*a* or V*b*; more rarely by I*b*. Without a petrofabric analysis of the host rocks it is impossible to assign even a relative age to the 'secondaries'.

Inclusions of uncertain origin

Occupying a position between the two main classes are a group of inclusions whose origin is less certain. By virtue of their occurrence they are clearly secondaries *sensu stricto*. Of these the least problematical are the minute inclusions decorating Boehm lamellae, which impart a reddish-brown colour to the quartz as a result of Tyndall light scattering (figure 3*g*). Closely associated are the arrays of small inclusions (< 5 μm) orientated at 90° to the deformation bands and elongated sub-grains. Both appear to have originated during the pre-depositional deformation of the quartz veins but are not necessarily contemporaneous.

Regional variation in inclusion assemblages

When considered regionally the fluid inclusion data for individual goldfields or sections of the Witwatersrand basin suggests a marked variation in the nature and origin of the vein quartz. This is most clearly illustrated by differences in the pre-depositional inclusion assemblages for separate geographical areas (figure 4). Quartz pebbles from the Klerksdorp–Dominion Reef area are significantly different from those of the East Rand and probably also from those of the O.F.S. and West Wits areas. Collectively, the evidence would appear to support a sedimentological model of multiple entry points into the basin (Brock & Pretorius 1964). A further observation not wholly reflected in the bulk mineral composition of the sediments is the persistence of a rather distinctive source for the vein quartz in the Klerksdorp region throughout the Dominion Reef and Upper Witwatersrand periods. Similarly, the dominance of type I*b* inclusions and presence of rutilated quartz implies a unique source for the East Rand quartz pebbles.

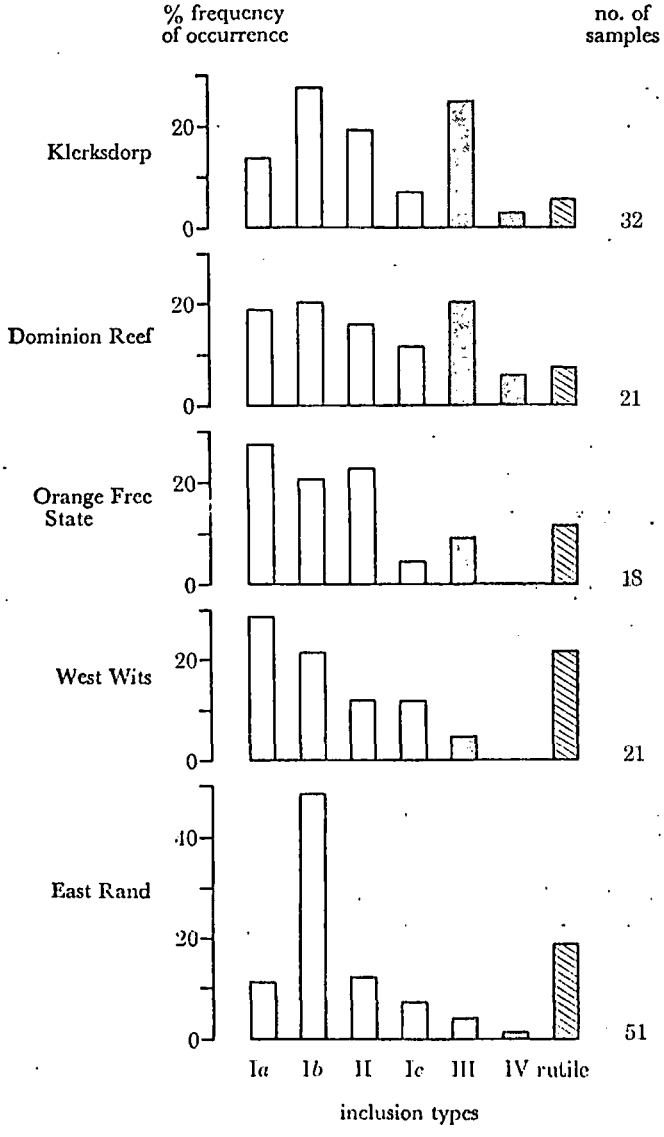

Figure 4. Regional variation in inclusion assemblages for the Witwatersrand orefield.

Correlation between uraniferous ores and CO_2 inclusions

After allowing for differences in the stratigraphic range of samples, several patterns emerge concerning the spatial and temporal distribution of uranium not discernible in the regional evaluation. Figure 5 shows the data re-plotted using a geological succession for the reefs suggested by Whiteside (1970). Of the six most economically important uraniferous reefs in the O.F.S., Klerksdorp, Dominion Reef, West Wits and East Rand areas, five are characterized by the presence of vein quartz pebbles containing type III or IV liquid CO_2 inclusions (i.e. the Intermediate, Leader, Vaal, Dominion and Kimberley UK9 reefs). The only exception is the Carbon Leader Reef of the West Wits which differs from the others in representing the best example of ore associated with hydrocarbon in the Witwatersrand Basin. Of the 19 major auriferous reefs studied, including the Afrikander Reef of the Rietkuil Syncline, vein quartz containing liquid CO_2 inclusions is present in only four cases (i.e. the Leader Reef of the O.F.S., the Black Reef, Ventersdorp Contact Reef and Vaal Reef of the Klerksdorp area). Both the Leader and Vaal Reefs are uranium producers and hence do not constitute real exceptions. Since the Black Reef and Ventersdorp Contact Reef represent a reworking of the underlying Upper Witwatersrand sediments it is conceivable that the quartz pebbles containing liquid CO_2 inclusions have been derived from the Vaal Reef.

The positive correlation between uraniferous banket ores and associated quartz pebbles containing type III and IV inclusions strongly supports the contemporaneous deposition of metal and associated sediments. Though favouring a syngenetic origin, the evidence offers no criteria for distinguishing between detrital uraninite and uranium precipitated chemically from the water in which the sediments were being laid down. In view of the work of Coetzee (1965), Hiemstra (1968), Liebenberg (1955) and Minter (1976), and the successful application of the 'placer' model, one must conclude that some uraninite, free from carbonaceous matter, is a primary detrital component. If this is correct, then the occurrence of vein quartz rich in liquid CO_2 inclusions reflects the presence or proximity of detrital uraninite. With regard to uranium in solution, a clue to the importance of this component may lie in our understanding of the hydrocarbon-rich ores and their relation to the banket ores. Brock & Pretorius (1964), De Kock (1964) and others have for many years advocated an algal origin for the 'carbon', implying growth and accumulation in a low-energy environment. Recent work by Hallbauer (1975) now appears to confirm this suggestion and demonstrates that simple organisms are capable of extracting Au and U from pre-existing minerals and depositing the elements inter- and intracellularly. Occupying the distal parts of alluvial fans, the hydrocarbon-rich ores probably represent the efficient biogenic extraction of U from solution in areas beyond the zone of active fan accretion.

Unfortunately, samples were not available from the eastern part of the West Wits area and hence it was not possible to test the concept of a distal to proximal facies change eastwards over the Bank Break from the Carbon Leader of the Blyvooruitzicht section to the more typical banket deposits of the Libanon section. However, unless the area was located at the confluence of two alluvial fans one should expect some detrital uraninite together with diagnostic vein quartz in the adjacent Libanon section. Further south, in the O.F.S. and Klerksdorp areas, hydrocarbon-rich ores in the Basal and Vaal Reefs share their horizons with typical banket type ores. In describing the geology of the O.F.S. (central section), McKinney (1964) notes

supergroup/group	formation	Orange Free State section	Klerksdorp section	Dominion Reef section	West Wits section	East Rand section
Transvaal			*Au. Black Reef			
Ventersdorp			*Au+(U). V.C.R.		Au. V.C.R.	
Upper Witwatersrand	Elsburg	Au. Elsburg	Au. Elsburg			Au. Elsburg
	Kimberley	Au. 'A' Reef				Au. Kimberley UK7 *U+Au. Kimberley UK9
	Bird	*U+Au. Leader Basal	*U+Au. Vaal			
	Main	*U+(Au). Intermediate			Au. M.R.L.	Au. M.R.L.
			Au. Ada May		U+Au.C.L.	
Lower Witwatersrand	Jeppestown				Au. N.L.	Au. Footwall
				Au. Afrikander		
	Government Reef					
	Hospital Hill					
Dominion Reef						
				*U+(Au). Dominion		

KEY: * Vein Quartz containing type III or IV liquid CO_2 inclusions. **Au**, Gold; **U**, Uranium; V.C.R., Ventersdorp Contact Reef; M.R.L., Main Reef Leader; C.L., Carbon Leader; N.L., North leader.

FIGURE 5. Correlation between uraniferous reefs and the presence of vein quartz containing liquid carbon dioxide-type inclusions.

that economic amounts of uranium are only found in the centre of the basin where carbon is more abundant. The present data suggests a predominance of quartz pebbles containing type III and IV inclusions in the southern section (Virginia) and their absence in the northern section (Freddies). This is in keeping with a southerly proximal facies related to a movement of sediment from south to north as inferred from palaeocurrent direction. In the Klerksdorp area, Minter's work (1976) confirms the importance of the association 'uranium-hydrocarbon' in the Vaal reef orebody but from an exhaustive treatment of sedimentological and mine data he derives a close relationship between reef isopachs and uranium values, which combined with the observed hydraulic equivalence of uraninite with other heavy minerals, strongly supports the case for a major detrital component. The alluvial fan complexes of the O.F.S. and Klerksdorp areas may therefore represent situations where both the detrital and solution components of syngenetic uranium are developed at the same stratigraphic horizon.

Origin of the uranium

Concerning the significance of the association U-CO_2, the spatial relationship for the basin does not prove a genetic affinity in the source area. Inclusion data for the 'primaries' does suggest, however, that *P–T–X* conditions during vein formation were typical of those for hydrothermal uranium mineralization. Tugarinov & Naumov (1969) in describing various uranium deposits in the U.S.S.R. report a temperature range of 350 to 50 °C and pressure range of 2000 to 400 bar. This agrees closely with the temperature range for intergranitic uranium veins in the Massif Central, given by Poty, Leroy & Cuney (1974). Both groups record a pronounced enrichment of CO_2 in the orefluids; a feature interpreted as indicating uranium transport as uranyl carbonate complexes. Tugarinov & Naumov also note that whereas uraninite is the most stable mineral above 250 °C, pitchblende is characteristic of the lower temperature deposits. Opinions differ as to the distinction between these two phases, but whatever terminology is used the less resistate 'pitchblende' would be more susceptible to solution during weathering. Furthermore, since the 'secondaries' were of a low temperature type it is unlikely that post-depositional fluids were responsible for the development of the allogenic uraninite phase.

The marked contrast in gross mineralogy of the Dominion Reef and Upper Witwatersrand systems has promoted several workers to advocate separate origins for the uraninites. The abundance of accessory garnet, monazite, columbite and zircon in the older sediments is taken as evidence for a pegmatitic source whereas the relative absence of these minerals in the younger sediments is indicative of a non-pegmatitic source. If, however, one assumes the diagnostic quartz pebbles reflect the depositional environment of quartz-rich uraniferous bodies in the hinterland, then the similarity in inclusion assemblages for the Dominion Reef and Klerksdorp areas implies that the uraninites were formed under similar conditions (figure 4). This apparent contradiction can best be explained by considering the uranium to have been derived from a suite of uraniferous veins emplaced in a terrain of variable metamorphic and granitic rocks, the heavy mineral content of the reefs being determined by the mineralogy of the eroded country rocks. Furthermore the discrete distribution of uranium in the basin also implies a restricted distribution in the source areas such that the influx of uranium was controlled by the occurrence and erosion of these veins. With the exception of the Black Reef and Ventersdorp Contact Reef it is doubtful whether a reworking of older

mineralized sediments, as proposed by Vos (1975) for the gold ores, could produce conglomerates uniquely defined by the presence of one particular type of vein quartz.

Recent work by Touret (1971), Hoefs & Touret (1975), and Hollister & Burruss (1976) has demonstrated the important rôle of supercritical H_2O–CO_2 fluids during high-grade metamorphism and migmatization. Lambert & Heier (1968) have also shown that increasing metamorphism is accompanied by a progressive loss of U and Th from the system. Given the extreme mobility of uranium in carbonated fluids, a situation where both processes were operating simultaneously would create the optimum conditions for uranium remobilization. Such a situation may have existed in the granite–greenstone belts of the Kapvaal craton surrounding the Witwatersrand Basin. In the Barberton area, Hunter (1968) and Viljoen, Saager & Viljoen (1970) describe the intrusion of volatile-rich metasomatic granites and migmatitic granite complexes along the margins of older low-volatile tonalitic gneiss domes. A concomitant expulsion of CO_2-rich fluids, enriched in uranium may have triggered an additional remobilization of uranium from the metavolcanic/sedimentary cover to be redeposited at higher levels as uraniferous quartz veins. Depending upon the source of the metal and conditions during its extraction and precipitation, one would expect the Th/U ratio of the resultant uraninite to vary accordingly.

As a corollary, it is suggested that the relative proportions of detrital uraninite and uranium in solution entering the Witwatersrand Basin were governed by the mineralogical character of the uraniferous veins; a high solution component reflecting a predominance of pitchblende in that part of the source area.

Conclusions

The pebbles of vein quartz, characteristic of the mineralized oligomictic conglomerates, show considerable variation in the degree of intercrystalline deformation and the development of fluid inclusions, both within and between samples. These features indicate the heterogeneous origin of the quartz, not always apparent in hand specimens. According to differences in morphology, mode of occurrence and relative phase proportions, the inclusions may be classified into five main types. Using these differences together with the associated dislocation creep phenomena and crystallographic orientation of adjacent pebbles it is possible to distinguish between pre- and post-depositional events.

As shown by the progressive modification of pre-existing inclusions corresponding to changes in the intensity of deformation, the inclusions also record the pre-depositional metamorphism of the parent quartz veins. The effects, though variable, cannot be discounted entirely and must be considered when assessing the phase relations for primary and pseudosecondary inclusions.

The 'primaries' or pre-depositional inclusions are represented by all five types, of which those containing liquid CO_2 are the most distinctive. Their presence, especially where coexistent with high vapour two phase inclusions, indicates formation at elevated temperatures and pressures. P–T–X data for this group provides direct information on physico-chemical conditions in the source area.

The 'secondaries' or post-depositional inclusions are less well developed and represented by only the lowest temperature types. The temperature régime as defined by these inclusions appears too low to account for the deposition of uraninite but is adequate to account for a later secondary remobilization of uranium by circulating groundwaters.

Regional variation in pre-depositional inclusion assemblages follows a coherent geographical

pattern, implying a systematic variation in the source areas for individual sections of the Witwatersrand basin. Within each section there is a positive correlation between uraniferous banket ores and the presence of vein quartz containing liquid CO_2 inclusions. This suggests a syngenetic origin for the uranium and though the hydrocarbon-rich ores appear at first to contradict this model it is thought they represent the precipitation of uranium from solution by organic matter in areas beyond the zone of active fan accretion; and hence beyond the areas of significant detrital uraninite.

Data for the 'primaries' demonstrates that conditions during vein formation in areas supplying uranium to the basin were typical of those for hydrothermal uraninite/pitchblende deposits, especially with regard to the enrichment of CO_2 in the fluids.

The marked similarity in inclusion assemblages for the Klerksdorp and Dominion Reef areas suggests that the contrasting bulk mineral composition of the Dominion Reef and Upper Witwatersrand Systems may not have a direct bearing on the origin of the associated uraninite, but more a reflection of the country rocks adjacent to the uraniferous quartz bodies. The discrete distribution of uranium in the basin implies a restricted distribution in the hinterland such that the influx of uranium was controlled by the occurrence and erosion of these uranium enrichments.

Given the important rôle of supercritical H_2O–CO_2 fluids during high grade metamorphism and migmatization, it is proposed that the intrusion of migmatitic granite complexes into the granite–greenstone belts of the Kapvaal craton was responsible for the remobilization of uranium and its subsequent deposition in contiguous quartz veins.

Future research

The obvious exploration potential given by the ability to recognize uraniferous horizons from a study of inclusions in pebbles of vein quartz needs to be developed more fully. If integrated with routine pebble counts, as practised by several mining companies, fluid inclusion studies may provide a much better understanding of the distribution of U and Au within particular reefs. An important extension of the present work should be the sampling of areas as yet untested (i.e. the West Rand, South Rand and Evander goldfields). Satisfactory confirmation of this model for the Witwatersrand Basin opens up the possibility of using this technique to evaluate similar uranium prospects in the eastern Transvaal, northern Natal and ultimately other oligomictic quartz conglomerate sequences in Brazil, Australia, Canada and Algeria.

Equally, a more detailed characterization of inclusions for the auriferous reefs may provide criteria for differentiating between barren and mineralized conglomerates. The important rôle of uranium-bearing quartz veins would be greatly substantiated if it could be demonstrated that CO_2-rich inclusion fluids were uraniferous.

I should like to thank Dr S. H. U. Bowie for suggesting the study and my many colleagues in the Geochemical Division for their advice and constructive discussion during all stages of the work. I also wish to acknowledge H. C. M. Whiteside and A. G. Darnley for providing the specimens at Dr Bowie's request.

This paper is published by permission of the Director, Institute of Geological Sciences.

References (Shepherd)

Borchers, R. 1961 Exploration of the Witwatersrand System and its extensions. *Geol. soc. South Africa* **64**, lxvii–xcviii.

Brock, B. B. & Pretorius, D. A. 1964 In *The geology of some ore deposits in South Africa* (ed. S. H. Haughton), vol. 1, pp. 550–599. Geol. Soc. South Africa.

Coetzee, F. 1965 Distribution and grain-size of gold, uraninite, pyrite and certain other heavy minerals in gold-bearing reefs of the Witwatersrand Basin. *Geol. soc. South Africa Trans.* **68**, 61–88.

De Kock, W. P. 1964 In *The geology of some ore deposits in South Africa* (ed. S. H. Haughton), vol. 1, pp. 323–386. Geol. Soc. South Africa.

Ermakov, N. P. 1965 *Research on the nature of mineral-forming solutions* (ed. E. Roedder), p. 743. Pergamon Press.

Hallbauer, D. K. 1975 The plant origin of the Witwatersrand 'carbon'. *Minerals Sci. Engng.* **7**, 111–129.

Hiemstra, S. A. 1968 The mineralogy and petrology of the uraniferous conglomerate of the Dominion Reefs mine, Klerksdorp area. *Geol. soc. South Africa Trans.* **71**, 1–65.

Hoefs, J. & Touret, J. 1975 Fluid inclusion and carbon isotope study from Bamble granulites (South Norway). *Contrib Mineral. Petrol* **52**, 165–174.

Hollister, L. S. & Burruss, R. C. 1976 Phase equilibria in fluid inclusions from the Khtada Lake metamorphic complex. *Geochem. cosmochim. Acta.* **40**, 163–175.

Hunter, D. R. 1968 The pre-Cambrian terrain in Swaziland with particular reference to the granite rocks. Unpubl. Ph.D. Thesis, University of Witwatersrand, Johannesburg.

Kalyuzhnyy, Vl. A. & Voznyak, D. K. 1969 Thermodynamic and geochemical characteristics of mineral-forming solutions of Zanorysh-type pegmatites (from liquid inclusions in minerals). *Geochem. Int.* **6**, 208–220.

Krendelev, F. P., Zozulenko, L. B. & Orlova, L. M. 1973 Properties of solutions that have metamorphosed metalliferous conglomerate as shown by the study of gas–liquid inclusions in quartz pebbles and regenerated minerals. *Dokl. Earth Sci. Sect.* **212**, 160–163.

Lambert, I. B. & Heier, K. S. 1968 Geochemical investigations of deep-seated rocks in the Australian shield. *Lithos* **1**, 30–53.

Liebenberg, W. R. 1955 The occurrence and origin of gold and radioactive minerals in the Witwatersrand System, the Dominion Reef, the Ventersdorp Contact Reef and the Black Reef. *Geol. soc. South Africa Trans.* **58**, 101–223.

McKinney, J. S. 1964 In *The geology of some ore deposits in South Africa* (ed. S. H. Haughton), vol. 1, pp. 445–506. Geol. Soc. South Africa.

Minter, W. E. L. 1976 Detrital gold, uranium, and pyrite concentrations related to sedimentology in the pre-Cambrian Vaal Reef placer, Witwatersrand, South Africa. *Econ. Geol.* **71**, 157–176.

Poty, B. P., Leroy, J. & Cuney, M. 1974 *Formation of uranium ore deposits* (Proc. Symp. Athens), pp. 562–581. Int. Atom. Energy Agency, Vienna, 1974.

Roedder, E. 1967 Metastable superheated ice in liquid-water inclusions under high negative pressure. *Science, N.Y.* **155**, 1413–1417.

Takenouchi, S. & Kennedy, G. C. 1965 The solubility of carbon dioxide in NaCl solutions at high temperatures and pressures. *Am. J. Sci.* **263**, 445–454.

Touret, J. 1971 Le faciès granulite en Norvège meridonale. Les inclusions fluides. *Lithos* **4**, 423–436.

Tugarinov, A. I. & Naumov, V. B. 1969 Thermobaric conditions of formation of hydrothermal uranium deposits. *Geochem. Int.* **6**, 89–103.

Viljoen, R. P., Saager, R. & Viljoen, M. J. 1970 Some thoughts on the origin and processes responsible for the concentration of gold in early pre-Cambrian of South Africa. *Mineral. Deposita.* **5**, 164–180.

Vos, R. G. 1975 An alluvial plain and lacustrine model for the pre-Cambrian Witwatersrand deposits of South Africa. *J. Sed. Petrol.* **45**, No. 2, 480–493.

White, S. & Treagus, J. E. 1975 The effects of polyphase deformation on the intra-crystalline defect structures of quartz. Parts 1 & 2. *N. Jb. Miner. Abh.* **123**, No. 3, 219–252.

Whiteside, H. C. M. 1970 *Uranium exploration geology* (Proc. panel, Vienna), pp. 49–74. Int. Atom. Energy Agency, Vienna, 1970.

Appendix I

Tables 1–5: Tables of samples used for fluid inclusion studies according to geographical areas described in the text

Table 1. East Rand area

polished thin section no.	sample no.	mine property	stratigraphic horizon	material
1968	1	Daggafontein	Main Reef	conglomerate
1969	2	Daggafontein	Main Reef	conglomerate
1970	3	Daggafontein	Main Reef	conglomerate
1971	4	Daggafontein	Main Reef	conglomerate
1972	4	Daggafontein	Main Reef	conglomerate
1973	5	Daggafontein	Main Reef	conglomerate
1974	6	Daggafontein	Main Reef	conglomerate
1975	7	Daggafontein	Main Reef	conglomerate
1976	8	Daggafontein	Main Reef	conglomerate
1978	10	Daggafontein	Main Reef	conglomerate
1979	11	Daggafontein	Main Reef	conglomerate
1980	12	Daggafontein	Main Reef	conglomerate
1981	13	Daggafontein	Main Reef	conglomerate
1982	14	Daggafontein	Main Reef	conglomerate
1983	15	Daggafontein	Main Reef	conglomerate
1984	16	Daggafontein	Main Reef	conglomerate
1985	17	Daggafontein	Main Reef	conglomerate
1986	18	Daggafontein	Main Reef	conglomerate
1987	19	Daggafontein	Main Reef	conglomerate
1988	20	Daggafontein	Main Reef	conglomerate
1989	21	Daggafontein	Main Reef	conglomerate
1990	21	Daggafontein	Main Reef	conglomerate
1991	22	Daggafontein	Main Reef	conglomerate
1992	23	Daggafontein	Main Reef	conglomerate
1993	24	Daggafontein	Main Reef	conglomerate
1994	25	Daggafontein	Main Reef	conglomerate
1995	26	Daggafontein	Main Reef	conglomerate
2029	MK 1A	Daggafontein	Kimberley Reef	conglomerate
2030	MK 1B	Daggafontein	Kimberley Reef	conglomerate
2031	MK 2	Daggafontein	Kimberley Reef	conglomerate
2061	UG 9145	East Geduld	Main Bird	quartzite
2062	UG 9146	East Geduld	Main Reef	conglomerate
2063	UG 9147	East Geduld	Main Reef	conglomerate
2064	UG 9148	East Geduld	Main Reef	conglomerate
2065	UG 9149	East Geduld	Main Reef	conglomerate
2066	UG 9150	East Geduld	Main Reef	conglomerate
2067	UG 9151	East Geduld	Main Bird	quartzite
2068	UG 9152	East Geduld	Kimberley Reef (UK3)	conglomerate
2069	UG 9153	East Geduld	Kimberley Reef (UK3)	conglomerate
2070	UG 9154	East Geduld	Kimberley Reef (UK4)	quartzite
2071	UG 9155	East Geduld	Kimberley Reef (UK5)	conglomerate
2072	UG 9156	East Geduld	Kimberley Reef (UK7)	conglomerate
2073	UG 9157	East Geduld	Kimberley Reef (UK8)	quartzite
2074	UG 9158	East Geduld	Kimberley Reef (UK9)	conglomerate
2076	UG 9160	East Geduld	Kimberley Reef	conglomerate
2077	UG 9161	East Geduld	Kimberley Reef	quartzite
2078	UG 9162	East Geduld	Kimberley Reef	conglomerate
2099	A 232	East Geduld	Main Reef Leader	conglomerate
2100	A 233	East Geduld	Kimberley Reef	conglomerate
2108	MR 1	Springs	Main Reef Leader	conglomerate
2109	FR 1	Sallies	Footwall Reef	conglomerate
2110	VC 1	Sallies	Ventersdorp Contact Reef	conglomerate
2111	EC 1	Sallies	Elsburg Conglomerate	conglomerate

TABLE 2. WEST WITS AREA

polished thin section no.	sample no.	mine property	stratigraphic horizon	material
1940	1 A	West Driefontein	Main Reef	conglomerate
1941	1 B	West Driefontein	Carbon Leader	conglomerate
1942	2 A	West Driefontein	Main Reef	conglomerate
1943	2 B	West Driefontein	Main Reef	conglomerate
1944	3 A	West Driefontein	Carbon Leader	conglomerate
1945	3 B	West Driefontein	Main Reef	conglomerate
1946	3 C	West Driefontein	Main Reef	conglomerate
1947	3 D	West Driefontein	Main Reef	conglomerate
1948	3 D	West Driefontein	Main Reef	conglomerate
1949	4 A	West Driefontein	Main Reef	conglomerate
1950	4 B	West Driefontein	Carbon Leader	conglomerate
1951	5	West Driefontein	Carbon Leader	conglomerate
1952	6 A	West Driefontein	Carbon Leader	conglomerate
1953	6 B	West Driefontein	Carbon Leader	conglomerate
1954	6 C	West Driefontein	Carbon Leader	conglomerate
1955	6 C	West Driefontein	Carbon Leader	conglomerate
1956	7 A	West Driefontein	Carbon Leader	conglomerate
1957	7 A	West Driefontein	Carbon Leader	conglomerate
1958	7 B	West Driefontein	Carbon Leader	conglomerate
1959	8 A	West Driefontein	Main Reef	conglomerate
1960	8 B	West Driefontein	Main Reef	conglomerate
1961	8 B	West Driefontein	Main Reef	conglomerate
1962	9 A	West Driefontein	Carbon Leader	conglomerate
1963	9 A	West Driefontein	Carbon Leader	conglomerate
1964	9 A	West Driefontein	Carbon Leader	conglomerate
1965	9 B	West Driefontein	Main Reef	conglomerate
1966	9 B	West Driefontein	Main Reef	conglomerate
1967	9 B	West Driefontein	Main Reef	conglomerate
2084	A 217	Western Deep levels	Ventersdorp Contact Reef	conglomerate
2085	A 218	Western Deep levels	Carbon Leader	conglomerate
2086	A 219	Western Deep levels	North Leader	conglomerate
2087	A 220	Western Deep levels	Carbon Leader	conglomerate

TABLE 3. ORANGE FREE STATE AREA

polished thin section no.	sample no.	mine property	stratigraphic horizon	material
2052	V 1	Virginia	Basal Reef	conglomerate
2053	V 3	Virginia	Leader Reef	conglomerate
2058	V 2	Virginia	Basal Reef	conglomerate
2059	V 4	Virginia	Leader Reef	conglomerate
2093	A 226	Freddies	Elsburg Reef	conglomerate
2094	A 227	Free State Saaiplaas	Leader Reef	conglomerate
2095	A 228	President Steyn	Intermediate Reef	conglomerate
2096	A 229	President Steyn	'A' Reef	conglomerate
2097	A 230	Free State Saaiplaas	Basal Reef	conglomerate
2098	A 231	President Brand	Basal Reef	conglomerate
2102	FW 1	Freddies	Basal Reef	conglomerate
2103	FW 2	Freddies	Basal Reef	conglomerate
2104	FW 3	Freddies	Basal Reef	conglomerate
2105	FW 4	Freddies	Basal Reef	conglomerate
2106	FW 5	Freddies	Basal Reef	conglomerate
2107	FW 6	Freddies	Basal Reef	conglomerate
2112	FW 7	Freddies	Basal Reef	conglomerate
2113	T 1	Freddies	Basal Reef	conglomerate

TABLE 4. KLERISDORP AREA

polished thin section no.	sample no.	mine property	stratigraphic horizon	material
2032	VR 1	Vaal Reefs	Vaal Reef	conglomerate
2033	VR 2	Vaal Reefs	Vaal Reef	conglomerate
2034	VR 3	Vaal Reefs	Vaal Reef	conglomerate
2035	VR 4	Vaal Reefs	Vaal Reef	conglomerate
2036	VR 6A	Vaal Reefs	Vaal Reef	conglomerate
2037	VR 6B	Vaal Reefs	Vaal Reef	conglomerate
2038	VR 6C	Vaal Reefs	Vaal Reef	conglomerate
2039	VR 5	Vaal Reefs	Vaal Reef	conglomerate
2040	VR 7	Vaal Reefs	Vaal Reef	conglomerate
2041	VR 8	Vaal Reefs	Vaal Reef	conglomerate
2042	VR 9	Vaal Reefs	Vaal Reef	conglomerate
2043	VR 10	Vaal Reefs	Vaal Reef	conglomerate
2044	VR 11	Vaal Reefs	Vaal Reef	conglomerate
2045	VR 12	Vaal Reefs	Vaal Reef	conglomerate
2046	VR 13	Vaal Reefs	Vaal Reef	conglomerate
2047	VR 14	Vaal Reefs	Vaal Reef	conglomerate
2048	VR 15	Vaal Reefs	Vaal Reef	conglomerate
2049	VR 16	Vaal Reefs	Vaal Reef	conglomerate
2050	VR 17	Vaal Reefs	Vaal Reef	conglomerate
2054	VR 20	Vaal Reefs	Vaal Reef	conglomerate
2055	VR 21A	Vaal Reefs	Vaal Reef	conglomerate
2056	VR 21B	Vaal Reefs	Vaal Reef	conglomerate
2057	VR 22	Vaal Reefs	Vaal Reef	conglomerate
2060	VR 19	Vaal Reefs	Vaal Reef	conglomerate
2079	A 212	Western Reefs	Black Reef	conglomerate
2080	A 213	Western Reefs	MB 10 Reef	conglomerate
2082	A 215	Western Reefs	Ada May Reef	conglomerate
2083	A 216	Western Reefs	Ventersdorp Contact Reef	conglomerate
2088	A 221	Western Reefs	Vaal Reef	conglomerate
2089	A 222	Western Reefs	Ventersdorp Contact Reef	conglomerate
2090	A 223	Western Reefs	Elsburg No. 5 Reef	conglomerate
2091	A 224	Western Reefs	Dennys Conglomerate	conglomerate

TABLE 5. DOMINION REEF AREA

polished thin section no.	sample no.	mine property	stratigraphic horizon	material
1997	BR7 N1 A	Dominion Reefs	Dominion Reef	conglomerate
1998	BR7 N1 B	Dominion Reefs	Dominion Reef	conglomerate
1999	BR5 N2 A	Dominion Reefs	Dominion Reef	conglomerate
2000	BR5 N2 B	Dominion Reefs	Dominion Reef	conglomerate
2001	BR7 N2 A	Dominion Reefs	Dominion Reef	conglomerate
2002	BR7 N2 B	Dominion Reefs	Dominion Reef	conglomerate
2003	BR8 N2 A	Dominion Reefs	Dominion Reef	conglomerate
2004	BR8 N2 B	Dominion Reefs	Dominion Reef	conglomerate
2005	UG 9187	Dominion Reefs	Dominion Reef	quartzite
2006	BR8 N5 A	Dominion Reefs	Dominion Reef	conglomerate
2007	BR8 N5 B	Dominion Reefs	Dominion Reef	conglomerate
2008	BR9 52 A	Dominion Reefs	Dominion Reef	conglomerate
2009	BR6 N3 A	Dominion Reefs	Dominion Reef	conglomerate
2010	BR6 N3 A	Dominion Reefs	Dominion Reef	conglomerate
2011	BR10 N2 A	Dominion Reefs	Dominion Reef	conglomerate
2012	BR10 N2 B	Dominion Reefs	Dominion Reef	conglomerate
2013	UG 9184	Dominion Reefs	Dominion Reef	conglomerate
2014	BR8 N6	Dominion Reefs	Dominion Reef	conglomerate
2015	BR8 S2 A	Dominion Reefs	Dominion Reef	conglomerate
2016	BR8 S2 B	Dominion Reefs	Dominion Reef	conglomerate
2017	BR6 N4 A	Dominion Reefs	Dominion Reef	conglomerate
2018	BR6 N4 B	Dominion Reefs	Dominion Reef	conglomerate
2019	BR5 N3 A	Dominion Reefs	Dominion Reef	conglomerate
2020	BR5 N3 B	Dominion Reefs	Dominion Reef	conglomerate
2021	BR 952 B	Dominion Reefs	Dominion Reef	conglomerate
2022	UG 9181	Dominion Reefs	Dominion Reef	quartzite
2024	UG 9183	Dominion Reefs	Dominion Reef	conglomerate
2025	UG 9184	Dominion Reefs	Dominion Reef	conglomerate
2026	UG 9185 A	Dominion Reefs	Dominion Reef	conglomerate
2027	UG 9185 B	Dominion Reefs	Dominion Reef	conglomerate
2028	UG 9186	Dominion Reefs	Dominion Reef	conglomerate
2081	A 214	Afrikander Lease	Afrikander Reef	conglomerate
2101	A 234	Dominion Reefs	Dominion Reef	conglomerate

French Translations

Through this page acknowledgement was made in the April Journal to two members who offered their services in this connection.

The Society has received a third offer of assistance. Mr. J. P. Rees, former Editor of the Journal, has also offered to help with the translations.

The Society applauds the enthusiasm of these members and appeals to other members to assist with translations in German, Rumanian, Dutch and even Russian.

FURTHER MEASUREMENTS OF HEAT FLOW IN SOUTH AFRICA‡

By A. E. Carte and A. I. M. van Rooyen*†

Measurements of heat flow are given for 15 localities in South Africa. The values range from 1,0 to 1,8 μcal/cm² sec. Shield values tend to be lower than those outside the shield.

INTRODUCTION

Additional measurements of earth heat flow have been made in South Africa. Hitherto, practically all such measurements were confined to the goldfields of the Transvaal and Orange Free State or to the southern Karroo (Bullard, 1939; Carte, 1954; Gough, 1963). The observations have now been extended to other parts of the country. This work forms a contribution to the International Upper Mantle Project.

METHODS

The thermal conductivity of rock specimens was measured under pressure in a modified Birch-type of apparatus as used by Gough (1963). The specimens were disks about 6 mm in thickness. Their surfaces were ground parallel and plane to within the limits used by Bullard (1939). Practically all the measurements were made at a mean specimen temperature of 30 °C. The apparatus was calibrated with respect to fused silica and crystalline quartz.

Borehole temperatures were measured by either mercury maximum thermometers or a thermistor probe. In some cases the measurements were made by mining companies, using various types of electronic thermometers.

Accurate temperature measurements were made in one borehole (Roodepoort R57 near Klerksdorp, Transvaal) in 1939 and 1951 (Carte, 1954). These measurements agreed to within a few hundredths of a degree. During 1965, the depth of this hole was increased from almost 1 780 m to more than 3 000 m. Temperatures measured in August, 1966 agreed closely with the earlier measurements. This borehole therefore provides an excellent site for checking instruments for measuring borehole temperatures.

The arithmetic mean conductivity was used in the derivation of heat flow for regions in a borehole where the temperature gradient was constant. When numerous thin layers of different conductivity were encountered, the integrated thermal resistance was used in conjunction with the temperature difference. (Bullard, 1939).

RESULTS

The results of heat flow determinations at fifteen localities are summarized in Table I. Temperature gradients and mean thermal conductivities have been tabulated for regions where the temperature gradient remained constant. Otherwise only heat flow is given.

*National Physical Research Laboratory, C.S.I.R., Pretoria, South Africa.

‡First published in December, 1970 by the Geological Society of South Africa as part of a Symposium on the Upper Mantle Project held in July, 1969 and reprinted here by kind permission of the G.S.S.A.
†Permission to Publish received January, 1971.

TABLE I

Temperature gradients, thermal conductivity and heat flux at 15 localities in South Africa

Locality	Borehole	South latitude	East longitude	Elevation in meters above m.s.l.	Depth range in meters	Main rock types	Mean temperature gradient in °C/km	No. of conductivity samples	Mean conductivity in mcal cm sec °C	Heat flux in mcal.cm² sec
Cape Province										
Springbok	B I.M. 143 Nababeep flat mine	29°34'	17°46'	757	0–1 520	*Granite gneiss,* Nababeep gneiss	18,9	49	7,6	1,44
Springbok	B Z.020S Carolusberg West	29°40'	17°58'	995	0– 660	Nababeep gneiss	17,8	19	7,9	1,41
Sishen	C B.W.I Bishopswood	27°42'	22°53'	1169	240–1 040	Ongeluks lava, agglomerate	—	49	—	1,15
					790–1 040	Ongeluks lava	20,8	13	6,6	1,37
Sishen	C D.I.1 Dingle	27°51'	22°57'	1190	550– 850	*Ongeluks lava,* Ongeluks tillite, quartzite, conglomerate, shale	—	17	—	1,25
Petrusville area	C	30°	24°	—	300– 700	Shale (Ecca)	—	13	—	1,66
Aliwal North	C WE 1 66 Weltevrede	30°43'	26°47	1532	0–1 100	Sandstone, shale, dolerite	17,7	0	6,6	1,17
Swartberg	C SW 1 67 Oakham	30°10'	29°16'	1676	670–1 220	Sandstone, shale, dolerite, siltstone	21,3	53	6,0	1,28
Orange Free State										
Brandfort area	C	28°	26°	—	150– 670	Shale (Ecca)	26,0	15	5,5	1,43
					670–1 580	Shale (Lower Witwatersrand?)	17,7	11	7,6	1,35
Natal										
Bergville	C GSO 1 Hopewell	28°41'	29°23'	1150	310– 640	Sandstone, siltstone, dolerite, shale	31,9	8	5,0	1,60
					670– 850		25,7	6	7,3	1,80
					850–1 040		33,7	5	4,5	1,52
					60–1 040		29,8	33	5,5	1,64
Mtubatuba	C S 1 Somkele	28°21'	32°06'	100	150– 460	Sandstone, shale dolerite	21,2	7	7,1	1,51
					460– 790	sandstone, shale	26,9	10	6,1	1,64
					150– 820			24		1,62
Transvaal										
Potchefstroom	A EIE Leeuwpoort 356.IQ	26°25'	27°30'	1684	1 830–2 740	Ventersdorp lava	13,6	15	8,0	1,09
Rustenburg	A	25°	27°	—	150– 760	Norite, porphyritic-norite	19,3	10	5,4	1,04
					760–1 070	Mesocratic norite, leuco-norite, anorthosite	24,5	9	4,8	1,18
Barberton	A P.C. Shaft New Consort mine	25°41'	31°05'	677	730–1 340	Schist, shale	19,6	11	6,0	1,18
Sokhukune-land	A US9 Umkoanesstad	24°19'	29°54'	832	150– 610	Gabbro	21,2	14	5,3	1,12
Gravelotte	A WS 68 Wiegel shaft	23°54'	30°41'	513	240– 430	Schist and phyllite	10,8	14	10,4	1,12
					430– 600		11,9	12	12,7	1,51

A Archean
B Proterozoic
– Phanerozoic non-orogenic

TABLE 2
Thermal conductivities of various rocks at 30° C

Rock Type	Conductivity in mcal/cm sec °C		No. of Samples	Borehole No. and Locality
	Spread of values	Mean		
Agglomerate	7.8–11.5	9.1	5	B.W.1 Sishen
Anorthosite	3.7– 4.5	4.2	4	U S 9 Umkoanesstad and Rustenburg
Conglomerate		10.6	1	D.1.1 Sishen
Dolerite	10.0–12.1	11.1	4	Brandfort
	8.5–10.0	9.3	6	S.1 Somkele
Dolomite	13.4–10.2	11.4	8	E 1 E Potchefstroom
Gabbro	5.2– 5.4	5.3	6	U S 9 Umkoanesstad
Gneiss	6.0–10.3	7.2	25	FM.143 Springbok
	6.4–10.0	7.9	19	Z. 026 S Springbok
Gneiss, transition		9.2	1	FM143 Springbok
Granite gneiss	6.5– 8.8	7.7	19	FM143 Springbok
Granulite	7.3– 8.0	7.6	4	FM143 Springbok
Lava, Ongeluk	5.1– 9.0	6.5	42	B.W.1 Sishen
	5.5– 7.5	6.5	19	D.1.1 Sishen
Lava, Ventersdorp	6.6– 9.3	7.9	16	E 1 E Potchefstroom
Norite	[illegible]	5.4	2	U S 9 Umkoanesstad
	[illegible]	5.2	20	Rustenburg
Phyllite	8.6–10.9	9.5	12	W S 68 Gravelotte
Pyroxenite	7.0– 7.7	7.3	3	U S 9 Umkoanesstad and Rustenburg
Quartzite, Gamagara	12.5–13.2	12.8	2	D.1.1 Sishen
Sandstone	4.4– 8.4	6.5	19	S W 1/67 Swartberg
	4.3– 9.6	5.6	19	G S O 1 Bergville
	5.9– 7.6	6.7	8	S.1 Somkele
Schist	6.4– 8.6	7.2	4	G S O 1 Bergville
Schist, chloritic	13.4–15.1	14.3	2	W S 68 Gravelotte
Schist, mica	14.0–14.3	14.1	2	W S 68 Gravelotte
Schist, talc carbonate	10.0–15.8	12.5	8	W S 68 Gravelotte
Shale	3.8– 5.8	4.9	13	Petrusville
,,	3.8– 6.6	5.7	10	S W 1/67 Swartberg
,,	3.4– 5.6	4.7	14	G S O 1 Bergville
,,	4.9– 7.1	6.0	7	S.1 Somkele
,, (Lower Wits.)	6.4– 9.2	7.8	12	Brandfort
,, (Ecca)	4.3– 6.6	5.5	15	Brandfort
Siltstone	4.7– 6.9	5.8	22	S W 1/67 Swartberg
Tillite, Ongeluk	6.5– 9.9	8.1	7	D.1.1 Sishen

No rock core was available from the Aliwal North borehole. A weighted mean thermal conductivity was therefore derived from the Swartberg and Brandfort holes. These two holes are not far removed from the Aliwal North hole and have lithological logs similar to it. The derived mean conductivity was the same as the arithmetic mean conductivity of the four Karroo boreholes measured by Gough (1963).

Results from Potchefstroom have been included, even though it lies in the gold fields area, because measurements were made at a greater depth than the earlier ones.

Temperature measurements at Barberton were made in horizontal drill holes at various levels in a mine.

The thermal conductivities of various rocks are listed in Table 2. Most of these rock types have not been measured before. The results in conjunction with average heat flow values may therefore be helpful in the estimation of underground temperatures in places where no measurements have been made. Values for sandstone and shale have also been included even though thermal conductivity data for them have been published earlier. These rocks show great variation from specimen to specimen and many observations are required for meaningful averages.

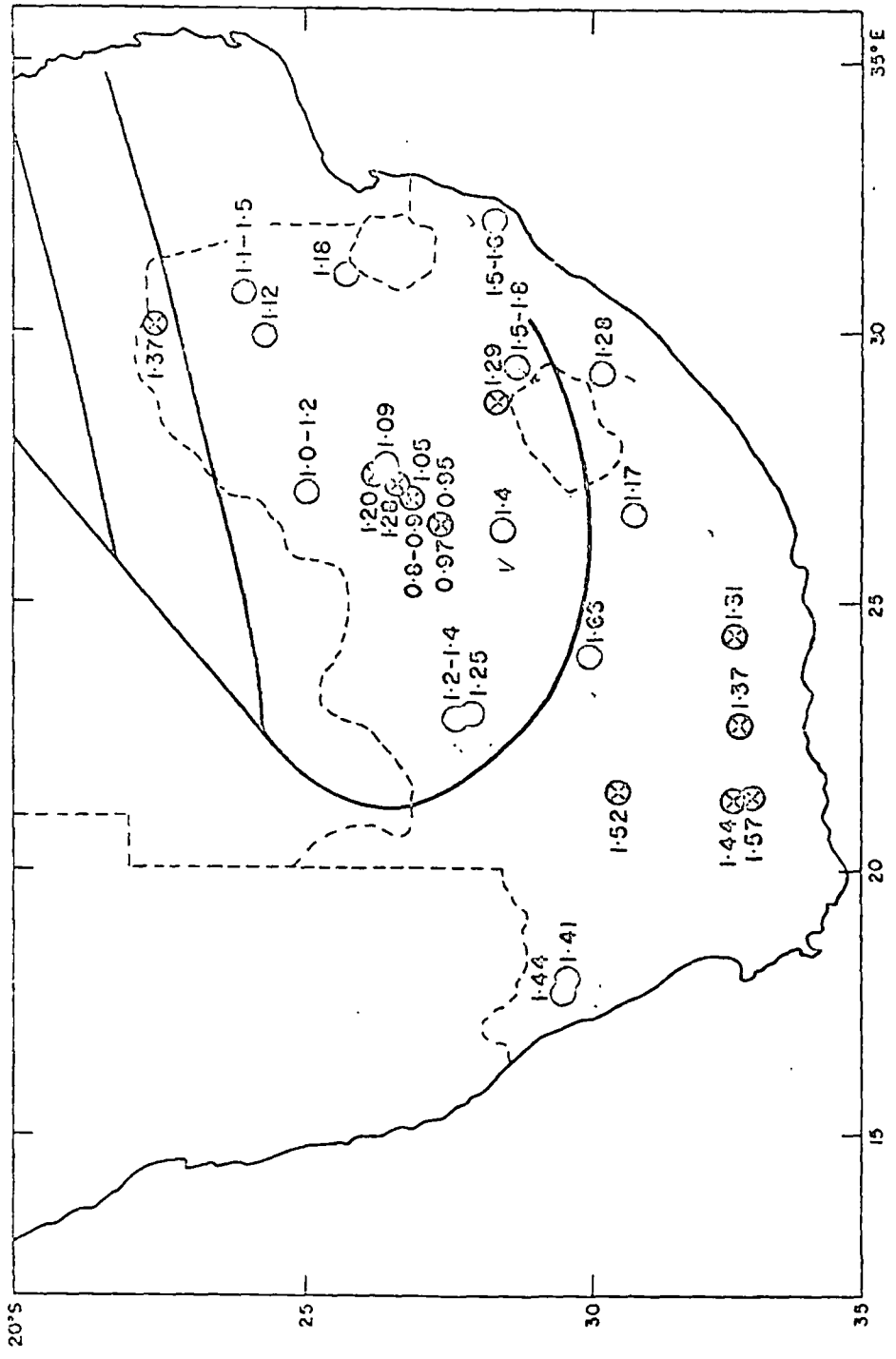
20°S
25
30
35
15
20
25
30
35°E
1·37
1·1–1·5
1·12
1·18
1·5–1·6
1·5–1·8
1·29
1·28
1·0–1·2
1·09
1·20
1·28
0·8–0·9
1·05
0·97
0·95
1·4
1·17
1·63
1·2–1·4
1·25
1·31
1·37
1·52
1·44
1·57
1·44
1·41

Fig. 1

DISCUSSION OF RESULTS

Every borehole has its own peculiarities which include drilling history, topographical situation and local stratigraphy. These will not be discussed in detail here, primarily because in spite of not having taken these differences into account the variation of heat flux with geographical location in South Africa is relatively small. The main limitation in the accuracy of the results is estimated to be determined by inadequate conductivity sampling, even though over 400 rock specimens were measured.

Several of the holes show a trend of increasing vertical heat flux with depth. This is apparent from the results in Table 1 for the holes at Sishen (Bishopswood), Rustenburg and Gravelotte. It also applies to Sishen (Dingle) and Petrusville. In all these cases the trend is consistent with the effects of steeply-dipping bedding planes and differences in thermal conductivity of contiguous layers leading to refraction of the heat.

Heat flow values have been plotted on a map of southern Africa (Figure 1). The solid line encloses the Precambrian shield as given by Vail (1966). This area is 2 600 my or more in age except where crossed by the Limpopo orogenic belt which is 2 000 my. The shield boundaries are not accurately known, particularly the southern boundary.

The lowest heat flow values all lie on the shield. Values for localities off the shield, or close to its indicated boundaries, tend to be higher than those on the shield. The averages are 1,1 for the shield and 1,4 μcal/cm^2 sec for places off the shield if the indicated southern boundary of the shield were moved 160 km northwards. The mean value for the 28 points shown in Figure 1 is 1,28 μcal/cm^2 sec.

ACKNOWLEDGEMENTS

Active help and permission to publish data were given by the following: O'Okiep Copper Company, Limited; Union Corporation Limited; Southern Oil Exploration Corporation (Pty.) Limited; Geological Survey of South Africa; Johannesburg Consolidated Investment Company, Limited; Eastern Transvaal Consolidated Mines, Limited; Consolidated Murchison (Tvl.) Goldfields and Development Company, Ltd.; South African Iron and Steel Industrial Corporation, Limited; Gold Fields of South Africa, Limited. The Rock Mechanics Division of the National Mechanical Engineering Research Institute cut and prepared most of the rock specimens.

This paper is published with the permission of the S.A. National Committee for the Upper Mantle Project.

REFERENCES

BULLARD, E. C., Heat flow in South Africa, Proc. Roy. Soc. London, A, *173*, 474–502, 1939.
CAPE, A. E., Heat flow in the Transvaal and Orange Free State, Proc. Phys. Soc., B, *67*, 664-672, 1954.
GOUGH, D. I., Heat flow in the Southern Karroo, Proc. Roy. Soc., A, *272*, 207–230, 1963.
VAIL, J. R., Distribution of non-orogenic igneous complexes in Southern Africa and their tectonic setting., 11th Ann. Rept. Res. Inst. African Geol., Univ. Leeds, 33–35, 1965/66.

STANDARD ENVELOPE SIZES

Readers will be delighted to know that in another two years there will be substantial uniformity in envelope sizes. The Universal Postal Union has decided that the minimum envelope size will be 90×140 mm. Also a surcharge will be placed on envelopes larger than 120×235 mm. In South Africa, the C6 and DL sizes (114mm×162 mm, and 110mm×220mm) are prescribed for correspondence purposes, and they are the only two sizes in the international standard series to fall within the range of preferred sizes of the Universal Postal Union. These two envelope sizes will accept A4 paper folded into 4, and 3, respectively.

Another long-overdue standardization is that of the size of cheques with a view to eliminating folding for postal transmission. The S.A. Bureau of Standards is still working on this one.

Phil. Trans. R. Soc. Lond. A. 286, 567–583 (1977) [567]
Printed in Great Britain

AREA
S. Africa
W.twat
Uran
Chrono

The geochronology of uraniferous minerals in the Witwatersrand Triad; an interpretation of new and existing U–Pb age data on rocks and minerals from the Dominion Reef, Witwatersrand and Ventersdorp Supergroups

By C. C. Rundle and N. J. Snelling
Institute of Geological Sciences, Geochemistry Division, 64–78 Gray's Inn Road, London WC1X 8NG

Uranium and lead analyses of rock samples from the Witwatersrand, Ventersdorp, and Transvaal supergroups give mainly discordant ages. Samples from the Upper Witwatersrand of the Orange Free State give $^{207}Pb/^{206}Pb$ ages of *ca.* 3000 Ma. These data when considered together with earlier total conglomerate U–Pb analyses from the Dominion Reef Supergroup lead to the conclusion that the uraniferous minerals of the Dominion Reef, Witwatersrand, Ventersdorp and Transvaal conglomerates are 3050 ± 50 Ma old. In the northern parts of the Witwatersrand Basin the parent uraniferous minerals experienced a major reworking at 2040 ± 100 Ma which brought about the partial or complete resetting of the original 3050 Ma age. Radiogenic lead released during this reworking crystallized as galena in veins and fissures which cut across the uraniferous conglomerate horizons. This reworking appears to have had little effect in the Orange Free State to the south. Its age and geographical extent suggest it was caused by thermal effects which accompanied the emplacement of the Bushveld Igneous Complex at 1950 ± 150 Ma.

Samples from the south, which were relatively unaffected by the *ca.* 2040 Ma reworking generally show the effects of recent uranium loss. In the northern part of the basin discordant age patterns characteristic of lead loss have been imposed on uranium–lead systems which were generally reset (partially or completely) by the *ca.* 2040 Ma event.

The presence of 3050 Ma old minerals in sedimentary sequences which are probably younger than *ca.* 2740 Ma suggests the simple interpretation that the uraniferous minerals are predominantly detrital.

1. Introduction

Auriferous and uraniferous quartz–pebble conglomerates occur in the Dominion Reef, Witwatersrand, Ventersdorp and Transvaal Supergroups of South Africa. These weakly metamorphosed sedimentary/volcanic successions rest with marked unconformity on a highly metamorphosed basement complex comprising the Older Granite and the Swaziland Sequence which together constitute an early Precambrian granite–greenstone terrain.

The three lower supergroups are closely related both areally and structurally, they appear to constitute a major geological cycle and have been named the Witwatersrand Triad (Hamilton & Cooke 1960). The maximum total thickness of the triad has been estimated to be about 15000 m of which nearly half is lava (Whiteside 1970).

Three main theories have been advanced to explain the presence of gold and uranium in the conglomerates. These are:

(1) The placer theory, which holds that the gold and uraninite are detrital. The theory was later modified to allow the gold to be dissolved and reprecipitated almost *in situ*.

(2) The hydrothermal theory, which considers that the gold, uraninite and certain other minerals, in particular sulphides, were introduced by hydrothermal solutions.

(3) The precipitation theory, which states that the gold and uranium were precipitated possibly together with pyrite during the deposition of the conglomerates or during subsequent diagenesis.

The main development of gold and uraninite bearing conglomerates occurs in the Upper Witwatersrand. Uraniferous conglomerates also occur in the Basal Sedimentary Formation of the Dominion Reef Supergroup. The Ventersdorp Contact Reef occurs at the base of the Ventersdorp Supergroup and is auriferous and uraniferous where it lies uncomformably on the eroded and bevelled beds of the Witwatersrand rocks. The gold and uraninite are here clearly derived from the underlying Witwatersrand sediments. The Black Reef which occurs in the overlying Transvaal Supergroup is locally auriferous and uraniferous. Here again it is accepted that the gold and other heavy minerals, including uraninite, were derived by the erosion of underlying Witwatersrand conglomerates.

		Area				
		1	2	3	4	5
Supergroup/ Group	Formation	Odendaalsrus–Welkom	Virginia	Klerksdorp	Carletonville	East Rand
Transvaal	Black Reef			212 Black Reef		
Ventersdorp	Contact Reef			216, 222 V.C.R.	217 V.C.R.	
Upper Witwatersrand	Elsburg	226 Elsburg Freddies		223 no. 5 Reef		
	Kimberley	229 'A' Reef		224 Dennys Conglomerate		233 Upper Kimberley
	Bird	228 Intermediate Reef, 231 Basal Reef	227 Leader Reef, 230 Basal Reef	221 Vaal Reef		
	Main				218, 220 Carbon Leader	232 Main Reef Leader

FIGURE 1. Stratigraphic correlations and sample location (1–5 as in figure 2).

The present investigation was made on conglomerates – bankets – from the main conglomerate horizons within the Witwatersrand, Ventersdorp and Transvaal Supergroups (see figures 1 and 2). Age determinations were made on 'total rock' specimens (cf. Nicolaysen, Burger & Liebenberg 1962). Rock for analysis was selected from the interstitial material between the quartz and other pebbles, avoiding as far as possible the inert pebbles. No claim is made that these total rock specimens reflect the bulk composition of the conglomerates. The method of sampling was adopted because microscopic examination shows that uraninite is frequently associated with exsolved, and presumably radiogenic galena, which occurs both as specks within the uraninites and as more completely exsolved rims. Normal mineral separation procedures bring about a mechanical separation of the uraninite and exsolved radiogenic galena (Nicolaysen *et al.* 1962) giving rise to discordant age patterns.

The analyses were made on a suite of conglomerates provided by Dr H. C. M. Whiteside and the analytical data are given in table 1. The specimens are all of typical 'banket' conglomerate composed of quartz and chert pebbles in a fine-grained matrix of quartz, phyllosilicates and opaques. Pyrite is the chief opaque mineral and occurs as allogenic, concretionary

authigenic, and reconstituted authigenic forms (Köppel & Saager 1974). Uraninite occurs as individual rounded grains lying within the quartzitic and sericitic matrix (the detrital form of Liebenberg 1958) and in some specimens is intimately associated with hydrocarbon. Secondary uraninite occurs as specks, patches and veinlets in the matrix and also in the hydrocarbon.

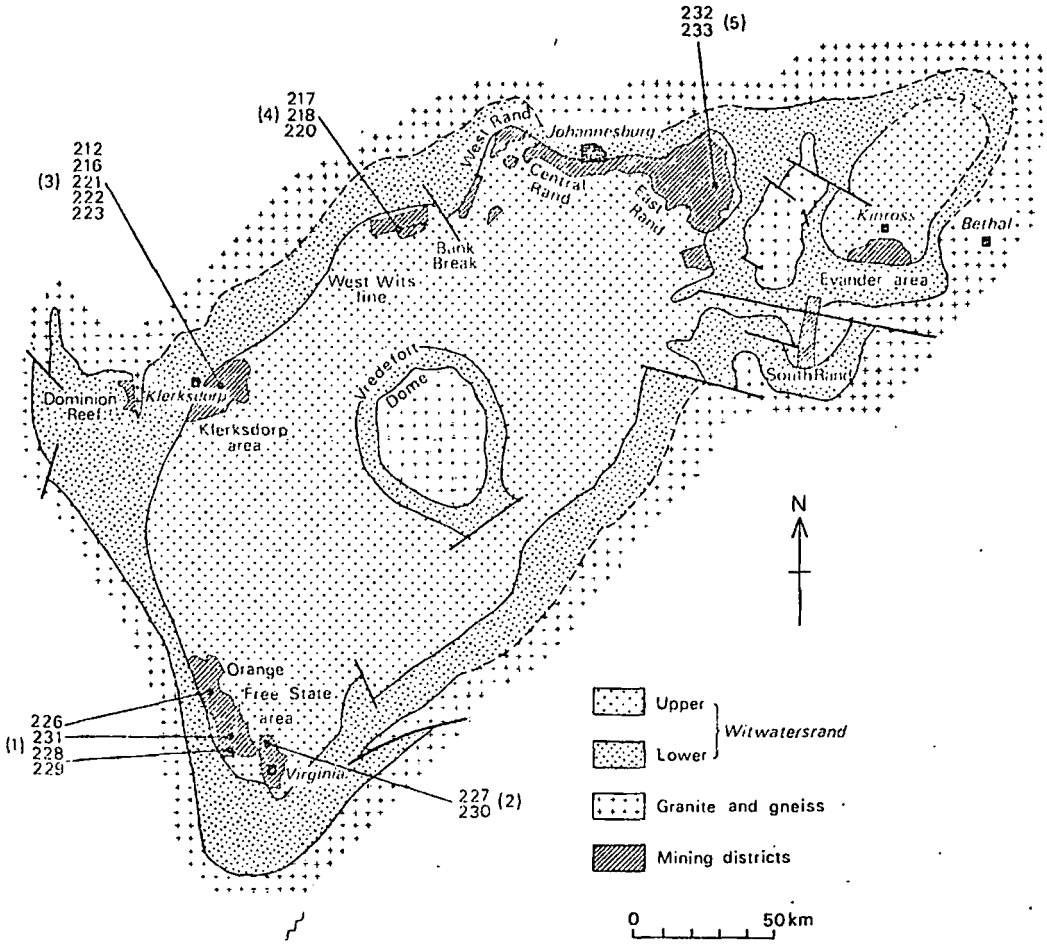

FIGURE 2. Simplified geological map of the Witwatersrand Basin beneath the Ventersdorp and younger cover. Sample locations 1–5 as in figure 1.

2. ANALYTICAL METHODS AND PRECISION

Portions of the matrix, avoiding as far as possible the pebbles, were cut in the form of cubes about 2 cm in size, fragmented in a percussion mortar and finely ground in a Tema swing mill (grain size < 75 μm). The approximate concentrations of U and Pb were then determined by X-ray fluorescence analysis. Samples for analysis were decomposed in a mixture of hydrofluoric and perchloric acids (Aristar grade) and after evaporation to dryness the residues were dissolved and made up to 100 ml in 1.2 M hydrochloric acid. Minute amounts of residue sometimes proved insoluble and consisted of unattacked sample – chromite, rutile and traces of zircon – and crystalline perchlorates which spectrographic analysis showed to be free of uranium and lead.

Appropriate aliquots of the rock solution were taken for lead isotope analysis and for isotope dilution analysis of Pb and U using ^{208}Pb and ^{235}U enriched tracers respectively. Uranium and

lead were separated using ion exchange columns of Dowex 1 × 8 resin, lead was further purified by dithizone extraction, and uranium by precipitation as hydroxide with ammonia gas. The precipitated hydroxides were dissolved and repassed through the ion exchange column and finally iron was extracted with di-isopropyl ether.

Mass spectrometric analyses were made using a Thomson C S F THN 206, 60°, 30 cm radius mass spectrometer. Samples were loaded on a rhenium filament together with silica gel and phosphoric acid. Ion beam intensities were measured from a chart recorder for samples 212, 218, 221, 226, 228, 229, 230 and 231. Subsequently a digital recording system using voltage to frequency conversion became operative.

Lead isotope ratios were monitored throughout the investigation by analysis of the NBS lead isotope standard SRM. 981. The following results were obtained: (1) by chart measuring, $^{206}Pb/^{204}Pb = 16.914 \pm 0.014$, $^{207}Pb/^{204}Pb = 15.445 \pm 0.012$; (2) by digital output, $^{206}Pb/^{204}Pb = 16.946 \pm 0.007$, $^{207}Pb/^{204}Pb = 15.498 \pm 0.008$. Catanzaro, Murphy, Shields & Garner (1968) give the following ratios for this standard: $^{206}Pb/^{204}Pb = 16.937$, $^{207}Pb/^{204}Pb = 15.491$.

Estimates of precision in the determination of uranium, lead and lead isotope ratios have been obtained from replicate data. Pooled standard deviations have been determined as follows:

(1) Uranium: concentration range 39–87 parts/10^6, pooled standard deviation ± 1 part/10^6; concentration range 100–215 parts/10^6, pooled standard deviation ± 2.2 parts/10^6; concentration range 1000–1500 parts/10^6, pooled standard deviation ± 22.2 parts/10^6.

(2) Lead: concentration range 18–28 parts/10^6, pooled standard deviation ± 0.35 part/10^6; concentration range 190–350 parts/10^6, pooled standard deviation ± 1.5 parts/10^6; concentration range 750–1100 parts/10^6, pooled standard deviation ± 4.2 parts/10^6.

The precision is thus generally better than ± 2 % for uranium and ± 1.5 % for lead. Applying these uncertainties to the data, and reducing them by a factor of $N^{-\frac{1}{2}}$ when N replicates have been made, the standard errors on the U/Pb ratios are less than ± 2.2 % with the exception of 223 (± 3.3 %), 217 (± 4.2 % and 224 ± 6 %). For sample 230 which has an extremely low uranium content of 2.78 parts/10^6 the standard error has been calculated using duplicates of 2.77 and 2.79.

Replicate determinations of lead isotope ratios on these samples gave pooled standard deviations as follows: $^{206}Pb/^{204}Pb$ and $^{207}Pb/^{204}Pb < 30$, ± 0.27; $^{206}Pb/^{204}Pb$, and $^{207}Pb/^{204}Pb > 30$, < 60, ± 0.17; $^{206}Pb/^{204}Pb$ and $^{207}Pb/^{204}Pb > 60$, < 300, ± 0.37. These precision estimates are relatively poor compared with those obtained on the NBS standard galena. They presumably reflect additional uncertainty introduced by sampling, chemical processing and blank correction.

Errors in the $^{207}Pb^*/^{235}U$ and $^{206}Pb^*/^{238}U$ ratios have been calculated by combining in the appropriate way the above precision estimates. The common lead correction results in an error enhancement on the lead isotope ratios by a factor of $M/(M-C)$ where M is the measured ratio and C the assumed common lead ratio. Samples 217 and 212 are most strongly effected by this error magnification, and assuming the Rosetta common lead correction the $^{206}Pb/^{204}Pb$ errors are enhanced by a factor of 2.8 and 1.6 respectively and the $^{207}Pb/^{204}Pb$ errors by a factor of 9 and 4.7.

The percentage errors on the ages are less than those on the appropriate D/P ratios by a factor $\dfrac{(D/P)}{(1+D/P)\ln(1+D/P)}$. For a 2000 Ma sample this factor is 0.43 for the $^{207}Pb/^{235}U$ age and 0.86 for the $^{206}Pb/^{238}U$ age. For a 3000 Ma sample the factors are 0.32 and 0.8 respectively.

TABLE 1. NEW U–Pb DATA, TOTAL CONGLOMERATE SAMPLES FROM THE UPPER WITWATERSRAND GROUP, VENTERSDORP CONTACT REEF, AND THE BLACK REEF (TRANSVAAL SUPERGROUP)

	concentration parts/10^6		Pb isotope ratios			calculated ages Ma		
sample	U	Pb	206/204	207/204	208/204	$t^{206}Pb/^{238}U$	$t^{207}Pb/^{235}U$	$t^{207}Pb/^{206}Pb$
212	85.73	82.49	34.64	18.35	40.49	1493 ± 30	2089 ± 40	2738 ± 105
216	246.3	182.5	116.4	32.62	38.03	2506 ± 25	2577 ± 15	2632 ± 25
217	25.48	98.34	22.29	16.45	34.28	2985 ± 105	3046 ± 65	3084 ± 215
218	60.75	25.77	574.4	82.80	56.75	2112 ± 24	2051 ± 15	1998 ± 10
220	513.9	168.0	2686	364.3	96.26	1804 ± 20	1952 ± 15	2110 ± 10
221	1486	778.7	139.9	33.27	40.76	1985 ± 15	2168 ± 10	2344 ± 20
222	319.7	179.8	330.9	74.83	46.82	2434 ± 25	2609 ± 10	2746 ± 25
223	772.4	345.7	274.9	57.61	48.52	1968 ± 55	2250 ± 30	2513 ± 10
224	12.41	16.83	91.82	26.83	64.71	3330 ± 150	2810 ± 60	2453 ± 45
226	39.50	23.00	60.99	21.41	41.73	1497 ± 30	1885 ± 30	2341 ± 65
227	403.3	485.9	61.53	24.33	32.29	2927 ± 25	2904 ± 16	2887 ± 45
228	102.3	187.7	77.80	29.05	49.54	4077 ± 50	3411 ± 20	3038 ± 35
229	216.5	348.7	56.90	23.26	36.32	3441 ± 30	3090 ± 20	2867 ± 50
230	2.78	17.00	52.58	22.94	35.78	8127 ± 20	4416 ± 25	2974 ± 35
231	1051	1070	119.7	37.13	38.37	3211 ± 25	3046 ± 15	2937 ± 35
232	234.8	115.8	539.8	98.35	49.71	2345 ± 30	2403 ± 15	2451 ± 10
233	1063	300.0	948.4	243.2	74.99	1398 ± 25	2251 ± 20	3150 ± 10

Decay constants: $\lambda^{235}U = 0.98485 \times 10^{-9}$ a^{-1}, $\lambda^{238}U = 0.15525 \times 10^{-9}$ a^{-1}.
Common lead correction ratios: $^{206}Pb/^{204}Pb = 12.52$, $^{207}Pb/^{204}Pb = 14.13$, $^{208}Pb/^{204}Pb = 32.35$.

212 Black Reef, Western Reefs mine.
216 Ventersdorp Contact Reef, Western Reefs mine.
217 Ventersdorp Contact Reef, Western Deep Levels mine.
218 Carbon Leader, Western Deep Levels mine, 100–69 2E.
220 Carbon Leader, Western Deep Levels mine, 97/60 Pillar Line (Reef Drive).
221 Vaal Reef, Western Reefs mine.
222 Ventersdorp Contact Reef, Western Reefs mine.
223 Elsburg No. 5 Reef, Western Reefs mine.
224 Dennys Conglomerate, Western Reefs mine.
226 Elsburg Series, Freddies Consolidated mine.
227 Leader Reef, Free State Saaiplaas mine.
228 Intermediate Reef, President Steyn mine.
229 'A' Reef, President Steyn mine.
230 Basal Reef, Free State Saaiplaas mine.
231 Basal Reef, President Brand mine.
232 Main Reef Leader, East Rand area, E. Geduld mine.
233 Kimberley Reef, East Rand area, E. Geduld mine.

3. AGE LIMITS TO THE WITWATERSRAND SUPERGROUP

Early attempts to assign age limits to the Witwatersrand Supergroup have been summarized by Hales (1960). At that time it was clear that some granitic members of the basement complex underlying the Witwatersrand Triad were at least 3000 Ma old. Hales further reported that Rb–Sr whole-rock studies by Schreiner on Dominion Reef acid volcanics indicated an age of about 3000 Ma. Mendelssohn, Burger, Nicolaysen & de Villiers (1958) had previously reported a lead–lead age of 2160 ± 100 Ma on an authigenic monazite from a vein cutting Witwatersrand sediments which was generally accepted as setting a younger limit to the age of the Supergroup.

Nicolaysen *et al.* (1962) made U–Pb determinations on a detrital monazite and total conglomerate from the Dominion Reef conglomerate. Their data are given in table 2. Ages have been recalculated using the most recently determined uranium decay constants (Jaffey *et al.* 1971).

Although the monazite showed a discordant U–Pb age pattern indicative of uranium loss, the lead–lead age of 3120 ± 100 Ma† was accepted as its age of formation, and since the

† See comments by Nicolaysen *et al.* (1962, footnote, p. 18) concerning the interpretation of this age.

monazite is unquestionably detrital it set an older limit to the Dominion Reef Supergroup. This was further confirmed by results on three total conglomerate specimens which contain small, oval uraninites, considered to be detrital in origin, together with various other detrital heavy minerals and subhedral secondary uraninite. One sample gives a virtually concordant age of 3060 ± 70 Ma (B153) while the other two, KCG1 and KCG4, although showing a lead loss discordant age pattern, give $^{207}Pb/^{206}Pb$ ages of 3048 ± 100 Ma and 3018 ± 100 Ma respectively. Although the presence of subhedral uraninites suggests some degree of recrystallization, it is clear that total conglomerate B153 has remained a closed chemical system with respect to both U and Pb. An age of about 3060 ± 70 Ma can thus be accepted as dating an episode or uraninite mineralization in the pre-Dominion Reef basement and sets an older limit to the Dominion Reef and younger deposits.

TABLE 2. U–Pb DATA, DOMINION REEF CONGLOMERATES
(Nicolaysen *et al.* 1962)

	Concentration		Pb isotope ratios			calculated ages/Ma		
sample	% U	% Pb	206/204	207/204	208/204	$t^{206}Pb/^{238}U$	$t^{207}Pb/^{235}U$	$t^{207}Pb/^{206}Pb$
KCG Mon	0.332	0.981	195	58	596	3640 ± 120	3322 ± 120	3120 ± 100
B 153	2.46	1.77	571	142	52.6	3075 ± 100	3059 ± 100	3050 ± 100
KCG 1	0.201	0.112	249	68.3	62.6	2182 ± 110	2654 ± 120	3048 ± 100
KCG 4	0.520	0.350	326	84.7	69.1	2648 ± 110	2862 ± 120	3018 ± 100

KCG 1 Monazite concentrate, Dominion Reef conglomerate, Klerksdorp Consolidated Mines Ltd.
B 153 Total < conglomerate, Upper Reef in the Bramley 6, N3 section of the Dominion Reefs Mine.
KCG 1, KCG 4 Total conglomerate reef from the upper zone, showing supergene alteration, of the Klerksdorp Consolidated Mines Ltd mine.
Ages recalculated according to revised decay constants (Jaffey *et al.* 1971):
$\lambda^{235}U = 0.98485 \times 10^{-9}\ a^{-1}$, $\lambda^{238}U = 0.15525 \times 10^{-9}\ a^{-1}$.
Common lead correction ratios: $^{206}Pb/^{204}Pb = 12.52$, $^{207}Pb/^{204}Pb = 14.13$, $^{208}Pb/^{204}Pb = 32.35$.

In 1964 Allsopp reported whole-rock Rb–Sr determinations on various basement granites from the Western Transvaal. An intensive study was made of the Schweizer Reneke granite which intrudes a complex belt of schists some 320 km southwest of Johannesburg. The granite is overlain unconformably by rocks of the Ventersdorp Supergroup. Allsopp's data gave an isochron corresponding to an age of 2700 ± 55 Ma ($\lambda = 1.39\ 10^{-11}\ a^{-1}$) with an initial $^{87}Sr/^{86}Sr$ ratio of 0.704 ± 0.005. Recalculation of these data, allowing for errors (as quoted by Allsopp) in both coordinates, by the method of Williamson (1968) gives a slightly different result of 2740 ± 20 Ma with an initial $^{87}Sr/^{86}Sr$ ratio of 0.703 ± 0.001. Allsopp also reported apparent ages on a suite of granite samples, some from boreholes and others from small isolated exposures. Ages were calculated assuming an initial $^{87}Sr/^{86}Sr$ ratio of 0.705 and gave results agreeing within experimental error either with the age of the Johannesburg–Pretoria granite (3200 ± 65 Ma, Allsopp 1961, 1964) or the Schweizer Reneke granite. One of the granite samples which gave an apparent age of 2720 ± 100 Ma was overlain by Lower Witwatersrand rocks (borehole sample An952), another sample (borehole RSPIC) gave an apparent age of 2820 ± 55 Ma and was overlain by sediments of the Dominion Reef. However, Allsopp considered it likely that sample RSPIC had suffered chemical alteration, since it occurred only 0.9 m beneath the Dominion Reef contact. Although not absolutely conclusive, these data strongly indicate that the Witwatersrand Triad is younger than *ca.* 2740 Ma. The Ventersdorp rocks certainly are,

and there is no reason to believe that the episode of granite intrusion dated at 2740 ± 20 Ma occurred after the deposition of the Witwatersrand sediments and before the formation of the Ventersdorp rocks. The apparent age of An 952 (2720 ± 100 Ma) accords with this view but it must be admitted that an age calculated assuming an initial $^{87}Sr/^{86}Sr$ ratio must be viewed with caution.

More recently van Niekerk & Burger (1964, 1969*a*, *b*) have reported lead–lead and uranium lead ages on lavas from the Dominion Reef and Ventersdorp Supergroups so providing both lower and upper limits to the time of deposition of the Witwatersrand Supergroup. They quoted ages of 2800 ± 109 Ma and 2300 ± 80 Ma respectively. Only lead–lead data are available for the Dominion Reef lavas; regression of these data weighted according to the quoted errors, and calculation of the age using the most recently determined uranium decay constants, gives a somewhat younger age of 2725 ± 75 Ma. Similar treatment of the Ventersdorp lavas gives an age of 2290 ± 85 Ma. Two zircons from these lavas give discordant age patterns indicative of uranium loss and yield a concordia intersection age of 2285 ± 50 Ma, identical within error limits with the aforementioned lead–lead age.

The age of the Schweizer Reneke granite and the Dominion Reef lavas cannot be resolved, suggesting that the unroofing of the granite and subsequent deposition of the Dominion Reef sediments and lavas occurred in a relatively short time. This is compatible with the observations that the Dominion Reef rocks were deposited on an uneven floor suggesting that there was insufficient time for a peneplain surface to develop.

The younger limit to the age of the Witwatersrand deposits is thus set by the Ventersdorp age determination of 2290 ± 85 Ma. For the older limit we suggest it is appropriate to adopt the weighted mean age of the Schweizer Reneke granite and the Dominion Reef lavas, namely 2740 ± 19 Ma.

4. Previous research on the U–Pb geochronology of the Witwatersrand

The results of previous U–Pb age determination studies on uraninite and thucholites mainly from the Witwatersrand sediments by Louw (1954) and Horne & Davidson (1955) have been summarized and discussed by Holmes & Cahen (1957). The data, plotted on a concordia diagram are shown in figure 3. The concordia diagram has been constructed, and ages calculated using the recently revised uranium decay constants. Rosetta lead has been used for the common lead correction. However, if it is assumed that the ages reflect a major rejuvenation at about 2040 Ma (see below) then a more radiogenic common lead correction will be appropriate. Any lead incorporated in the rejuvenated uraninites would, at that time, have an isotopic composition comparable to that of the extracted lead. This lead has a variable isotopic composition and defines a secondary isochron reflecting mixing of entirely radiogenic lead with original *ca.* 3000 Ma old common lead (Burger, Nicolaysen & de Villiers 1962). We have accordingly adopted one of the most radiogenic of these leads, namely NPRL No. 163, $^{206}Pb/^{204}Pb = 23.32$, $^{207}Pb/^{204}Pb = 18.21$; for the alternative common lead correction and the appropriate data points are indicated by vertical crosses (see comments below, §5).

The calculated ages are in the main discordant and in some cases affected by uncertainties concerning the common lead correction. However, Holmes & Cahen (1957) and later Burger *et al.* (1962) considered that three samples yielded concordant or nearly concordant ages which

were not too dependent on assumption concerning the common lead correction and which 'appear to have started their history 2040 ± 100 million years ago' (Burger *et al.* 1962). The greatest age was given by a sample from the Dominion Reef ($^{207}Pb/^{206}Pb$ age = 2760 Ma) with the remaining samples giving $^{207}Pb/^{206}Pb$ ages in the range *ca.* 2000 Ma to 2540 Ma. Holmes & Cahen (1957) proposed two hypotheses to explain the age patterns. The first implied that the uraninites were of two distinct generations, the oldest having an age in excess of 2760 Ma and the youngest being about 2000 Ma old. The second considered that all the uraniferous minerals were of the same age as the Dominion Reef uraninite and hence older than 2760 Ma. Concerning the cause of the discordant ages Holmes & Cahen were particularly impressed with the number of $^{206}Pb/^{238}U$ ages in the 1200 Ma to 1400 Ma range and suggested an important reworking causing lead loss at this time.

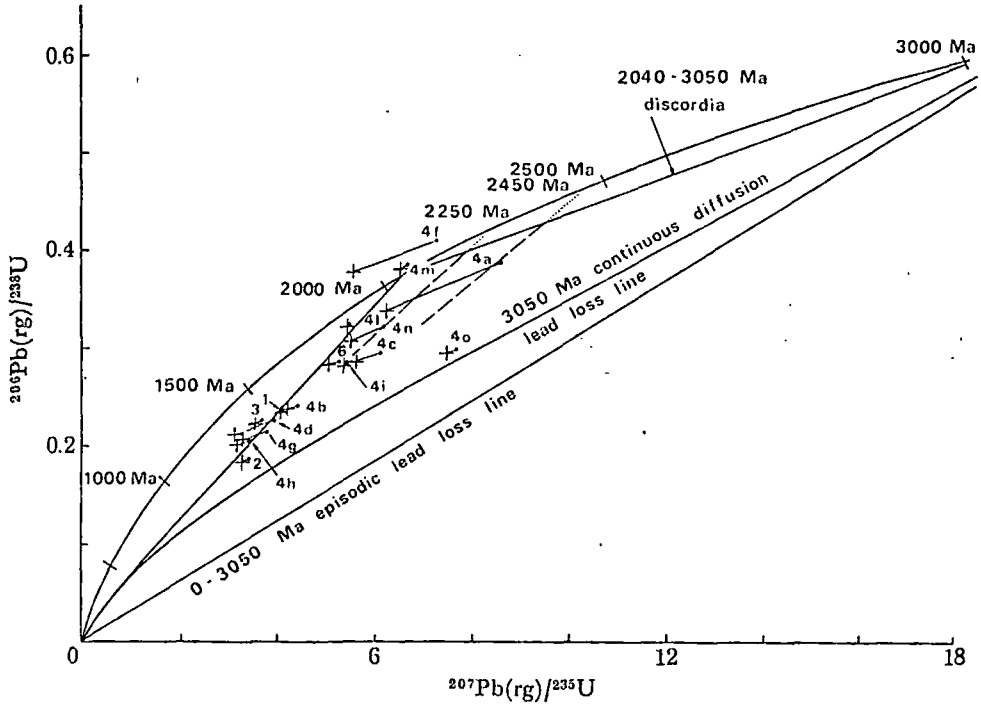

FIGURE 3. Concordia diagram showing data points for previous uraninite and thucholite U–Pb age determinations. Sample numbers refer to Holmes & Cahen (1957), Table 1, suite V11 (sample V11, 1 uses lead isotope data H. 1).

From consideration of the distribution of the data points on a concordia diagram, Wetherill (1956) suggested that the Witwatersrand uraninites and thucholites 'were formed 2040 ± 50 million years ago and suffered loss of lead because of some alteration or leaching process 200 ± 150 million years ago'. Wetherill further noted certain minor regularities which, if real, could be interpreted as two additional groups of minerals having true ages of 2250 Ma and 2450 Ma which had also experienced lead loss at *ca.* 200 Ma. Wetherill had interpreted the data solely on the basis of episodic lead loss. Nicolaysen (1957), however, had previously shown that the characteristic lead-loss pattern of discordant ages could equally arise from continuous loss of lead by solid diffusion. When plotted on concordia the lead loss by diffusion trajectory for a *ca.* 2040 Ma sample hardly differs over much of its length from the discordia

chord resulting from episodic lead loss at 200 Ma (Tilton 1960). In the present case the distinction is somewhat irrelevant, lead loss is clearly indicated and could equally reflect continuous diffusion or episodic loss related to the thermal disturbances which may have been associated with the widespread Karroo volcanism. Before further consideration of this earlier U:Pb data it is appropriate to review the findings of Burger *et al.* (1962) concerning the isotopic composition of lead from galenas from the Witwatersrand and Orange Free State, which led to the formulation of their hypothesis concerning the evolution of the Witwatersrand uraninites, and also to consider the new data obtained during this investigation.

Burger *et al.* noted not only the strongly radiogenic nature of the lead in galenas occurring in veins cutting the uraniferous conglomerates of the Witwatersrand and Dominion Reef, but also the fact that many of them displayed regular linear relations when plotted on a $^{207}Pb/^{204}Pb$ against $^{206}Pb/^{204}Pb$ diagram, and that the lines so defined passed through or close to the isotopic composition of lead from the Rosetta Mine galena. This is one of the least radiogenic terrestrial leads and occurs in rocks equivalent to those underlying the Witwatersrand deposits. The linear relations (metachrons or secondary isochrons) of the Witwatersrand, Dominion Reef and Rosetta galenas imply that they have evolved by the mixing of Rosetta type lead with radiogenic lead resulting from uranium decay. Burger *et al.* summarize the evolution of these galenas as follows:

(1) At some time in the past, an original or 'parent' uraninite was present in a particular region. The time of crystallization of the parent uraninite is denoted t_s.

(2) The uraninite was associated with varying amounts of a primary lead. Isotopically the Rosetta lead is, as indicated above, an appropriate primary lead.

(3) In parts of this region uraninite crystals were subjected to a sudden chemical alteration at time t_m. Some lead was separated from the parent uraninite ores. This lead would consist of radiogenic lead formed between t_s and t_m, together with some primary or common lead originally present in the uraniferous minerals.

Burger *et al.* show that if the alteration at time t_m affects a series of uraninite ores with different U/Pb ratios the separated lead will have different but linearly related isotopic ratios, and will define a metachron or secondary isochron.

The major postulate made by Burger *et al.* was to identify the parent uraninite with the oval and spherical uraninite grains present in the Witwatersrand conglomerates and considered by many works to be of detrital origin. They showed that these uraninites were at least 2550 million years old (this limit becomes 2602 Ma using new decay constants and the recalculated metachron slope; see below) and noted the apparent discrepancy between this minimum age and the conclusion reached by other workers, namely that certain of the Witwatersrand uraninites appeared to have started their present chemical history about 2040 Ma ago.

Faced with this dilemma they proposed that a parent uraninite may undergo a solid-state chemical alteration such that lead is selectively removed from the crystal, and that the oval and spherical Witwatersrand uraninites had undergone such a rejuvenation about 2040 million years ago. They noted Liebenberg's observation (1958) that lead occurs as small veinlets and specks of galena in the uraninite while other uraninites are surrounded by thin rims of more completely exsolved galena, and suggested that with complete mobilization this exsolved lead is deposited as galena in veins cross-cutting the uraniferous conglomerate horizons. Thus at about 2040 Ma parts of the Witwatersrand Basin experienced a thermal event of sufficient intensity to locally mobilize lead present both as a trace component in the

Witwatersrand detrital sulphide, and that generated over the preceding 1000 Ma in the uraninites and thucholites. This lead was mixed and deposited as galena in minor cross-cutting quartz veins. The great majority of these veins are entirely barren of uranium, gold or sulphides, and only carry sulphides, including galena, where they cut or lie within the mineralized conglomerates.

In more recent time further mobilization of both uranium and lead has occurred, as is testified by the presence of secondary uranium minerals in mine workings, and three-stage galenas (Burger *et al.* 1962, section VI (*b*)).

We would note that the new uranium decay constants, some new analyses of galenas from cross-cutting quartz veins (Köppel & Saager 1974) and refinements in the method of calculating regression lines necessitate slight modifications to the original treatment of the metachrons. Following Köppel & Saager (1974) the original galena isotopic data given by Burger *et al.* have been corrected on the basis of the measurements of the U.S. Geological Survey lead standard reported by them, and by Catanzaro *et al.* (1968). These modified data have been regressed following the method of Williamson (1968). Samples 33, 34 and 35 of Burger *et al.* (1962) have been excluded from the regression of the Witwatersrand galenas since we agree with Köppel & Saager (1974) that they may represent three-stage leads. Two additional galena samples analysed by Köppel & Saager (1974) have been included. The Witwatersrand main trend and the Dominion Reef galenas give metachrons or secondary isochrons of slopes 0.386 ± 0.003 and 0.413 ± 016 respectively. At the two-sigma level there is no significant difference between these metachrons. Their weighted mean, however, is strongly influenced by the high precision of the Witwatersrand metachron which largely reflects the high precision of Köppel & Saager's measurements on two extremely radiogenic samples. We accordingly think it more realistic to take an unweighted mean of the two slopes, namely 0.399 ± 0.019. Adopting 2040 Ma as the age of rejuvenation the metachron equation gives the age of the parent uraniferous mineral phases as 3065 ± 100 Ma, somewhat older than the age of 2980 ± 100 Ma (= 2911 Ma using revised decay constants) originally proposed by Burger *et al.* 1962).†

5. The significance of new total rock U–Pb analyses

The new analytical data are given in table 1. Ages have been calculated using the isotopic composition of lead from the Rosetta galena for the common lead correction.

The ages fall into two groups, one composed of samples yielding $^{207}Pb/^{206}Pb$ ages of *ca.* 3000 Ma, namely 217, 227, 228, 229, 230, 231 and 233, while the second gives younger ages. Two of the *ca.* 3000 Ma samples, 217 and 227, give concordant ages of 3029 ± 55 Ma 2921 ± 13 Ma respectively. Of the remaining samples in this group, 228, 229, 230 and 231 show a typical uranium loss pattern of ages while sample 233 shows a lead loss pattern. We would suggest that a first approximation to the age of the *ca.* 3000 Ma samples is given by regression of their 207/204 against 206/204 ratios (figure 4). The regression applies the appropriate pooled standard deviation to each ratio, and yields a best-fit line of 2945 ± 40 Ma. Sample 233 was excluded

† Slope of metachron or secondary isochron

$$= \frac{\exp(\lambda 235 t_s) - \exp(\lambda 235 t_m)}{137.8\,[\exp(\lambda 238 t_s) - \exp(\lambda 238 t_m)]}$$

where $\lambda 235$ and $\lambda 238$ are the decay constants for ^{235}U and ^{238}U respectively, and t_s and t_m are as defined in the text.

from the regression because its extremely high ratios dominate the calculation. The Rosetta lead fits this line within limits of error so providing independent justification for the use of this lead for the common lead correction. The mean square of weighted deviates (hereafter m.s.w.d., Brooks, Hart & Wendt 1972) is high (about 4), indicating that the scatter of data points about the best-fit line is greater than can be accounted for by experimental error alone. The inclusion of 233 in the regression gives a significantly greater age of 3090 ± 30 Ma with no improvement of the fit of data points about the line.

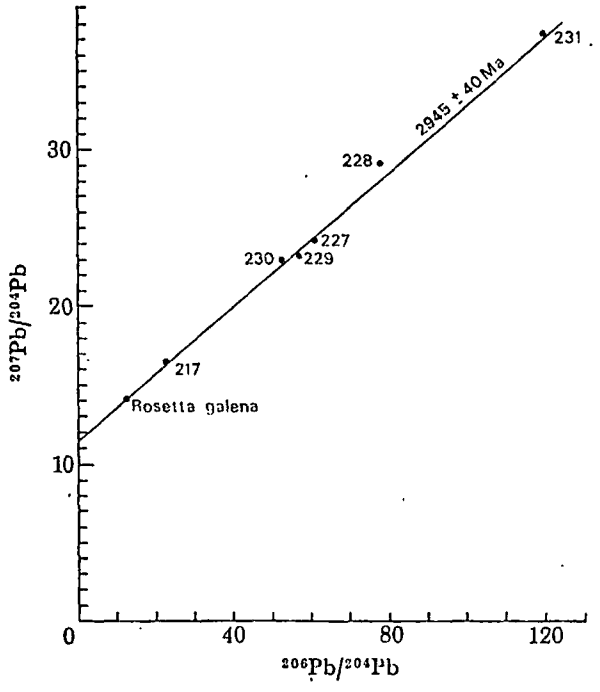

FIGURE 4. $^{207}Pb/^{204}Pb$ against $^{206}Pb/^{204}Pb$ plot for Upper Witwatersrand and Ventersdorp Contact Reef samples giving lead/lead ages of *ca.* 3000 Ma.

This *ca.* 3000 Ma-old suite of samples includes total conglomerates from both the Upper Witwatersrand and Ventersdorp Contact Reef. The age immediately suggests an affinity with the uraniferous minerals of the Dominion Reef and it is pertinent to plot the Dominion Reef total conglomerate and monazite data (Nicolaysen *et al.* 1962) on concordia together with the *ca.* 3000 Ma Witwatersrand and Ventersdorp samples (figure 5). It will be seen that total conglomerate samples 233, KCG1, KCG4, 217, B153, 228, 230, and detrital monazite KCG M give a good linear array. The best-fit line through these points gives a slope of 0.0329 ± 0.0007, and an intercept of − 0.0262 ± 0.0111. The m.s.w.d. is only 0.4, indicating that all scatter of points about the line can be accounted for by experimental error alone and the line intersects concordia at 3050 ± 50 Ma. Thus all these samples can be regarded as having been derived from parent rocks containing 3050 ± 50 Ma uranium bearing minerals, some have experienced recent lead loss (233, KCG1 and KCG4), others recent uranium loss (KCG M, 228 and 230), while others have remained closed systems with respect to U and Pb and yield concordant ages not significantly different from 3050 ± 50 Ma (217, 3029 ± 55 Ma and B153, 3061 ± 25 Ma).

It might be argued that the inclusion of sample 230, which has extremely high 206*/238 and 207*/235 ratios, has a dominant effect on the regression calculation. However, it can be

shown that exclusion of this sample has no significant effect on the calculation and results in a 3060 ± 50 Ma intersection of the regression line with concordia, an effectively zero intercept, and an identical m.s.w.d.

Samples 227, 231 and 229 lie appreciably to the left of this line and their inclusion in the regression calculation, although giving a similar chord/concordia intersection of 2975 ± 60 Ma results in a significantly higher m.s.w.d. of 3.4. Thus scatter of these data points about the best-fit line is greater than can be accounted for by experimental errors alone, indicating that samples 227, 231 and 229 have experienced geochemical disturbance in addition to recent lead or uranium loss.

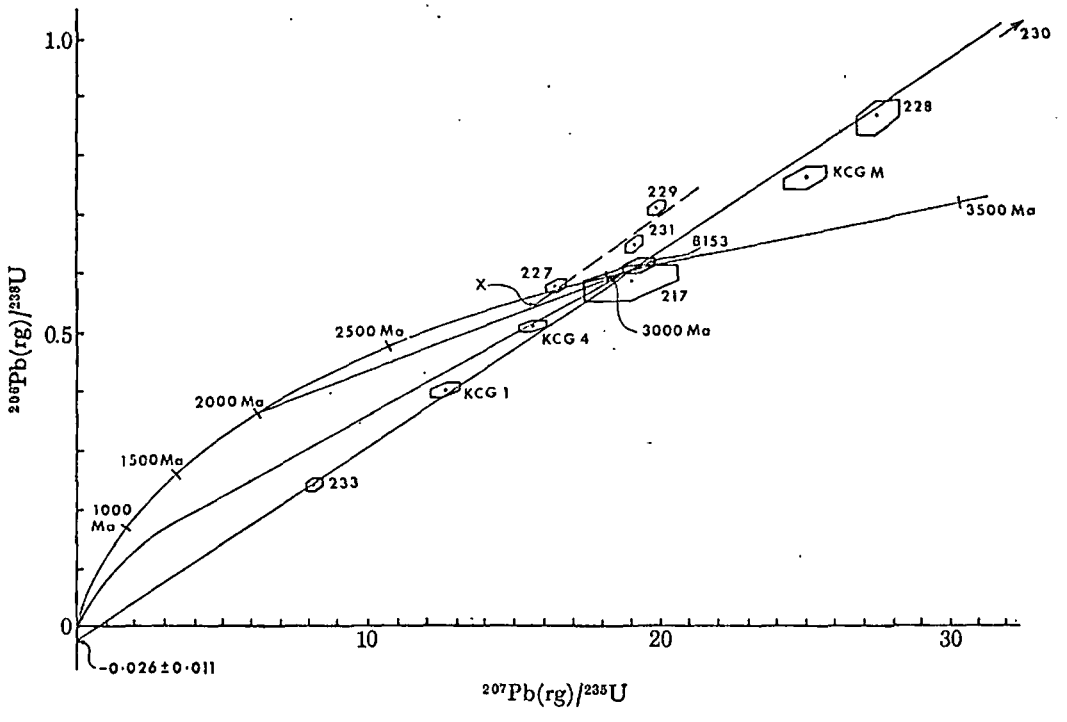

FIGURE 5. Concordia plot of *ca.* 3000 Ma-old samples from the Dominion Reef, Witwatersrand and Ventersdorp Supergroups. Sample 230 cannot be shown.

We suggest that this disturbance can be correlated with the 2040 Ma reworking proposed by Burger *et al.* (1962). Lead loss from rock samples occurring at this time would cause their data points to migrate along a chord between 3050 Ma and 2040 Ma. Two samples analysed in the course of this investigation (216 and 232, figure 6) in fact plot on the 3050 Ma/2040 Ma chord within limits of error and it will be noted that the use of a more radiogenic common lead correction merely displaces the data points along the chord. This effect is to be expected since the radiogenic common lead is one of the galenas from the Witwatersrand metachron. Burger *et al.* (1962) postulated that this lead was extracted at *ca.* 2040 Ma from a *ca.* 3000 Ma parent uraninite. If this postulate is correct then the use of the isotopic composition of any galena which plots on the Witwatersrand metachron as a 'radiogenic' common lead correction, is bound to move the respective data points along a trajectory parallel to the 2040 Ma/3050 Ma discordia. Sample 218 (figure 6) is virtually concordant irrespective of the common lead correction with a weighted mean of ^{206}Pb/^{238}U and ^{207}Pb/^{235}U ages of 2065 ± 13 Ma. This does not differ

significantly from the reworking age of 2040 ± 100 Ma, proposed by Burger *et al.* and it is clear that sample 218 experienced rejuvenation and virtually complete lead loss at this time.

Samples 227, 229 and 231 which we have shown to lie significantly to the left of the extension of the zero to 3050 Ma chord, thus show the effect of recent uranium loss imposed on slight lead loss at 2040 Ma, i.e. lead loss at 2040 Ma moved the data points a little way along the 3050 Ma/2040 Ma chord to about a point *X*, figure 5, and recent uranium loss caused the data points to move off the 2040 Ma/3050 Ma chord along trajectories away from zero and across concordia. Such a trajectory is indicated by a dashed line in figure 5. It will be observed that recent uranium loss from sample 227 was just sufficient for the datum point to come to rest on concordia and the sample provides a possibly unique case of accidental concordance.

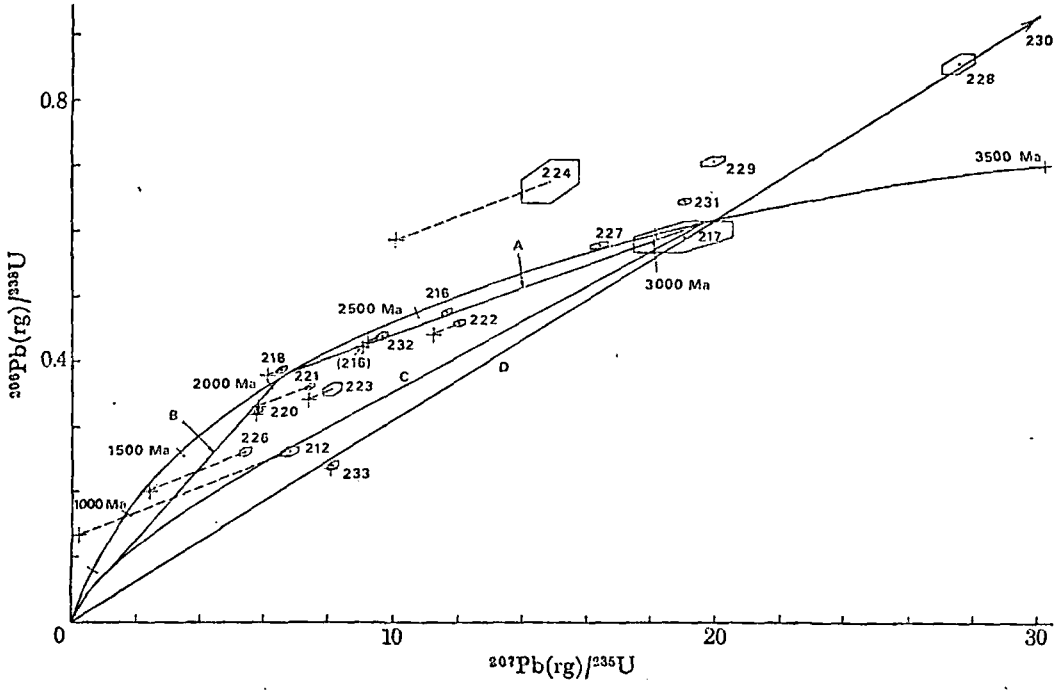

FIGURE 6. Concordia plot of 'total conglomerates' from the Witwatersrand, Ventersdorp and Transvaal Supergroups. Line A, *ca.* 3050 Ma/2050 Ma discordia; line B, *ca.* 2050 Ma lead loss by continuous diffusion trajectory; line C, *ca.* 3050 Ma lead loss by continuous diffusion trajectory; line D, recent episodic lead loss trajectory from *ca.* 3050 Ma sample.

These results provide a striking confirmation of the hypothesis first advanced by Burger *et al.* (1962) concerning the evolution of uraniferous minerals in the Witwatersrand Supergroup which predicts an age of the parent uranium minerals of 3065 ± 100 Ma, virtually identical with the estimate of 3050 ± 50 Ma derived above. The results carry the implication that the uraniferous conglomerates of the Dominion Reef, Witwatersrand and Ventersdorp Supergroups contain a common suite of parent uraniferous minerals. The age of 3050 ± 50 Ma for this parental suite is significantly older than the older limit to the deposition of the Witwatersrand sediments (2740 ± 19 Ma) and implies that the uraniferous minerals are detrital in origin.

With the exception of sample 224 the remaining samples (212, 220, 221, 222, 223 and 226) when plotted on the concordia diagram (figure 6) all fall within the triangular area bounded by the 2040 Ma/3050 Ma, zero/2040 Ma, and zero/3050 Ma chords. We suggest that these samples originally contained 3050 Ma-old uranium minerals which suffered variable lead loss

in response to the 2040 Ma reworking such that their data points were distributed along the 2040 Ma/3050 Ma chord. Subsequent lead loss, either episodic or by continuous diffusion, would then cause the data points to migrate into the triangular region defined above. It is not possible to decide which lead loss process was operative. Thus sample 220 must have experienced virtually complete resetting at 2040 Ma and now plots on the 2040 Ma lead loss by continuous diffusion trajectory. However, over most of its course this trajectory does not differ from the 200 Ma/2040 Ma episodic lead loss chord. Similarly, although the discordant age pattern of sample 212 is completely explicable in terms of lead loss by continuous diffusion from a 3050 Ma parent (it plots on the 3050 Ma continuous diffusion trajectory), it could equally reflect partial resetting in response to the 2040 Ma reworking involving about 50 % lead loss at that time, with further lead loss in response to a more recent (*ca.* 200 Ma) disturbance.

Sample 224 plots above concordia and gives a uranium loss discordant age pattern. We consider that this reflects a similar history to that experienced by samples 227, 229 and 231. In this case considerable lead loss ($\approx$ 50 %) from a 3050 Ma parent occurred in response to the 2040 Ma reworking moving the data point about half way down the 2040 Ma/3050 Ma chord. Recent uranium loss then caused the point to move away from the origin, and across concordia to its present position.

It is now appropriate to reconsider the early uraninite/thucholite U–Pb age determinations in the light of the above considerations. Wetherill (1956) had observed that most of the determinations when plotted on concordia fell on or close to a 200 Ma/2040 Ma chord indicating episodic lead loss at 200 ± 150 Ma from a 2040 Ma parent (see figure 3). Over most of its length the 200 Ma/2040 Ma chord hardly differs from the 2040 Ma lead loss by continuous diffusion trajectory so that the discordant age patterns of samples 1, 2, 3, 4*b*, 4*g*, 4*h* and 4*l* can be equally well explained in terms of episodic lead loss at 200 Ma or lead loss by continuous diffusion since 2040 Ma. Sample 4*f* plots above concordia and its age pattern can be explained in terms of recent uranium loss effecting a 2040 Ma parent. All these samples could have evolved from 3050 Ma old parent uraninites which experienced virtually complete resetting at 2040 Ma.

Of the remaining samples, 4*a*, 4*c*, 4*i*, 4*n* and 6 are considered to have had an original age of 3050 Ma but experienced only partial lead loss in response to the 2040 Ma resetting event such that they plotted on the 2040 Ma/3050 Ma chord. Subsequent lead loss, either in response to a more recent resetting event (200 ± 150 Ma?), or by continuous diffusion, caused the data points to migrate into the triangular area bounded by the 2040 Ma/3050 Ma, zero/2040 Ma, and zero/3050 Ma chords along trajectories indicated by dashed lines in figure 3. It is the extension of these trajectories across the 2040 Ma/3050 Ma chord on to concordia (indicated by dotted lines in figure 3) which led Wetherill (1956) to suggest the existence of *ca.* 2250 Ma and *ca.* 2450 Ma parent uraninites. There is clearly no need to postulate the existence of uraninites of these ages.

Sample 4*o* is from the Dominion Reef Supergroup and plots within error limits on the 3050 Ma lead loss by continuous diffusion trajectory. Nicolaysen *et al.* (1962) had previously noted that the discordant age pattern of this particular specimen could be explained solely in terms of such lead loss and showed that the true age of the uraninite would be about 3040 Ma.

6. Some conclusions

Total rock U–Pb analyses on samples from the Witwatersrand Ventersdorp and Transvaal Supergroups, together with earlier data reported by Nicolaysen *et al.* (1962) from the Dominion Reef Supergroup show that the uraniferous minerals in the conglomerates constitute a 3050 ± 50 Ma-old system. This system experienced a major reworking at 2040 ± 100 Ma which varied in intensity, but locally resulted in a complete resetting of U:Pb ages to *ca.* 2040 Ma in both uraninites and total rock. Radiogenic lead released during this reworking crystallized as galena in veins and fissures which cut across the uraniferous conglomerates. Isotopically these leads define a metachron or secondary isochron the slope of which is fully consistent with a *ca.* 2040 Ma reworking extracting lead from a *ca.* 3050 Ma parent uraniferous mineral.

Subsequent loss of lead or uranium has produced a plethora of discordant ages. In some cases it appears most likely that the lead and uranium loss occurred in very recent time and that the lead loss was episodic rather than by continuous diffusion. In other cases lead loss by continuous diffusion is possible, but there remains no objective way of distinguishing between lead loss by continuous diffusion from a 3050 Ma uraniferous parent mineral, and lead loss by either continuous diffusion or episodic loss from a 3050 Ma parent mineral which had previously undergone partial resetting in response to the *ca.* 2040 Ma reworking. Many of the separated uraninites analysed by the earlier workers show evidence of virtually complete resetting at *ca.* 2040 Ma. Their lead loss age patterns, however, can be interpreted either in terms of an episodic loss at 200 ± 150 Ma, a resetting event that can be correlated with the Karroo volcanism, or by continuous diffusion since 2040 Ma.

There is considerable indication of an areal control to the discordant age patterns. Thus samples from the Upper Witwatersrand to the south in the Orange Free State (regions 1 and 2 of figure 2, the Odendaalsrus–Welkom–Virginia area) show little effects of the 2040 Ma reworking, evidence of recent uranium loss, and no evidence of recent lead loss (see figure 5).

Total conglomerates from the Dominion Reef in the Klerksdorp area analysed by Nicolaysen *et al.* (1962) are either concordant (B153) or show evidence of an episodic recent lead loss, but, like the samples from the Orange Free State area, show little if any effects of the 2040 Ma reworking. A separated uraninite from the Dominion Reef gives a discordant age pattern which can be interpreted solely in terms of continuous lead loss from a *ca.* 3050 Ma parent. A separated detrital monazite shows evidence of recent uranium loss (see figure 5).

With the exception of sample 233 (E. Rand, E. Geduld Mine) and possible 212 (Basal Reef, Western Reefs Mine) the remaining total conglomerates analysed in this work all show very strong effects of the *ca.* 2040 Ma reworking (figure 6). These samples are all from the Klerksdorp, Carletonville, and E. Rand areas. Sample 233 gives a discordant age pattern unaffected by the *ca.* 2040 Ma reworking. Sample 212 comes from the Black Reef in the Transvaal System and plots on the 3025 Ma lead loss by continuous diffusion trajectory. As pointed out above, however, the discordant age pattern could equally well be due to recent episodic lead loss from a 3050 Ma parent which had previously been partially reset at 2040 Ma.

Sample 224, a strongly sheared rock from the Dennys conglomerate in the Western Reefs mine shows the effects of recent uranium loss following the 2040 Ma reworking. Samples 218, 216, and 232 have remained closed chemical systems with respect to uranium and lead since the 2040 Ma reworking, while the remaining samples, namely 220 221, 222, 223 and 226 have all experienced lead loss since the 2040 Ma reworking.

The problem of the correlation of the 2040 Ma old reworking of the Witwatersrand uraninites with a specific geological thermal event was fully discussed by Nicolaysen *et al.* (1962). They were unable to come to a definite conclusion, however, because of the uncertainty concerning the age of the Ventersdorp volcanism. It is now clear that the reworking of the uraninites at *ca.* 2040 Ma occurred after the Ventersdorp volcanism. We suggest that the occurrence of galenas, rich in radiogenic lead which plot on the Witwatersrand metachron, in cross-cutting veins in the Black Reef implies that the *ca.* 2040 Ma reworking is of late or post Transvaal age. This thermal event could thus be correlated with volcanic manifestations in the Transvaal Supergroup and the emplacement of the Bushveld Complex dated at 1950 ± 150 Ma, as suggested by van Niekerk & Burger (1964). In this connection we would note that all the analysed total rocks which show the effect of *ca.* 2040 Ma reworking come from the northern parts of the Witwatersrand Basin, i.e. the nearest to the Bushveld Complex.

The presence of 3050 ± 50 Ma-old uraniferous minerals in the Dominion Reef and Witwatersrand sediments which we have argued must have been deposited after about 2740 ± 19 Ma, carries with it the simple implication that the uraniferous minerals (originally mainly uraninite) are of detrital origin.

It might be argued that some of the uranium in the Witwatersrand sediments was deposited from solution either at the time of sedimentation or during diagenesis. Such uranium–lead systems would plot on concordia at about 2550 Ma but would mix with the older detrital component to generate a chord between 2550 Ma and 3050 Ma. We see no evidence of such a chord. It must be remembered, however, that most of the analysed samples have been affected to some extent by the 2040 Ma rejuvenation, and by subsequent loss of lead or recent loss of uranium. It would be virtually impossible to distinguish between disturbed detrital systems and disturbed systems with both detrital and authigenic components. The data presented here can be interpreted entirely in terms of a 3050 Ma old U–Pb system; the earlier work on separated uraninites and thucholites and on galenas fully supports this interpretation. We would suggest that authigenic mineralization has made at the most only a minor contribution to the total uranium in the Witwatersrand Basin.

We are indebted to our colleagues for their help and encouragement. We would in particular thank Dr S. H. U. Bowie at whose suggestion the work was undertaken, Dr I. G. Swainbank for much advice and help with the analytical work, and Mr R. D. Beckinsale for stimulating discussion which contributed greatly to the interpretation of the discordant ages advanced here. The analysed samples were generously provided by Dr H. C. M. Whiteside.

The investigations reported in this paper form part of the research programme of the Institute of Geological Sciences and are published with the permission of the Director.

References (Rundle & Snelling)

Allsopp, H. L. 1961 Rb–Sr age measurements on total rock and separated-mineral fractions from the Old Granite of the Central Transvaal. *J. geophys. Res.* **66**, 1499–1508.

Allsopp, H. L. 1964 Rubidium–strontium ages from the Western Transvaal. *Nature, Lond.* **204**, 361–363.

Brooks, C., Hart, S. R. & Wendt, J. 1972 Realistic use of two-error regression treatments as applied to rubidium–strontium data. *Rev. Geophys. Space Phys.* **10**, 551–557.

Burger, A. J., Nicolaysen, L. O. & de Villiers, J. W. L. 1962 Lead isotopic composition of galenas from the Witwatersrand and Orange Free State, and their relation to the Witwatersrand and Dominion Reef uraninites. *Geochim. cosmochim. Acta.* **26**, 25–59.

Catanzaro, E. J., Murphy, T. J., Shields, W. R. & Garner, E. L. 1968 Absolute isotopic abundance ratios of common, equal-atom and radiogenic lead isotopic standards. (*U.S.*) *Natl. Bur. Standards J., A. Phys. Chem.* **72A**, 261–267.

Hales, A. L. 1960 Research at the Bernard Price Institute of Geophysical Research, University of Witwatersrand, Johannesburg. *Proc. R. Soc. Lond.* A **258**, 1–26.

Hamilton, G. N. G. & Cooke, H. B. S. 1960 *Geology for South African students*, 4th edition. Johannesburg: Central News Agency.

Holmes, A. & Cahen, L. 1957 Géochronologie africaine 1956. *Mem. Acd. Sci. colon., Cl. Sci. nat. med.* 8°, **5**, 169.

Horne, J. E. T. & Davidson, C. F. 1955 The age of the mineralization of the Witwatersrand. *Bull. Geol. Surv. Gt. Brit.* **10**, 58–73.

Jaffey, A. H., Flynn, K. E., Glendenin, L. E., Bentley, W. C. & Essling, A. M. 1971 Precision measurements on half-lives and specific activities of ^{235}U and ^{238}U. *Phys. Rev. Ser. C* **4**, 1889–1906.

Köppel, V. H. & Saager, R. 1974 Lead isotope evidence on the detrital origin of Witwatersrand pyrites and its bearing on the provenance of the Witwatersrand gold. *Econ. Geol.* **69**, 318–336.

Liebenberg, W. R. 1958 The mode of occurrence and theory of origin of the uranium minerals and gold in the Witwatersrand ores. *Proceedings of the Second International Conference on the Peaceful Uses of Atomic Energy, Geneva*, 1958, vol. **2**, pp. 379–387. New York: United Nations.

Louw, J. D. 1954 Geological age determinations on Witwatersrand uraninites using the lead isotope method (with appendix by F. W. E. Strelow). *Trans. Geol. Soc. S. Afr.* **57**, 209–230.

Mendelssohn, E., Burger, A. J., Nicolaysen, L. O. & de Villiers, J. W. L. 1958 Age of monazite crystals from the Sub-Nigel Mine, Witwatersrand. *Abstr. Ann. Congress Geol. Soc. S. Africa.*

Nicolaysen, L. O. 1957 Solid diffusion in radioactive minerals and the measurement of absolute age. *Geochim. cosmochim. Acta*, **11**, 41–59.

Nicolaysen, L. O., Burger, A. J. & Liebenberg, W. R. 1962 Evidence of the extreme age of certain minerals from the Dominion Reef conglomerates and the underlying granite in the Western Transvaal. *Geochim. Cosmochim. Acta* **26**, 15–23.

Tilton, G. R. 1960 Volume diffusion as a mechanism for discordant lead ages. *J. geophys. Res.* **65**, 2933–2945.

van Niekerk, C. B. & Burger, A. J. 1964 The age of the Ventersdorp System. *Ann. geol. Surv. S. Africa* **3**, 75–86.

van Niekerk, C. B. & Burger, A. J. 1969*a* Lead isotopic data relating to the age of the Dominion Reef lava. *Trans. geol. Soc. S. Africa* **72**, 37–45.

van Niekerk, C. B. & Burger, A. J. 1969*b* The uranium–lead isotopic dating of South African acid lavas. *Bull. Volcanologique* **32**, 481–498.

Wetherill, G. W. 1956 An interpretation of the Rhodesia and Witwatersrand age patterns. *Geochim. comochim. Acta* **9**, 290–292.

Whiteside, H. C. M. 1970 Volcanic rocks of the Witwatersrand Triad. In *African magmatism and tectonics* (eds T. N. Clifford & I. G. Gass). Edinburgh: Oliver and Boyd.

Williamson, J. H. 1968 Least-squares fitting of a straight line. *Can. J. Phys.* **46**, 1845–1847.

Phil. Trans. R. Soc. Lond. A. 286, 527–548 (1977) [527]
Printed in Great Britain

Uranium mineralization of the Witwatersrand and Dominion Reef systems

By P. R. Simpson and J. F. W. Bowles
Institute of Geological Sciences, Geochemical Division, 64–78 Gray's Inn Road, London WC1X 8NG

[Plates 1–10]

Preface

The problem of the origin of the mineralization of the Witwatersrand and Dominion Reef has been one of the great controversies of the past 50 years. Any new attempt to solve it requires the application of the most up-to-date mineralogical techniques including the combined use of ore microscopy with electron microprobe analysis, radioisotope and stable isotope determinations, fission-track studies of uranium distribution, and detailed analysis of fluid inclusions. All these skills have been brought to bear in the work described in this and the two papers following, and although unequivocable results have not yet been obtained, important new information on the bimodal nature of the uranium mineralization has been established.

The significance of this study, which illustrates the application of techniques that will become more commonplace as the 21st century approaches, lies in providing essential information on the origin of uranium in quartz pebble conglomerates. More than 35 % of known uranium reserves occur in such rocks, particularly in Canada and South Africa but also, as recently reported, in Algeria. Previously many geologists have held that uranium can only be enriched to economic grades in Precambrian rocks if anoxygenic atmospheric conditions prevailed at the time of sedimentation. However, the remarkable similarity between the sub-economic concentrations of thorian uraninite in the present-day Indus Valley and that of the Dominion Reef and Witwatersrand System as well as other evidence invalidates any such concept.

Further work is required to complete the story of the Witwatersrand mineralization and it is hoped that multidisciplinary investigations will continue. The full resolution of the genesis of the mineralization could result in new discoveries that are essential to the availability of uranium for future energy needs.

S. H. U. Bowie, F.R.S.

Uranium-bearing minerals in the Witwatersrand and Dominion Reef sediments have been studied by ore microscopic, electron microprobe, fission track and neutron activation analytical methods to determine the controls of uranium mineralization. In the Dominion Reef, which represents a high-energy banket type of depositional environment, allogenic thorian uraninite occurs in hydraulic equivalence with allogenic pyrite, quartz and possibly also gold in the sediments which have uranium–thorium ratios between 3.1 and 5.6 indicating substantial amounts of thorium-rich resistate minerals.

The Witwatersrand sediments have uranium–thorium ratios ranging between 7.1 and 19.6 indicating lesser amounts of resistates which is consistent with the lower-energy depositional environment. The proximal or nearshore deposits are of banket type but are distinguished from the Dominion Reef by the abundance of concretionary pyrite formed within the Basin and the presence of carbonaceous matter. The distal

deposits formed at greater distance from the shoreline contain decaying organic material which has precipitated both uranium and gold from solution. Subsequent metamorphism has resulted in the formation of carbonaceous material bearing finely disseminated low-thorium pitchblende and a fine dissemination of gold associated with sulphides and arsenides.

Further evidence of the existence of uranium in solution is to be found in the banket deposits. In this case fine disseminations of uranium (> 500 parts/10^6) occur in clay minerals within concretionary pyrite nodules and in lenticles formed of clay minerals in Witwatersrand banket deposits. They represent reduction-deposition of the soluble uranyl ion below the sediment–water interface where conditions are reducing.

Allogenic thorian uraninite from the present-day Indus river has a texture, composition and association with gold and pyrite similar to allogenic uraninite in the Witwatersrand and Dominion Reef System. Thorian uraninite is a stable phase over large distances in this river. Hence it would appear quite unnecessary to postulate a reducing atmosphere for the transportation of detrital uraninite. Moreover the retention of sulphate and uranyl ions in solution in the model proposed here suggests that the atmosphere was oxidizing at the time of deposition. This conclusion indicates the likely occurrence in younger sediments of mineralization of this type provided the necessary geological criteria are met.

Introduction

Uranium mineralization in the Witwatersrand and Dominion Reef sediments is presently and has been, since its discovery by Cooper in 1923, the subject of debate and speculation as to its origin.

Mineralization has been described variously as the product of hydrothermal processes by Graton (1930) and sedimentary processes by Ramdohr (1958) and others. The detrital hypothesis for the origin of uraninite has been taken to account for all primary mineralization in the Basin by some workers. This idea has been further developed to the point where a reducing atmosphere was invoked as an essential prerequisite to the transportation of detrital uraninite grains (Liebenberg 1955; Grandstaff 1975). This has led to the notion that uraniferous conglomerates are thereby restricted by these atmospheric conditions to the Archaean or early Proterozoic (Robertson 1974).

The purpose of this study is to re-evaluate the uranium mineralization using mineralogical methods since the implications of the earlier work for the further discovery of uraniferous conglomerates would appear to be unduly restrictive.

All specimens available to the authors were sectioned for study to obtain as broad a view of the principal types of mineralization as possible, though it is appreciated that the coverage of this Basin is by no means as complete as could be wished. The outline geology, principal mining areas, and section numbers of specimens studied, are shown in figures 1 and 2.

In pursuing this investigation, two questions have been uppermost in our minds: firstly, does the formation of these and similar deposits elsewhere require a reducing atmosphere, or merely reducing conditions of deposition beneath the sediment/water interface; and secondly, what are the respective rôles of uranium as detrital grains of uraninite and as uranyl ions in solution. Answers to these two questions will have considerable relevance to the understanding of the mode of formation and estimating the potential for new discoveries of this type of mineralization.

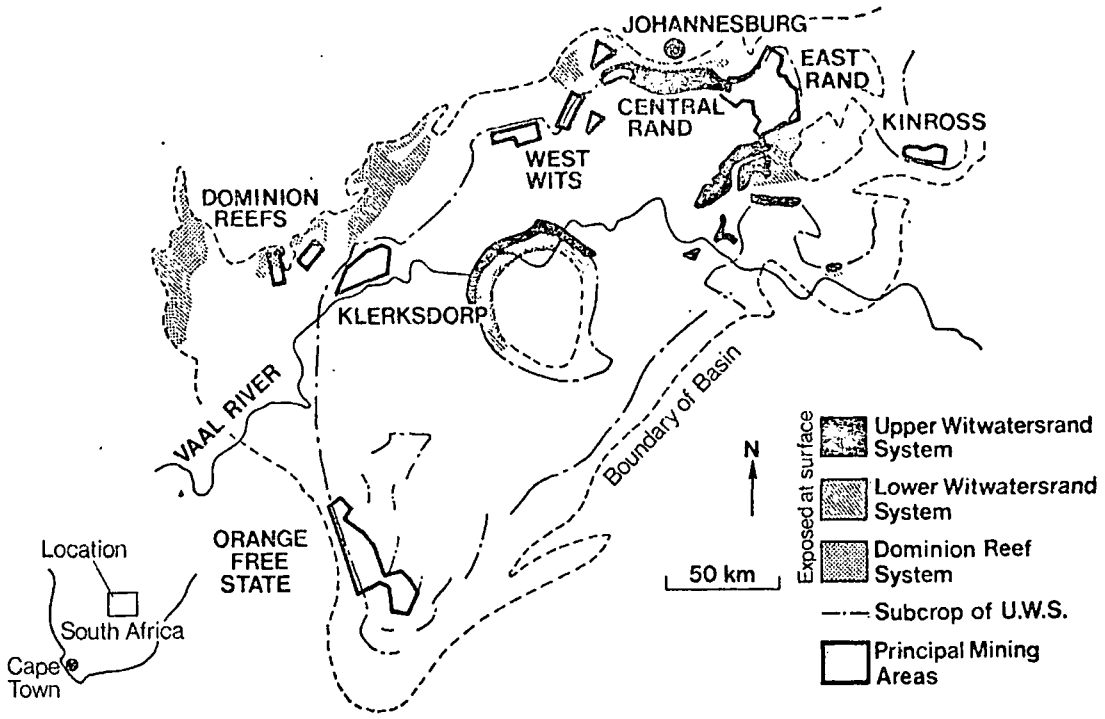

FIGURE 1. Map of the Witwatersrand Basin illustrating sub-Ventersdorp geology and showing principal mining areas.

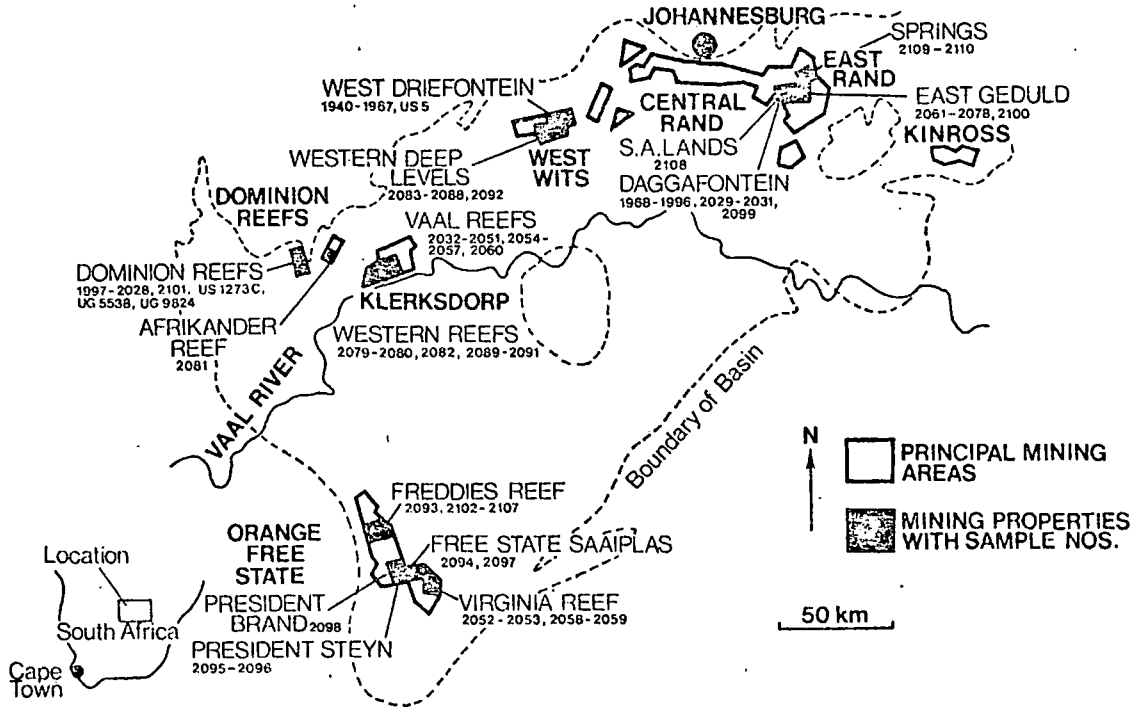

FIGURE 2. Map of the Witwatersrand Basin illustrating principal mining areas and sample localities. The numbers in small print refer to polished thin sections. Polished sections from the reference collection are prefixed (UG, US).

Experimental methods

The details of the complex mineralization and the distribution of uranium were elucidated by ore microscopy, electron probe microanalysis and fission track registration. The techniques of the first have been recently described by Bowie, Simpson & Atkin (1975) and the last is discussed below in the section on uranium micromapping.

The electron probe analyses were undertaken with a Cambridge Microscan-5 instrument fitted with a Canberra energy dispersive analytical system. The latter was used for the analysis of Ti, Mn, Fe, Pb, Th, U and Y, whilst Ca and Ce were analysed simultaneously by the Bragg spectrometers of the microprobe. X-rays from each specimen were counted for 250 s at a low beam current of 1×10^{-9} A, which conditions were suitable for both analytical systems. Data were reduced by a PDP11 computer, which calculates concentrations of the elements present at one analytical point while the next is being analysed. This technique enables an analysis for nine elements to be produced every 4 to 5 min. Pure metals were used as standards for Mn, Fe, Th and U, a rare-earth glass REE-3, kindly provided by the University of Oregon (Drake & Weill 1972) for Ca, Y and Ce, and chemically analysed rutile and galena for Ti and Pb respectively. The analytical methods for wavelength-dispersive analysis described by Bowles (1975) were used for Ca and Ce. In another paper, Bowles (in preparation) describes the quantitative analytical programme for the energy-dispersive equipment and compares selected results with those obtained with the Bragg spectrometers. The results are closely comparable for all elements with the exception of uranium for which the energy-dispersive results are consistently 3 % lower than the Bragg spectrometer results. Investigation has shown that as between the pure metal and the oxide there is a change in the ratio of the $L\alpha_1$ to $L\alpha_2$ intensities. The lower resolution of the energy-dispersive equipment records both X-ray emissions as a single peak, so that a variation in the ratio does not affect the results. The analyses presented here for uranium and thorium are those obtained using the energy-dispersive equipment. The measured concentrations were corrected using the quantitative correction programme devised by Mason, Frost & Reed (1969).

Mineralogical evidence

Pyrite

Pyrite is the principal opaque mineral of the Witwatersrand and Dominion Reef Systems. In hand specimen rounded grains of pyrite, commonly known as 'buckshot' (Feather & Koen 1975), display clearly defined sedimentary features with well-developed bedding and cross-bedding in layers also containing sand-sized grains of quartz. In the pebble-size conglomerate, pyrite occurs as a discrete disseminated phase together with other sand-sized constituents, principally quartz, in the matrix. Radioactivity is closely associated with pyritic zones in the hand specimen and those were therefore selected for more detailed investigation. Indeed, the presence of pyrite in the hand specimen is one of the clearest indications of the likely presence of anomalous radioactivity in the suite of specimens studied.

Ramdohr (1958), Saager (1970) and Köppel & Saager (1974), distinguished three types of pyrite in the Witwatersrand ore: I, allogenic; II, concretionary authigenic; and III, reconstituted authigenic. Type I pyrite has rounded and abraded outlines; it is completely fresh, is uniformly compact and homogeneous, and has a distinctive range of inclusions (figure 3*a*,

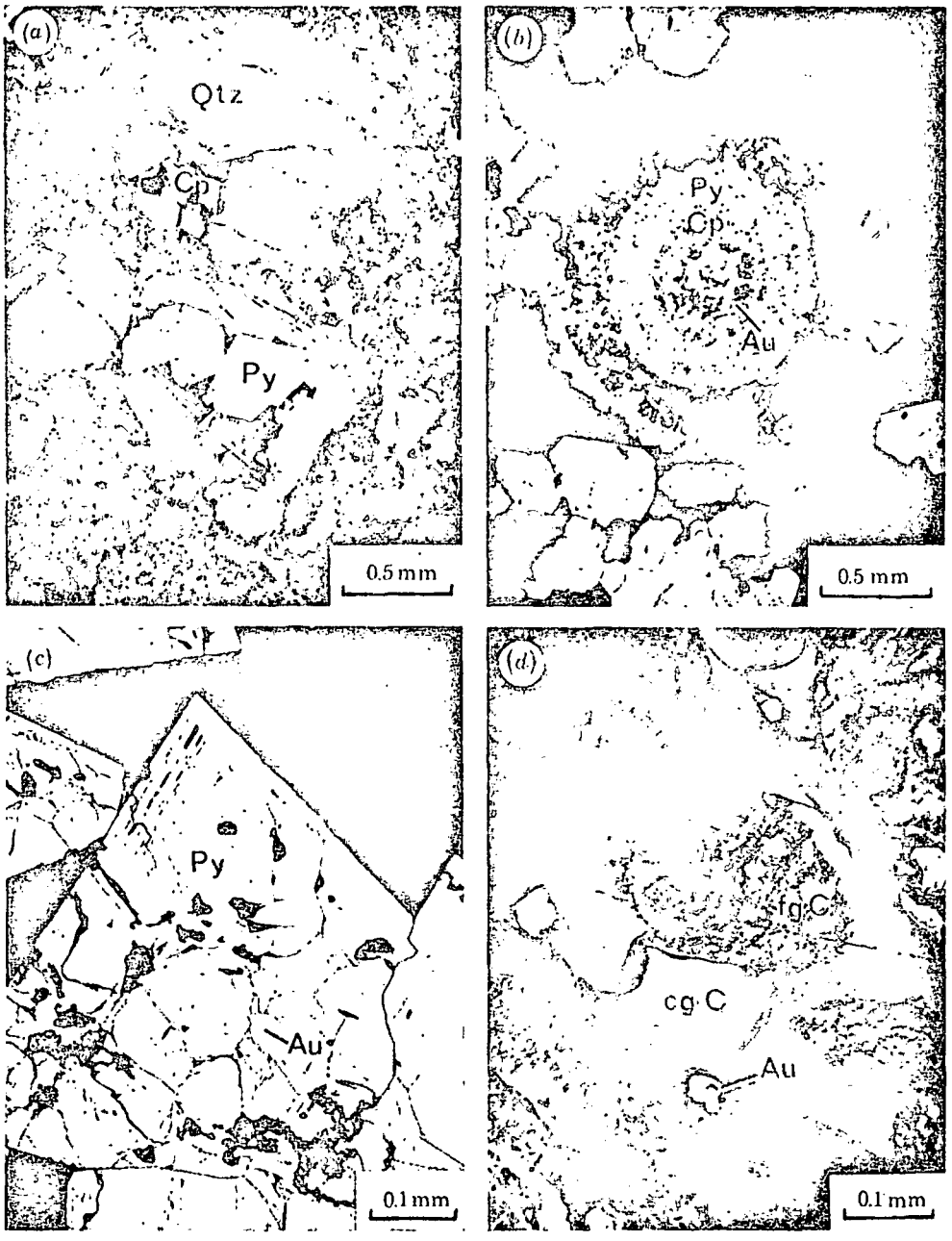

FIGURE 3 (*a*) Banket ore sample showing allogenic pyrite (Py), chalcopyrite (Cp) and quartz (Qtz); Dominion Reef, (US1273C), reflected light, air.

(*b*) Concretionary pyrite of spherical type composed of alternate layers of pyrite (Py) and chalcopyrite (Cp) with a grain of gold (Au). Silicates occur in the body of the concretion and particularly in the rim, as well as in the porous matrix (black). West Driefontein, West Wits (PTS 1966), reflected light, oil.

(*c*) Authigenic reconstituted pyrite (Py) containing gold (Au). West Driefontein, West Wits, (PTS 1958), reflected light, oil.

(*d*) Carbonaceous matter showing coarse (cgC) and fine-grained (fgC) carbon, with gold (Au). Carbon Leader, West Wits (US 5), reflected light, oil.

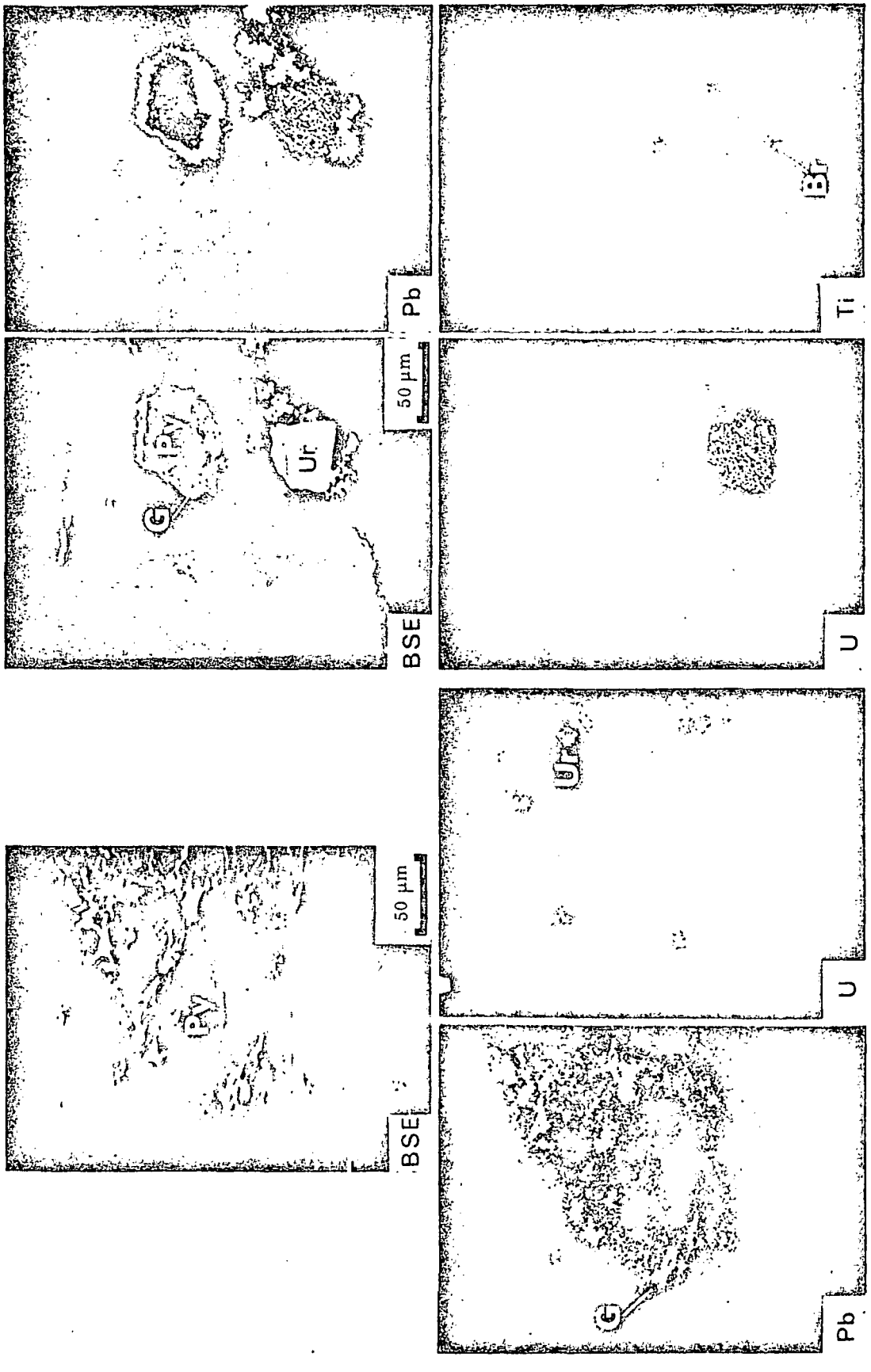

FIGURES 4 AND 5. For description see opposite.

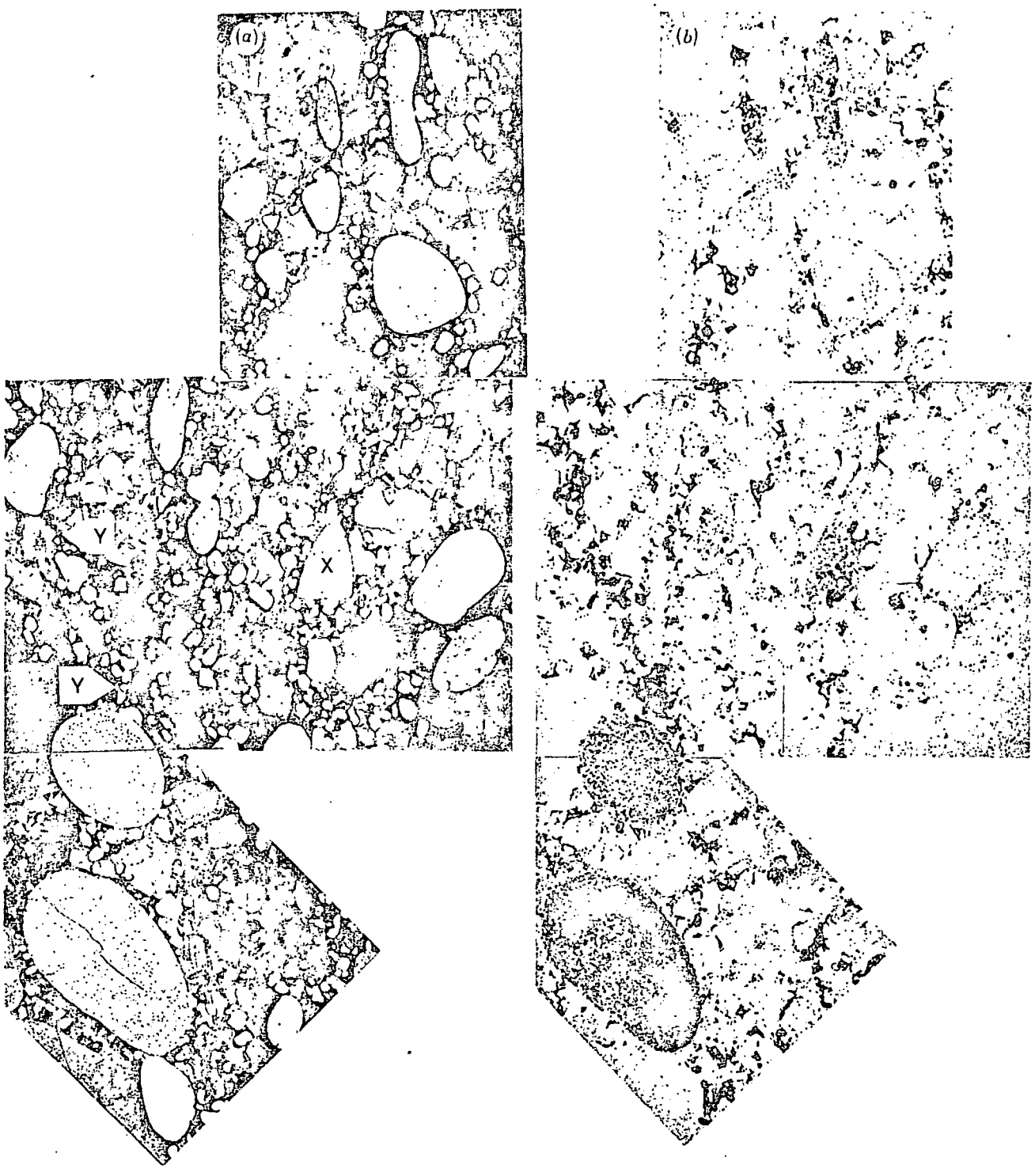

FIGURE 6. (*a*) Reflected light and (*b*) corresponding Lexan print showing a uraniferous pyritic band consisting of larger concretionary and smaller allogenic pyrite (white). Uranium is enriched in some concretionary pyrite grains but not in others (see Lexan print). One concretionary pyrite grain (*X*) has been fractured and further worn before deposition. Uranium present in the matrix is accounted for by allogenic grains of uraninite (*Y*), and interstitial clay minerals; Basal Reef, President Brand, Orange Free State (PTS 2463B).

FIGURE 4. Electron probe scanning images showing allogenic pyrite (Py) containing galena (G) and rimmed by uraninite (Ur); Basal Reef, President Brand, Orange Free State (PTS 2463A).

FIGURE 5. Electron probe scanning images showing localized migration of radiogenic lead from uraninite (Ur) to the rim of an adjacent allogenic pyrite (Py) grain with formations of minor amounts of brannerite (Br); Basal Reef, President Brand, Orange Free State (PTS 2463A).

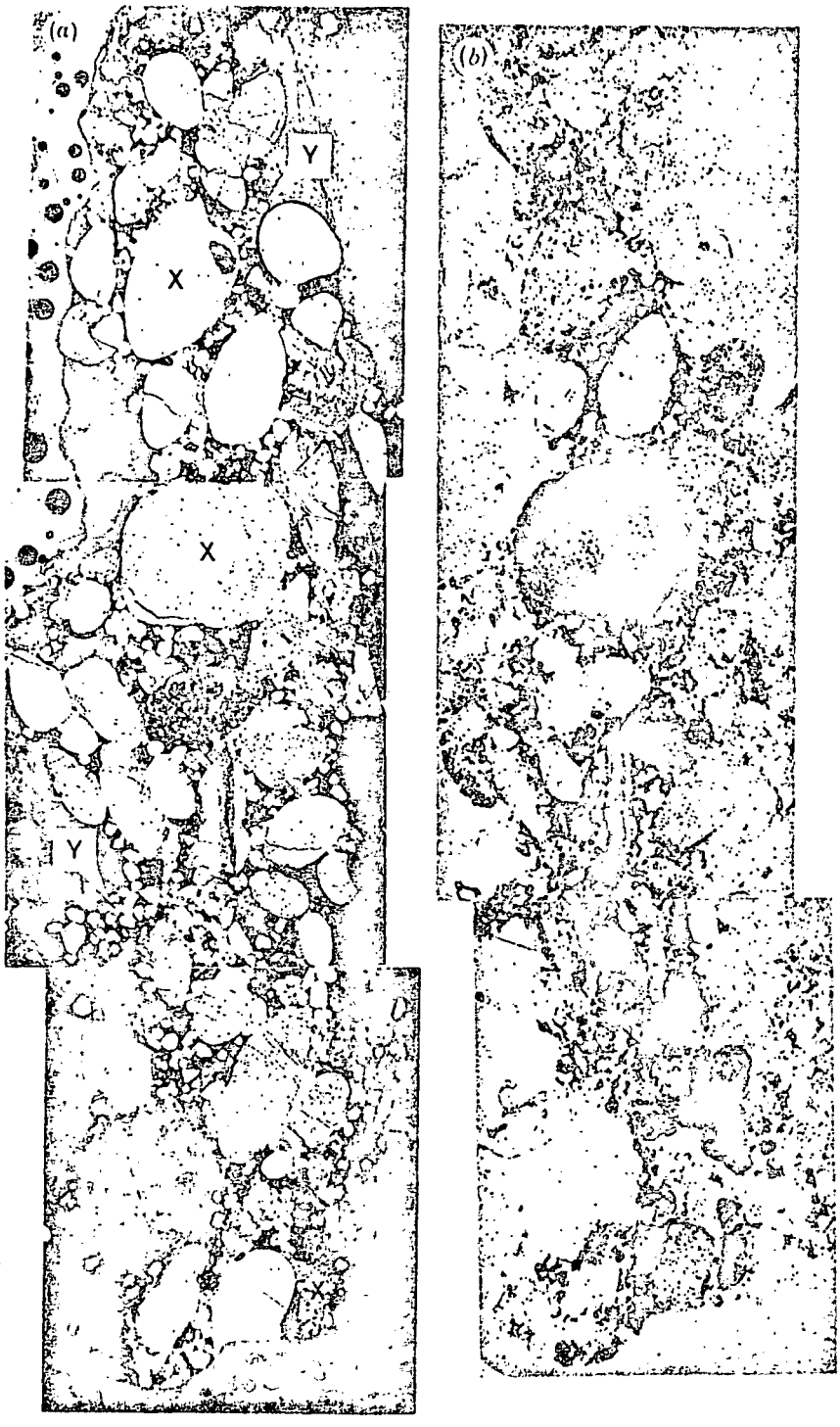

FIGURE 7. (*a*) Reflected light and (*b*) corresponding Lexan print showing uraniferous pyrite band consisting of mainly concretionary pyrite grains (white) which are a heterogeneous assemblage with regard to uranium enrichment (see Lexan print and compare grains marked *X*). Uranium present in the matrix is accounted for by the presence of allogenic grains of uraninite (*Y*) and interstitial clay minerals; Basal Reef, President Brand, Orange Free State (PTS 2463A).

plate 1). There is no doubt it is correctly described as allogenic. It is recognized in this study as the dominant pyrite type of the Dominion Reef System, whereas in the Witwatersrand any one of the three types may be dominant. Pyrite of this type also occurs partially or completely enclosed within very coarse quartz grains; it displays euhedral grain boundaries towards the host quartz, but has a sub-rounded and abraded margin where it forms the exterior of the composite grain (figure 3*a*). Optical study and electron probe microanalysis indicate that galena is the commonest phase included in allogenic pyrite. The exsolution blebs of galena (figure 4, plate 2) are distinct from marginal intergrowths of pyrite and galena resulting from the migration of radiogenic lead from coexisting uraninite grains (figure 5, plate 2).

Pyrite of type II is present in variable amounts in all samples studied from the Witwatersrand System. It is readily distinguished from type I by its porous nature and from type III by its rounded outline. The concretions are generally coarser than coexisting allogenic pyrite, ranging from granular to coarse sand size, although the individual pyrite crystallites that form the concretions are often 10 μm in diameter or less. However, in any one specimen the concretions are heterogeneous in nature with regard to shape, size and crystallite composition. Some concretions have spherically zoned alternating sulphide and silicate shells, others exhibit a layered structure. Some are so dark and fine-grained as to be indistinguishable from melnikovite or colloform pyrite, which is thought to represent a crystallized FeS_2 gel.

In the concretionary pyrite, the coarser crystallites, which are better crystallized and brighter, are texturally very similar to framboidal pyrite. The pore spaces between crystallites represent about 10% by volume of the concretions, although zones occur where the pyrite content may be as low as 10%. Even within one concretion the texture may be very variable, ranging from fine-grained disseminated pyrite to a more compact equigranular variety without pore spaces between crystallites. Saager & Mihálik (1967) proposed that these concretions formed *in situ* since they claimed the 'extremely delicate nature of the concretions exclude any long transport distance'. However, it should be noted that the crystallites forming the concretions are in most cases interconnecting, thereby providing a rigid skeleton, and the pore spaces between crystallites are filled by a matrix comprising quartz and a 7 Å clay mineral (unidentified) which provides additional strength to the concretions. Most of these composite structures have survived later metamorphism and deformation relatively unaltered. Moreover, coexisting detrital quartz granules show appreciable pressure solution effects along their margins, though both allogenic and concretionary grains occurring in close proximity are undeformed, testifying to their relative rigidity and strength.

In our view the heterogeneity of the concretionary pyrite in any hand specimen and the evidence of some rounded granules that have apparently been fractured and abraded before deposition, indicate that most of the concretionary pyrite has been transported to its present location and did not form *in situ* (figure 6, plate 3). The variability of this pyrite in any particular sample is considered to reflect a source area and selective effects of transportation processes. The intimately intergrown nature of the sulphide and silicate phases in the concretions is most probably a primary feature inherited from the source area and is not due to subsequent introduction of silica, since the regular fine-scale laminations observed in some cases preclude the possibility of later introduction (figure 7, plate 4). Hallbauer (1975) has described sub-spherical concretions of this type extracted for study by scanning electron microscopy as 'pyritized mudballs' and this would appear to be a satisfactory, yet simple, genetic description accounting for much of the concretionary pyrite studied here. However, there are rare

occurrences of zoned spherical concretions. The example shown (figure 3*b*) has a thin inner zone of chalcopyrite with rare grains of gold, and a siliceous rim partially overgrown by pyrite. The spherical outline is clearly a primary feature and deductions about the extent to which transport may or may not have occurred, cannot in general, be made from a study of external form alone.

Electron probe scans of the concretionary pyrite in one specimen, 2463A, indicate that the lead content, represented by galena, varies widely in amount and distribution from concretion to concretion. In some (figure 8, plate 5) galena is rare. Others have a high content of disseminated galena in 10 μm grains uniformly distributed throughout the concretion (figure 9); and some have fine veinlets of galena probably representing later introduction of lead.

Pyrite of type III occurs as euhedral grains in the conglomerate matrix or forms overgrowths on detrital components. It is clearly authigenic in origin. Köppel & Saager (1974) report enrichments of chalcopyrite, sphalerite and galena associated with the development of this pyrite type and also remark that the presence of dykes instrusive into the Witwatersrand rocks has influenced its development. However, these authors attribute the bulk of this reconstituted pyrite to regional metamorphism. The presence of grains of gold, in some cases abundant, noted in pyrite of this type during the present study (figure 3*c*), indicates that gold and pyrite were locally remobilized and redeposited together.

Uraninite

Before describing the details concerning the analysed material, it is necessary to comment on the use of the terms uraninite and pitchblende. Uraninite is the name for the species as a whole including all of its varieties (Frondel 1958). Pitchblende is a variety of uraninite distinguished primarily by its appearance. In the Witwatersrand all detailed work to date shows that uraninite found there can be divided into two groups. A well-crystallized variety with significant thorium content, and a poorly crystallized variety which only occurs in association with organic matter and has a low thorium content. As these tend to be found in different environments it is important to distinguish between them, so in this paper 'uraninite' is restricted to the well crystallized variety and 'pitchblende' to the other.

Uraninite occurs as discrete allogenic grains varying in shape from euhedral to subrounded and rounded grains, usually within a limited size range in the fine to very fine sand sizes (0.06–0.25 mm) and is often fractured. It occurs in this form both in the Dominion Reef and Witwatersrand Systems. Thorium content is the best indicator of primary differences in populations of uraninite grains since lead content within and between grains may be quite variable due to exsolution and migration of radiogenic lead. This lead mobility has a greater effect on the uranium content than on thorium which has a more homogeneous distribution, and is less readily displaced. It is possible to observe in some cases the migration and reaction of radiogenic

---

DESCRIPTION OF PLATE 5

FIGURE 8. Electron probe scanning images showing a discrete galena (G) grain occurring in a low-lead type pyrite concretion (Py). Uranium is present in the interstitial clay phase (*c*). Compare with figure 9 showing lead distribution in a pyrite concretion from the same section Basal Reef, President Brand, Orange Free State (PTS 2463A).

FIGURE 9. Electron probe scanning images showing galena distribution (G) in concretionary pyrite of high-lead type. Compare with low-lead type in figure 8. Basal Reef, President Brand, Orange Free State (PTS 2463A).

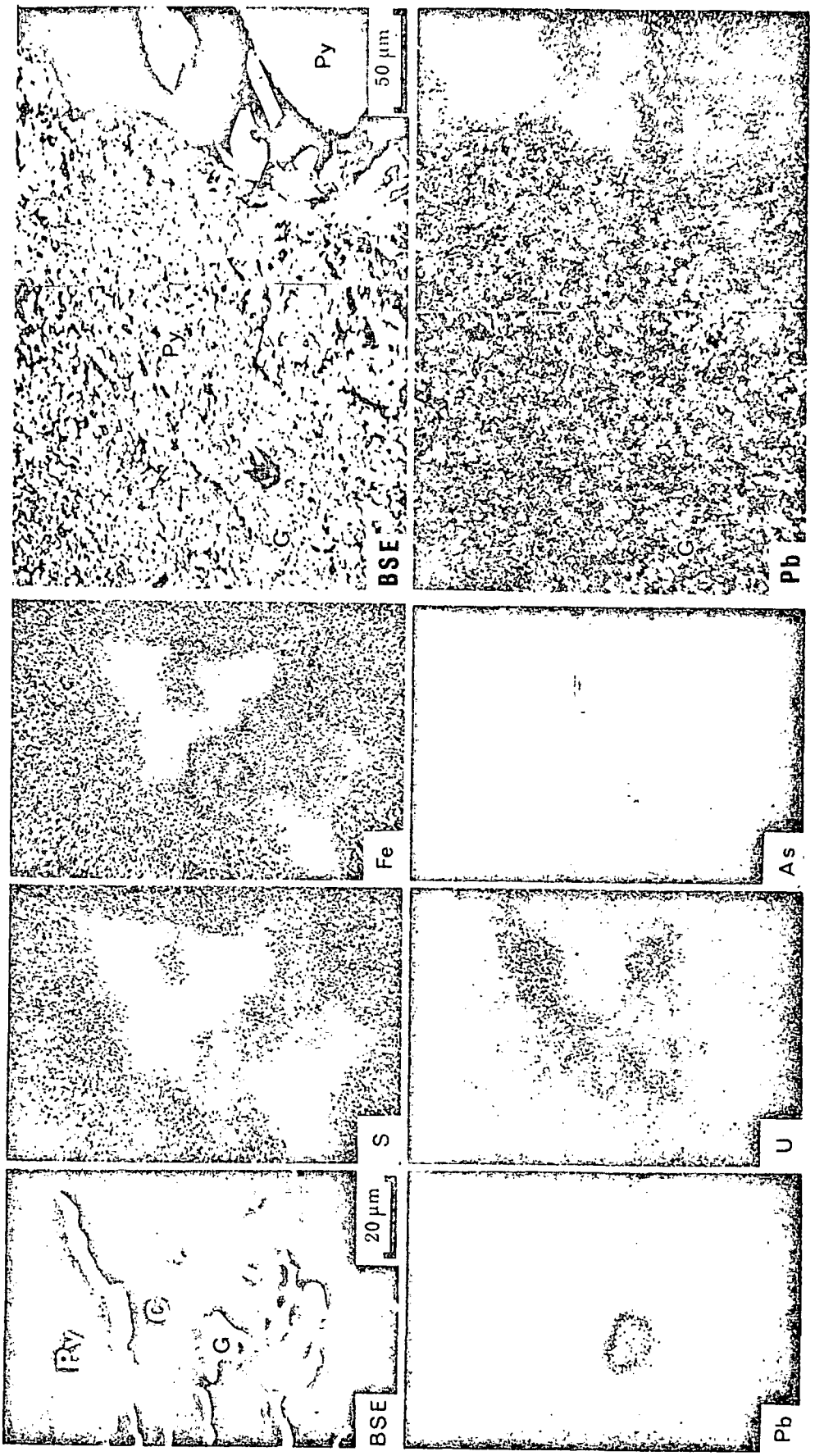

FIGURES 8 AND 9. For description see opposite.

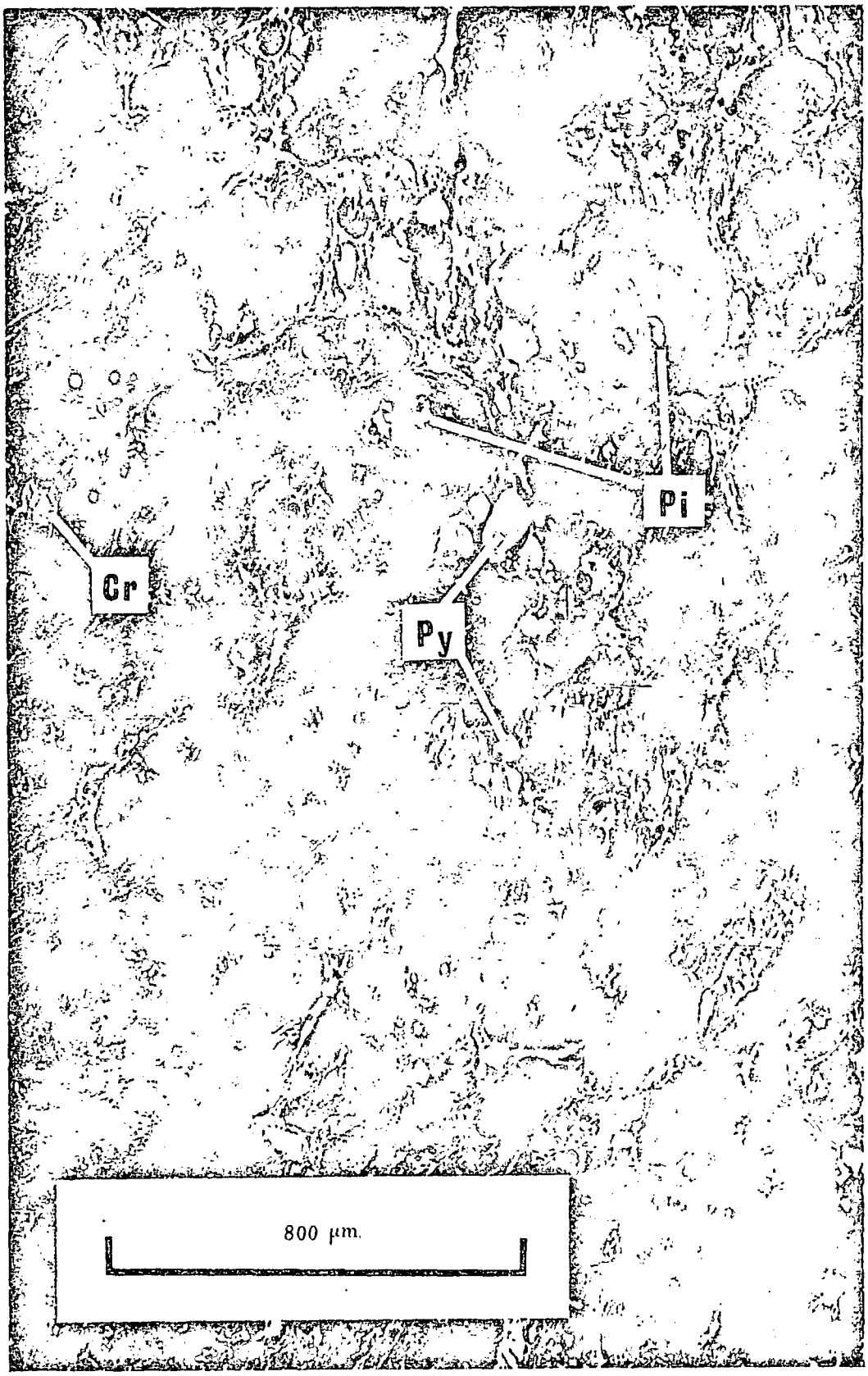

FIGURE 13. Electron probe backscattered electron image of granular carbonaceous material containing fine-grained particles of pitchblende (Pi) and gold in a carbonaceous matrix (black). Allogenic grains of pyrite (Py) and chromite (Cr) occur interstitially to the granular carbon but allogenic uraninite was not detected; Carbon Leader, West Wits (US 5).

lead with nearby allogenic sulphide to form a galena rim (figure 5). In the same section the close proximity of brannerite to decaying uraninite, with non-uraniferous titanium minerals at a greater distance is indicative of local migration and reaction of uranium with titanium minerals in the sediments.

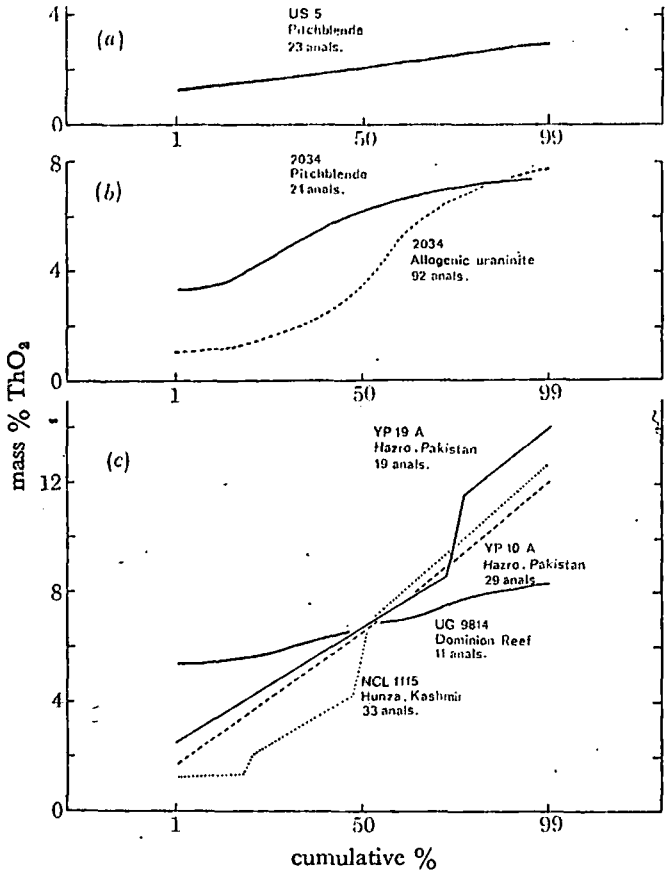

FIGURE 10. Cumulative frequency diagrams for ThO_2 obtained by electron probe microanalysis:

(*a*) Mass% ThO_2 of fine pitchblende grains in granular 'flyspeck' carbon, Carbon Leader, West Wits, (US 5).

(*b*) Mass% ThO_2 of coexisting granular allogenic uraninite and fine-grained pitchblende in columnar carbon, Vaal reefs, Klerksdorp (PTS 2034).

(*c*) Mass% ThO_2 of allogenic uraninite for one sample from the Hunza river, Kashmir a tributary of the Indus, two samples from Hazro, Pakistan on the Indus and one sample from the Dominion Reef.

Electron microprobe analyses show in this study that the Dominion Reef uraninite has a median ThO_2 content of 6.6 % with a range from 5.4 % to 8.4 % (figure 10*c*) and a median UO_2/ThO_2 ratio of 8.5 with a range from 6.4 to 10.9 (figure 11).

In the Vaal Reef of the Witwatersrand System, allogenic uraninite analysed in a columnar carbonaceous band (PTS 2034) has a median ThO_2 content of 3.5 % with a range from 0.9 to 9.1 % (figure 10*b*) and a median UO_2/ThO_2 ratio of 19 with a range of 8.3 to 48 (figure 11). The separate populations of ThO_2 in uraninite grains from the Dominion and Vaal Reefs were tested by analysis of variance methods and found to be significantly different at the 0.001 level, but variations within these populations are not significant. Significant positive correlation between calcium and manganese, and between iron and manganese is common to both uraninite populations.

The ThO_2 content, UO_2/ThO_2 ratio and correlation between calcium and manganese and iron and manganese probably reflect conditions of crystallization in the source area. The higher median UO_2/ThO_2 ratios for the Vaal reef uraninite and the lower Th content compared with uraninite from the Dominion Reef, indicates some variation in the source area for the two horizons. However, fluid-inclusion studies do not reveal any differences in the quartz pebbles (Shepherd, this volume).

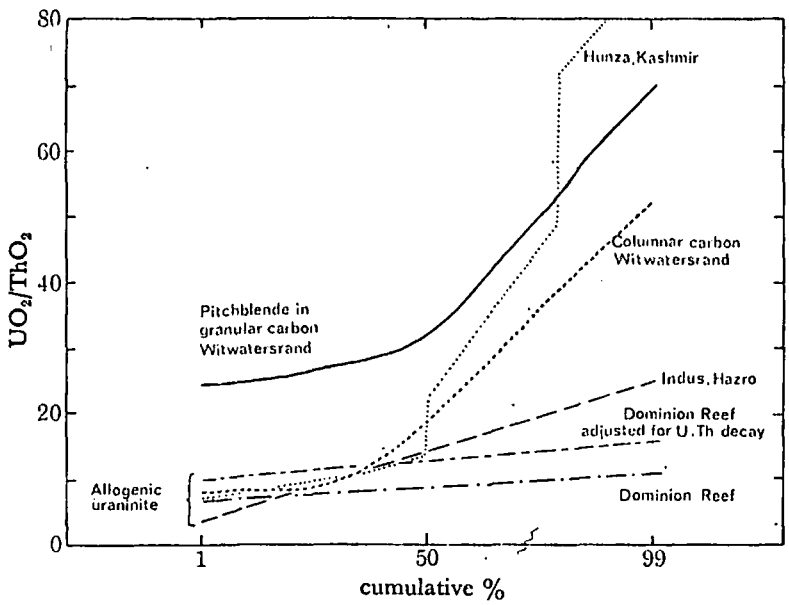

FIGURE 11. UO_2/ThO_2 ratios for separate populations of uraninite and pitchblende plotted on a cumulative frequency diagram. The highest median values are given by fine-grained pitchblende in granular carbon from the Carbon Leader (US 5). Allogenic uraninite from the Vaal reefs in the Witwatersrand (PTS 2034) has a lower ratio which is still higher than uraninite from the Dominion Reef (UG 9824). Detrital uraninite from the Indus river at Hazro (YP 10A and YP 19A) and the Hunza river, Kashmir, a tributary of the Indus, is plotted here for comparison with the Dominion Reef and Witwatersrand samples as they occur at present time. The Dominion Reef samples have also been recalculated to take account of decay of U and Th since crystallization at ~ 3000 Ma, and this correction tends to reduce the small difference between populations.

Grain size of uraninite and associated phases

A typical sample (UG 5538) from the Bramley section of the Dominion Reef mine, Klerksdorp, was examined in detail by grain-size analysis. Coexisting allogenic grains of quartz, pyrite, uraninite and gold were measured by means of the Humphries eyepiece micrometer, which can be used to classify grains directly according to the phi scale. Each population, except for gold, consisted of a hundred grains measured along the Feret diameter, which is the maximum grain length projected on to a fixed line. The populations appear to be single populations in each case resulting in linear cumulative frequency curves. Sample means and standard deviations were calculated in terms of phi units from which the standard error of the mean was obtained. This was transferred to a chart containing graphical results calculated for Stokes law and the square-root law combined (Tourtelot 1968), which indicates that quartz, pyrite and uraninite closely approximate to a hydraulically equivalent assemblage (figure 12). The gold grains counted were too few to be statistically significant, but nevertheless appear too small for exact hydraulic equivalence. This point was noted by Coetzee (1965), but no satisfactory explanation has yet been proposed.

Uraniferous and auriferous carbonaceous material

Uranium and gold in association with carbonaceous material is one of the most important modes of occurrence of these metals in the Witwatersrand Basin, particularly in view of the uniformly high grades of mineralization encountered and the wide lateral extent of such horizons as the Carbon Leader in the Far West Rand (Davidson & Bowie 1951; Bourret 1973).

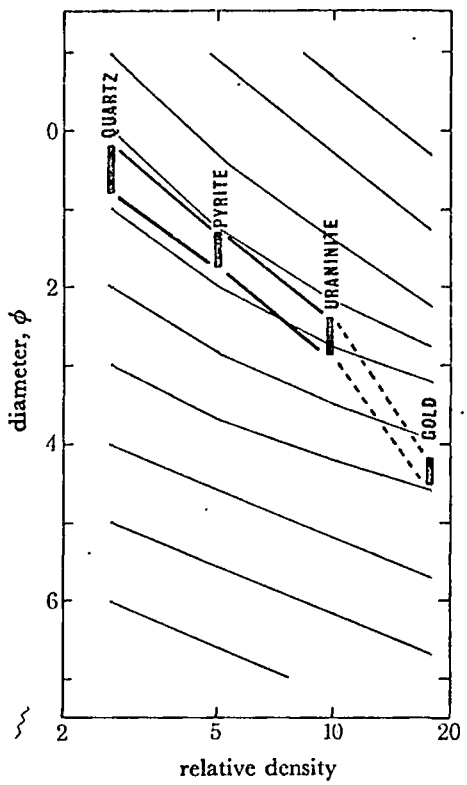

FIGURE 12. Standard error of the mean size for coexisting quartz, pyrite and uraninite plotted on the phi scale against specific gravity. The light curves are solutions for Stokes' law and the square-root law combined where they overlap. The relative grain sizes of the suite of minerals plotted in heavy type indicate that quartz, pyrite and uraninite are hydraulically equivalent. The gold is smaller than would be expected for hydraulic equivalence but the number of grains measured is inadequate for full statistical treatment, Bramley high grade, Dominion Reef (UG 5538), diagram after Tourtelot (1968).

Any satisfactory explanation of the nature of this metal-rich carbonaceous matter should take account of the following observations: (*a*) The Carbon Leader, which represents a most striking enrichment of uranium and gold, forms a very restricted horizon in the reef never greater than 13 mm thick (Davidson & Bowie 1951). (*b*) The consistently high levels of both uranium and gold over a wide lateral extent. (*c*) The higher UO_2/ThO_2 ratios in the carbonaceous type of mineralization compared with the banket type of both the Witwatersrand and Dominion Reef Systems, and its absence in the latter; (*d*) The absence of mineralization in certain occurrences of carbonaceous material. Some authorities consider the carbonaceous material represents fossilized remains of Precambrian plants (Hallbauer 1975). Whether such is its origin or not, there is little doubt that it has exercised a key rôle in the formation of these deposits.

The carbonaceous material comprises granular and columnar varieties, which have many features in common whilst differing in certain important aspects (Davidson & Bowie 1951). According to the analyses of Davidson & Bowie this material contains 43 % C and 2 % H and they called this phase hydrocarbon. However, we have not attempted to define the organic constituents of all the carbonaceous materials studied here and have therefore retained a more general nomenclature used by Vine *et al.* (1958).

The granular or 'fly speck' material (figure 13, plate 6) consists of ovoid to rounded grains (100–400 μm) with an interstitial matrix of sub-rounded allogenic pyrite, chromite and concretionary pyrite (~ 50 μm). The granules are partially moulded around interstitial grains, particularly where they lie along grain boundaries between granules (figure 13), but the carbonaceous matter at no point either replaces or invades the opaque minerals. The granules have mottled extinction under crossed polars in reflected light and contain two main phases of carbonaceous matter (figure 3*d*), consisting of relatively coarse-grained smooth areas with undulose extinction interspersed with fine-grained material having a similar reflectance of 14.3 % (Type (I) of Davidson & Bowie 1951, p. 6). The fine-grained material is veined along grain boundaries by a dendritic system containing pitchblende, gold, pyrite, galena and gersdorffite. The gold and gersdorffite are commonly intergrown, as are the gold and pitchblende. Galena tends to form separate grains, but is also intergrown with pyrite. These textural and mineralogical relationships have been confirmed by both scanning and quantitative electron probe analysis. The pitchblende has a median ThO_2 content of 2.0 % with a range from 1.1 to 2.9 % (figure 10*a*) and a median UO_2/ThO_2 ratio of 33 with a range from 25 to 69 (figure 11). Analysis of variance shows that this population is significantly lower in its ThO_2 content at the 0.001 level than all the other uraninite and pitchblende phases in the Witwatersrand and Dominion Reef. There is significant correlation between uranium and calcium (0.01 level) uranium and cerium (0.01 level), and PbO and ThO_2 (0.001 level). However, there is no correlation between calcium and manganese or between iron and manganese as for the allogenic uraninite, pointing to a distinct origin for the pitchblende in the granular carbon, which probably developed *in situ* during diagenesis and metamorphism.

The carbonaceous seam of the Carbon Leader usually occurs along the basal parting in quartz pebble conglomerate, and has a well-developed columnar structure normal to the bedding. It is linked with, but different from, the granular form described above. It consists of the same two carbon phases, occurring as lenticular to ovoid bodies with their long axes normal to the bedding. Individual bodies are cut by discontinuous vertical sutures which emphasize the overall columnar effect (figure 14, plate 7). Scanning electron-probe studies demonstrate that these sutures carry fine-grained pitchblende, brannerite, gold and other phases (figure 15, plate 7).

The inclusions within the columnar carbonaceous material are similar mineralogically to those in the granular material with one notable exception, namely the occurrence of coarse-grained uraninite, often subrounded and partly replaced by coarse-grained carbonaceous matter (figure 16, plate 8). This uraninite is concentrated along one margin of the carbon seam though not restricted to that margin. Analyses of neighbouring fragments show that they belong to groups within which the ThO_2 content is similar, but may differ very considerably from that in adjacent groups, indicating a chemically heterogeneous assemblage of uraninite crystals subsequently fragmented and replaced by carbonaceous matter (figure 17, plate 8). The chemistry of the allogenic uraninite grains has been described above and is shown in

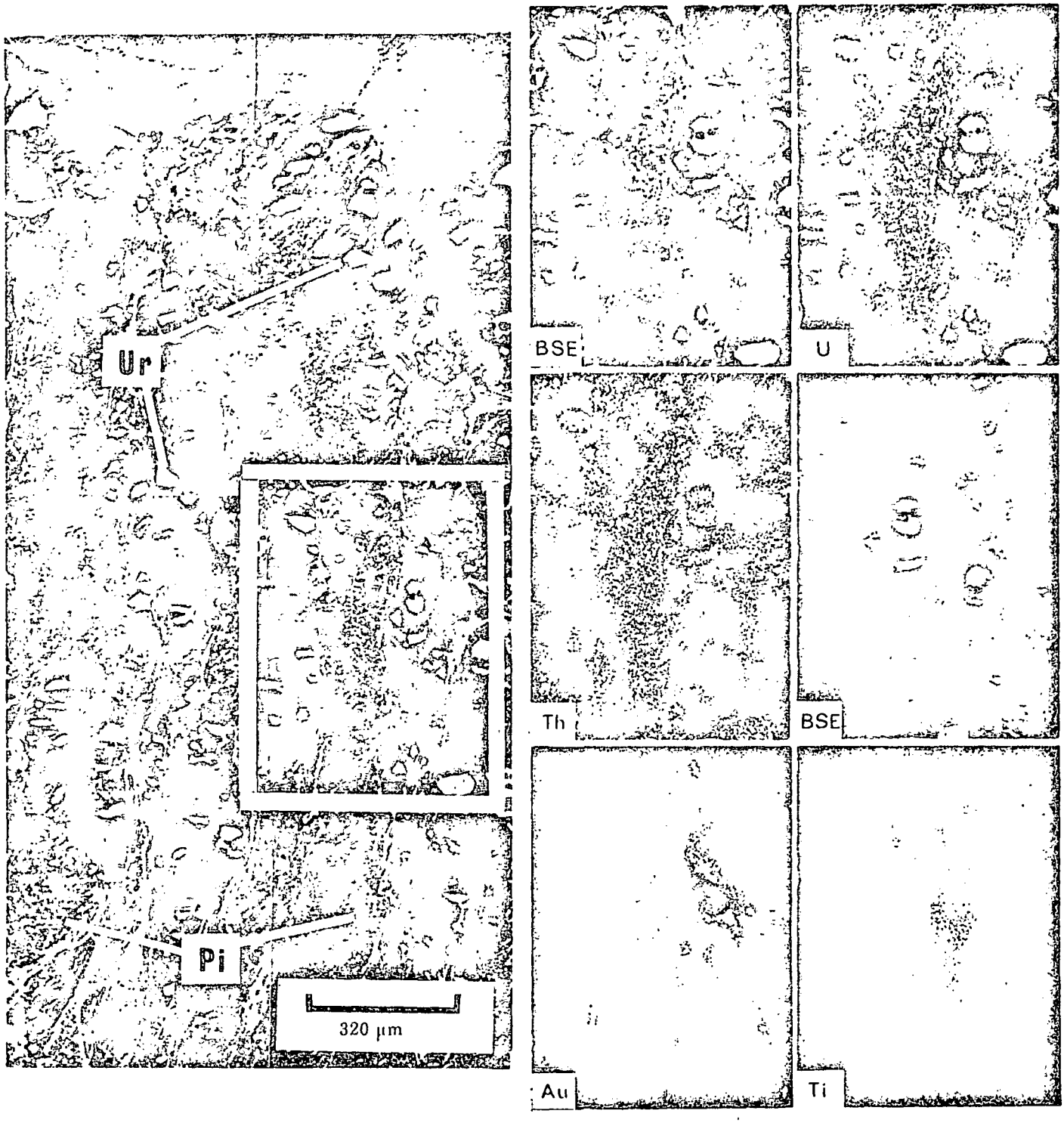

FIGURE 14. Electron-probe backscattered electron image of columnar carbon showing zones of coarse fragmented allogenic uraninite (Ur) and fine-grained disseminated pitchblende in a carbonaceous matrix (black). Vertical lineations of a strongly reflecting phase between these zones consist of fine disseminations of gold associated with brannerite, pitchblende and churchite; Vaal Reefs, Klerksdorp (PTS 2034).

FIGURE 15. Electron probe scanning images from two overlapping areas of columnar carbon within inset on figure 14 showing backscattered electron images and distribution of uranium and thorium corresponding to coarse-grained uraninite and fine-grained pitchblende. The latter is intimately associated with gold and a titaniferous phase, probably brannerite, in a carbonaceous matrix (black). Vaal Reefs, Klerksdorp (PTS 2034).

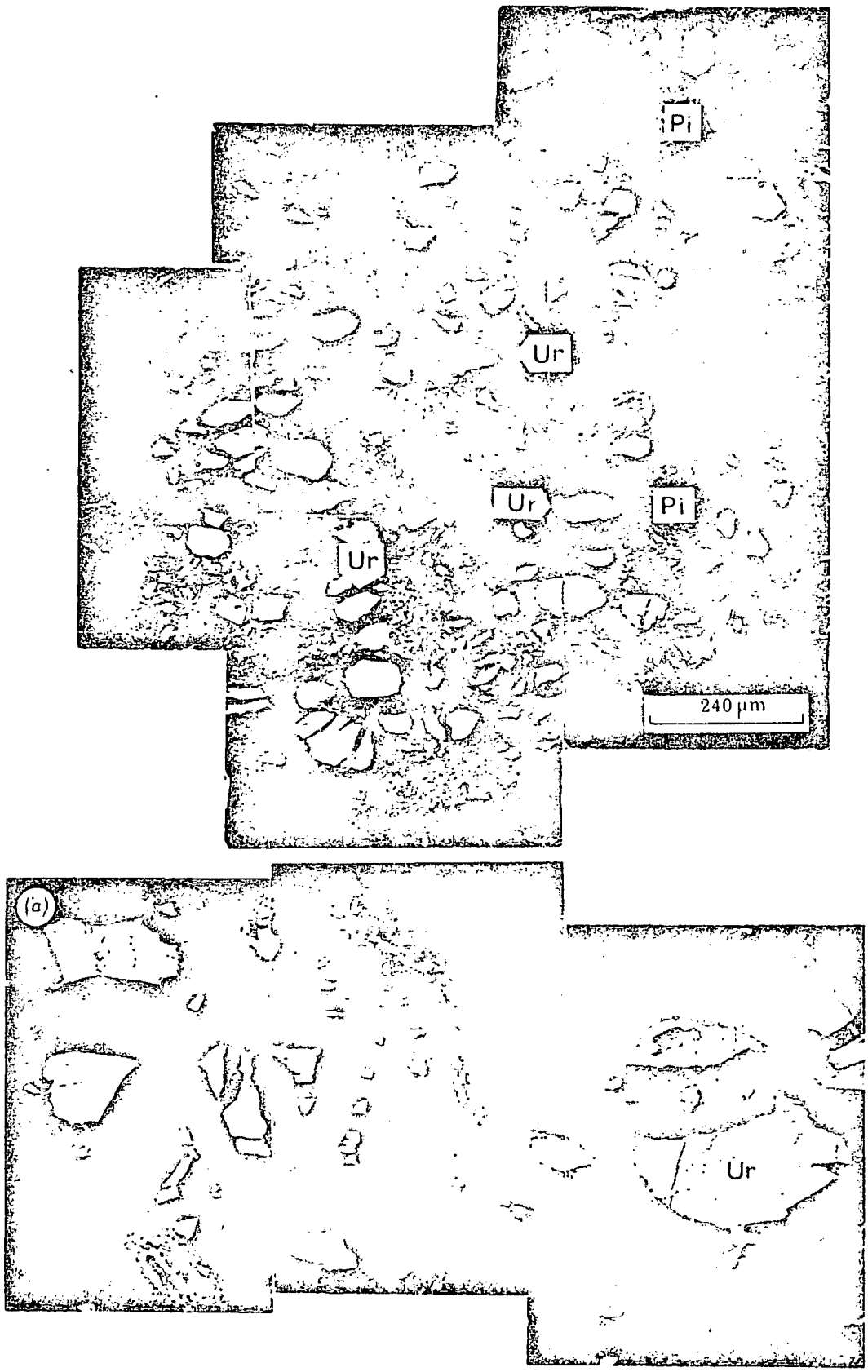

FIGURES 16 AND 17 (*a*). For description see opposite.

[redacted]s 10 and 11. Pitchblende, associated with partially replaced allogenic uraninite has a [redacted] higher thorium content than the pitchblende in the granular carbonaceous matter; it has a median ThO_2 content of 6.2 % with a range from 3.17 to 6.9 % (figure 10*b*) and a median UO_2/ThO_2 ratio of 9.0 with a range from 6.2 to 12.2. This population is significantly different from the coexisting coarse-grained allogenic uraninite (0.001 level), but not from the uraninite in the Dominion Reef. It is possible that the high thorium content is attributable to solution and redeposition of both uranium and thorium from the allogenic uraninite undergoing attack by carbonaceous matter.

The disseminated pitchblende in fine-grained columnar carbonaceous matter is optically and texturally very similar to that in the granular variety and is also intimately associated with galena, gersdorffite, gold and pyrite, forming an interconnecting dendritic texture of microcrystals in the manner previously described.

The outer margin of the carbonaceous matter, where it is in contact with allogenic pyrite, is a favoured site for gold concentration in the form of fine platelets. Internal pore spaces within carbonaceous matter are also an important site for the formation of complex intergrowths of uraniferous silicates, gold and gersdoffite. Partially replaced uraninite within carbonaceous material is also a common site for gold overgrowths. All these textures suggest that much of the

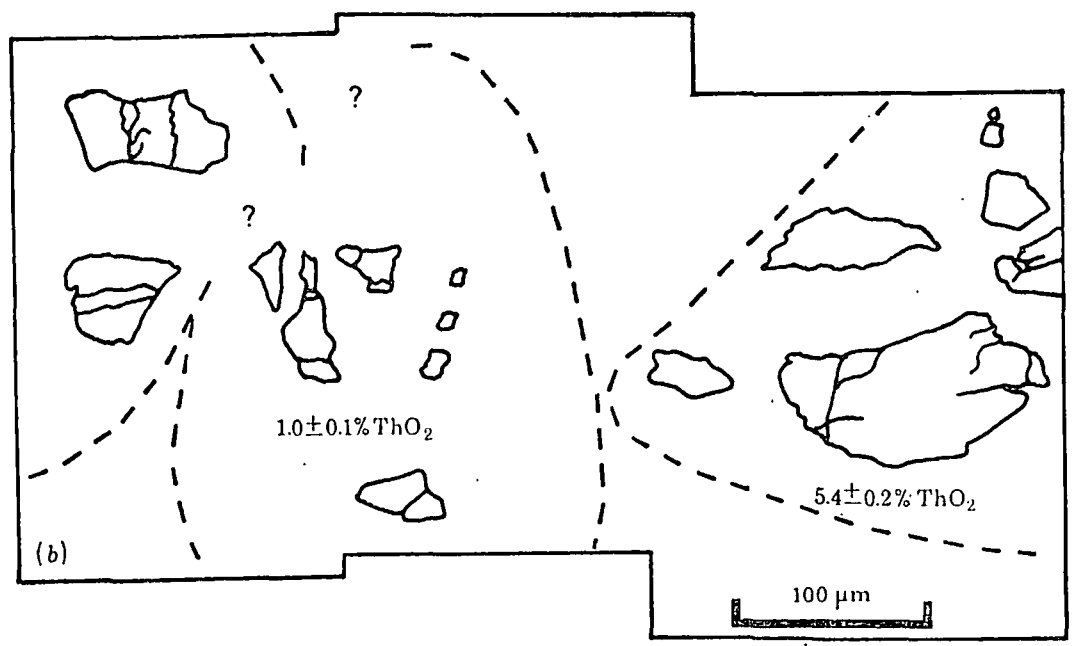

FIGURE 17(*b*).

DESCRIPTION OF PLATE 8

FIGURE 16. Electron probe backscattered electron image of columnar carbonaceous material showing clusters of coarse-grained allogenic uraninite crystals (Ur) partly digested by carbonaceous matter (black) with lobate zones of fine-grained pitchblende (Pi) in a carbonaceous matrix. Vaal Reefs, Klerksdorp (PTS 2034).

FIGURE 17. (*a*) Electron probe backscattered electron image showing uraninite within carbonaceous material. The destruction of large uraninite grains by the carbonaceous material is shown by the complementary outlines of adjacent grains and in the reconstruction of original grain outlines. (*b*) The ThO_2 content clearly demonstrates similarity within but differences between grains outlined, Vaal Reefs, Klerksdorp (PTS 2031).

gold, pitchblende, churchite (see below) and associated sulphides crystallized in their present position as a result of diagenetic or later metamorphic processes.

Churchite

A tenuous phase surrounds the fine-grained pitchblende of the columnar carbon (figure 18, plate 9). It contains major yttrium and phosphorous with the heavy rare-earth elements Gd, Tb, Dy, Er and Yb, corresponding to either xenotime (YPO_4) or churchite ($YPO_4.2H_2O$). Comparison of the rare-earth distribution (table 1) with that reported in the literature for xenotime and churchite points to an identity with the latter because of the distinct enrichment of the former in Dy, Er, and particularly Yb, relative to Gd.

This is particularly interesting in the present context, since xenotime is found principally in granitic pegmatites whereas churchite† can be formed by a combination of biochemical processes and diagenetic reactions close to the surface (Milton *et al.* 1944). In the occurrence des-

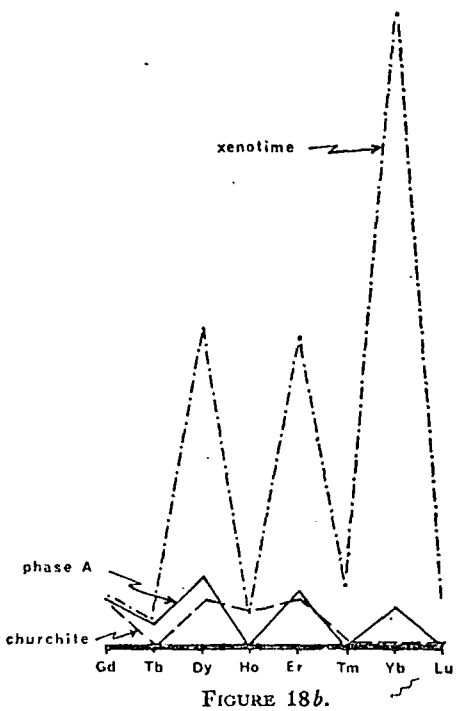

FIGURE 18*b*.

DESCRIPTION OF PLATE 9

FIGURE 18. (*a*) Electron probe scanning images of phase 'A' probably churchite, containing major Y and P which overgrows pitchblende (Pi). The example shown occurs in fibrous material within columnar carbon shown in figure 14. (*b*) The distribution of heavy rare-earth elements in phase A relative to gadolinium is compared here with examples of churchite and xenotime from the literature, Vaal Reefs, Klerksdorp (PTS 2034).

FIGURE 19 (*a*) and (*b*) Indus River uraninite.

(*a*) Uraninite grains from the Hunza river, Kashmir, a tributary of the Indus River. The uraninite grains usually show at least one crystalline face and several cubes are present. The grain shown in detail (*b*) exhibits alteration along discrete zones parallel to well-developed crystal faces. Most of the grains in the sample, however, are fresh and unaltered. No correlation between degree of alteration and ThO_2 content has been detected.

† Described as weinschenkite by Henrich (1935), Milton *et al.* (1944) and Pokrovskiy *et al.* (1965), but shown to be churchite by Claringbull & Hey (1953).

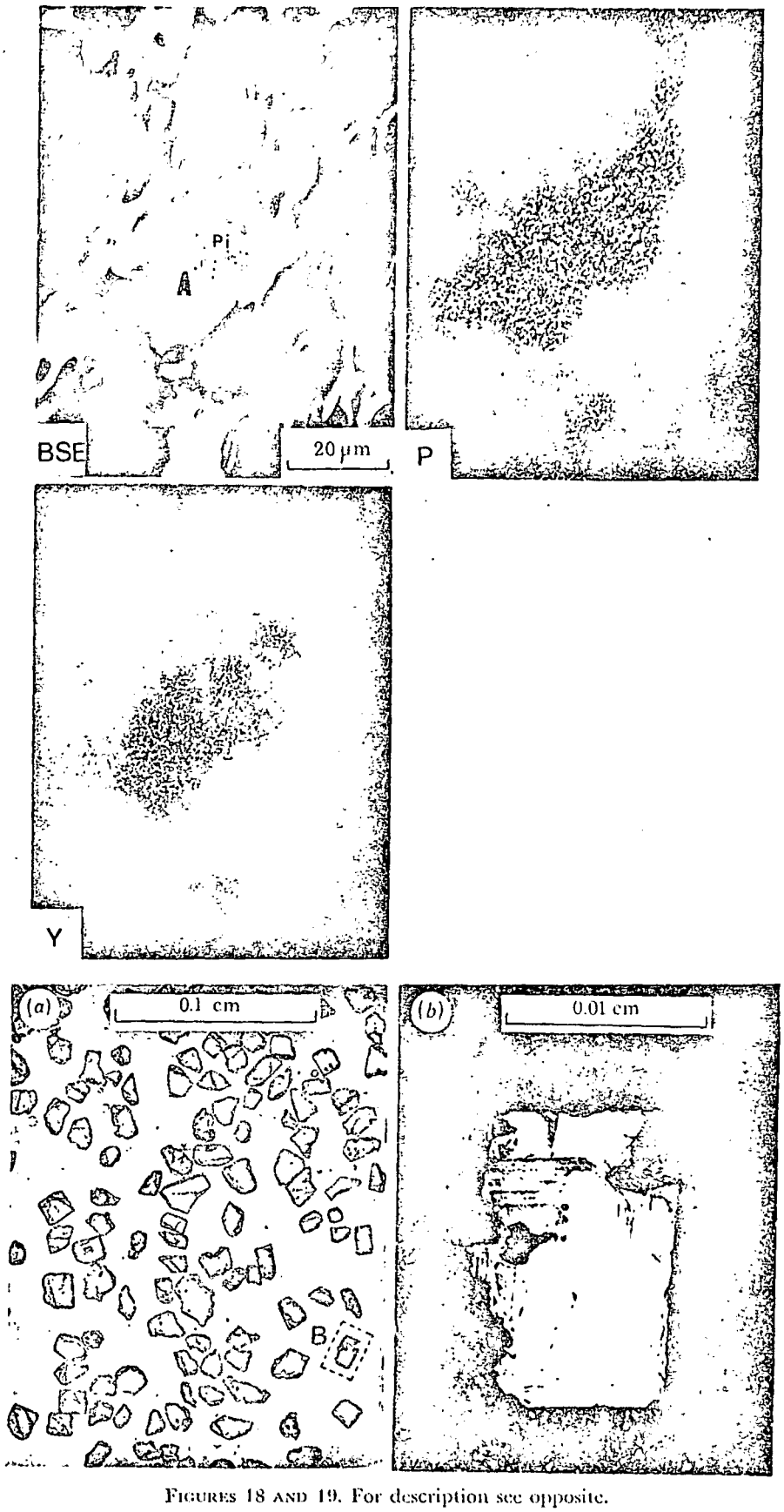

FIGURES 18 AND 19. For description see opposite.

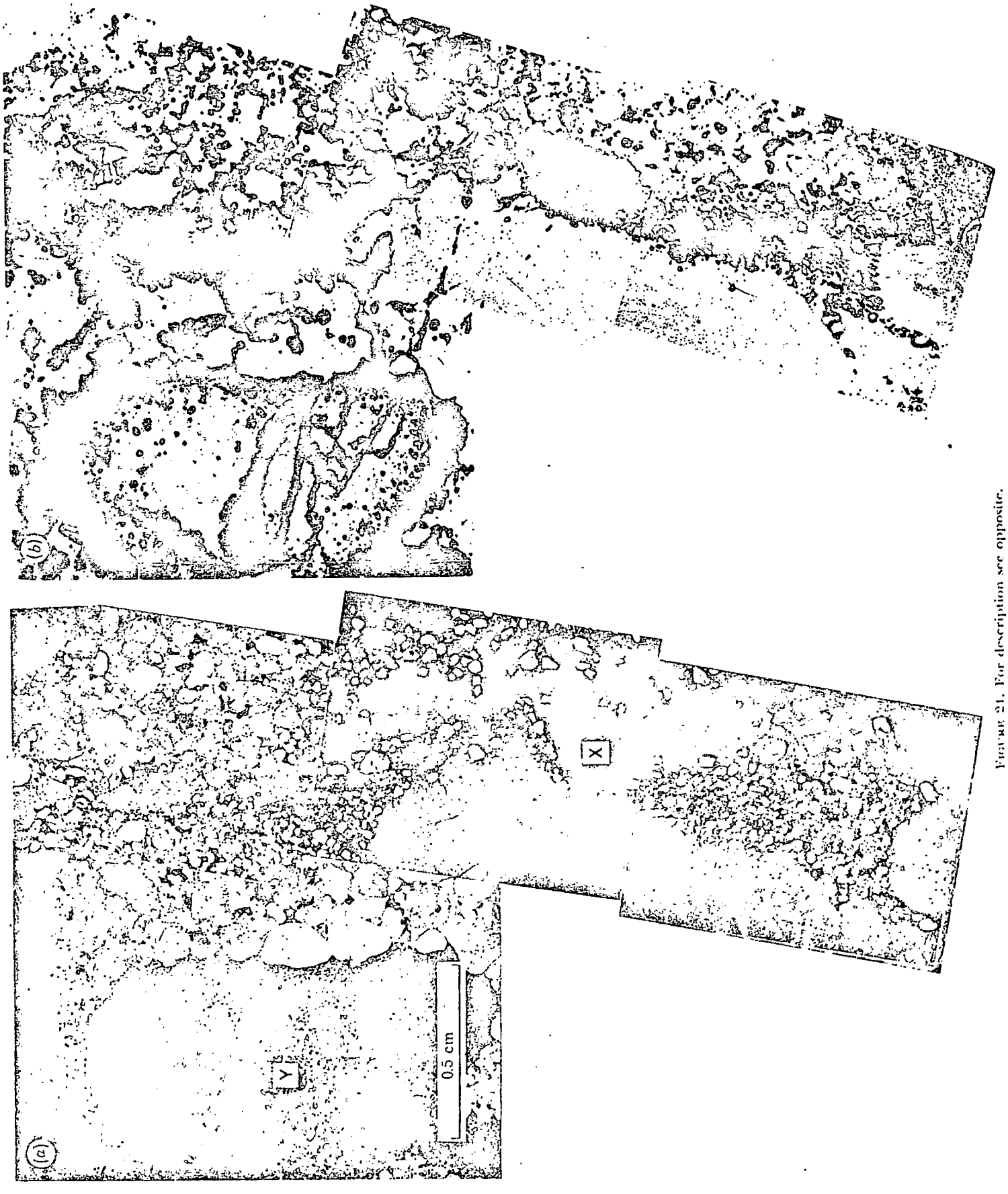

FIGURE 21. For description see opposite.

Indus river uraninite

Samples of uraninite from the Indus river were analysed by electron probe for comparison with the allogenic uraninite of the Dominion Reef and Witwatersrand Systems, and with a view to assessing the stability of uraninite as a detrital mineral in recent alluvial deposits. The samples had been collected from the Hunza river, a tributary of the Indus in Kashmir (Darnley 1962), and from the Indus alluvium near Hazro, Pakistan (Miller 1963).

The Hunza sample consists of a 99 % pure concentrate in which nearly all the uraninite grains have at least one well-defined crystal face and some show cubic form with little evidence of corrosion. They are in the very fine to fine range of sand size (0.05–0.20 mm) (figure 19, plate 9). Pyrite is present in the concentrate as euhedral cubes, fresh and untarnished, and as concretions. An extensive assemblage of radioactive resistate minerals and sulphides has also been reported (Darnley 1962).

The Hazro samples, which Miller (1963) had reported to contain both uraninite and gold, were also re-examined, involving the preparation of concentrates by vanner, superpanner and heavy liquids. The final concentrate contained in addition to uraninite: pyrite, arsenopyrite, uranothorite and a grain of gold. The sulphides were fresh, but many of the uraninite crystals, with at least one crystal face, had a distinct outer weathered zone, though beneath this they were fresh and homogeneous.

The ThO_2 content of one sample from the Hunza and two from Hazro are shown in figure 10*c*. The three populations exhibit no significant difference, indicating constancy in uraninite composition between sites 300 km apart. The mean UO_2/ThO_2 ratio for the Indus samples is shown in figure 11, to which has been added the ratio for the Dominion Reef uraninite adjusted for uranium and thorium decay to eliminate the effect of the greater age. There is no significant difference between the two uraninite populations after adjustment.

Viljoen (1963) regarded the lack of oxidation of detrital pyrite in the Witwatersrand System as evidence of an atmosphere free of oxygen and Liebenberg (1955) and Grandstaff (1975) considered a non-oxidizing atmosphere was necessary for uraninite transportation. Neither of these conclusions is supported by the evidence from the present-day Indus river, in which as we have seen uraninite, gold, pyrite and other sulphides form a stable assemblage over several hundred kilometres.

Geochemical evidence

Lead content of uraninite and pitchblende

Cumulative frequency curves for the lead content of selected uraninite and pitchblende phases are shown in figure 20. The data fall on four main distributions as follows: (1) relatively young (*ca.* 90 Ma) low-lead allogenic uraninite from the Indus, (2) pitchblende in granular carbon from the Carbon Leader in the Witwatersrand with intermediate lead content, (3) allogenic uraninite in the Witwatersrand and Dominion Reef with high lead content, and (4) pitchblende with high lead content intimately associated with allogenic uraninite in the Witwatersrand.

The intermediate lead content of the pitchblende sample US5 is consistent with the textural observation that this phase is younger than the allogenic uraninite and is formed *in situ* from the diagenesis and metamorphism of the carbonaceous host. The low thorium content of this phase is indicative of a low-temperature solution (thorium being relatively insoluble), from

which uranium was precipitated by absorption on decaying organic matter represented by the carbonaceous material in the section. The highest lead contents are given by the allogenic thorian uraninite phases which are probably a reflection of their greater age. Partial rejuvenation of the allogenic uraninite from the Witwatersrand resulted in the formation of a lead-rich pitchblende in sample 2034. However, the evidence from sample US5 indicates that the presence of allogenic uraninite is not essential for the formation of younger pitchblende, since

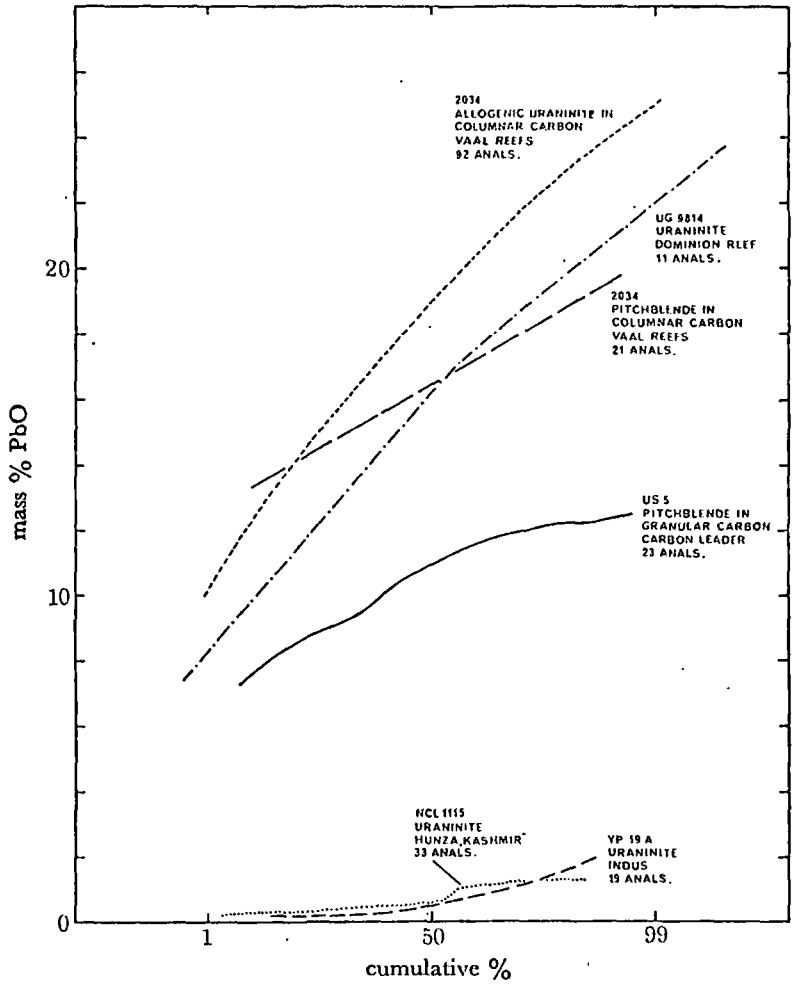

FIGURE 20. Cumulative frequency diagram of the PbO content of uraninite and pitchblende from Dominion Reef, Witwatersrand and Indus river sediments.

it may also form directly from the metamorphism of uranium-enriched carbonaceous material. Younger ages exhibited by pitchblende in the absence of allogenic uraninite should not be generally interpreted therefore as rejuvenation of an older allogenic uraninite, since in the example studied here pitchblende represents direct formation of this phase from a metal-enriched organic substrate; allogenic uraninite was not detected.

Uranium micromapping with thermal neutrons

The distribution of uranium in Witwatersrand and Dominion Reef samples was studied by the fission-track method using Lexan polycarbonate for the registration of fission fragments

from the induced fission of ^{235}U by thermal neutrons, as described by Price & Walker (1963), Kleeman & Lovering (1967) and Bowie, Simpson & Rice (1973). The method is ideal for providing information on the location of uranium in banket-type occurrences. The radioactive bands of interest can usually be included within the breadth of a single polished thin section and radiation doses can be adjusted so as to span concentration ranges. The samples studied here have been subjected to a dose of approximately 5×10^{16}n/cm^2 in order to obtain a lower detection limit of 0.01 parts/10^6 and track saturation at about 40 parts/10^6. This enables associations of uranium with mineralogical phases to be readily determined when the uranium is below the limits of detection by microprobe.

The results show that uranium is closely confined to discrete horizons both in the banket type and carbonaceous reefs, and that it not only occurs as grains of uraninite but also in a finely disseminated form. Thus uranium is present in pyrite concretions, within lenticular fragments comprising clay-size quartz, kaolinite and pyrophyllite, as a fine disseminated coating on allogenic pyrite grains otherwise uranium free, and, rarely, within dislocations and shears (figures 6, 7, and 21, plate 10).

Both microprobe and fission-track studies show the presence of uranium in the interstitial 7 Å clay phase in the pyrite concretions (figure 8), but fail to detect it in the pyrite itself. A combination of these techniques show that the uranium content of individual concretions is variable within a single reef over a distance of a few millimetres. Whereas some are virtually uranium-free, others are enriched in amounts readily detected by electron microprobe ($>$ 500 parts/10^6). Uranium enrichment occurs only in the rims of some concretions whereas in others, particularly the finer-grained melnikovitic types, the enrichment usually occurs throughout the concretion. This association of uranium with pyrite is particularly striking where it occurs surrounded by an essentially barren quartzitic groundmass, and in cases such as this the evidence for a primary association of uranium with the concretion is strong and probably related to deposition of uranium during the formation of the concretion. The uranium in the rims of concretions was probably absorbed during transport or diagenetically prior to lithification.

Allogenic pyrite is also closely associated with uranium but the uranium in the pyrite is below detection limit and in this case the uranium occurs in a secondary clay mineral forming a marginal overgrowth to the pyrite. This association is particularly well developed in allogenic pyrite occurring in close proximity to a carbonaceous band rich in uranium and gold (PTS 1944, West Driefontein). In this case the uranium was probably deposited *in situ* and subsequently incorporated into the clay mineral overgrowth which formed during diagenesis and metamorphism. This relationship between allogenic pyrite and overgrowths of fine-grained clay minerals and uranium has been recorded widely and is an important control in the deposition of uranium in the Witwatersrand System. The control is specific since uraniferous silicates overgrowing allogenic pyrite occur dispersed through a barren quartzite matrix and are readily identifiable and distinguishable from the textures produced by shearing and later introduction of uranium.

The association of uranium with lenticular to rounded granules consisting of quartz, kaolinite and pyrophyllite has been recognized in many of the Witwatersrand banket-type ores studied here. The uranium occurs disseminated throughout the granules and produces point sources of fission tracks which have not yet been correlated with any specific uranium mineral (figure 21). In some specimens this is the only uranium-bearing mode. The occurrence of these enriched

granules in a barren groundmass indicates that uranium enrichment most probably occurred either before deposition or at the latest during diagenesis. Larger rounded pebbles also occur, some consisting of quartz, pyrophyllite, kyanite and possible illite with secondary spherulitic structures.

In this case uranium occurs on what appears to be a leached and weathered margin and along a vermicular veinlet structure within the pebble. Enrichment in uranium during transport and diagenesis related to weathering of the pebble rim (figure 21) seems to be the most likely explanation of this occurrence. Regional metamorphism has tended to reduce the thickness of the uraniferous rim, which is best developed where weathered pebbles are relatively unaltered.

Neutron activation analysis of whole rock samples

Instrumental neutron activation analysis of whole-rock samples was undertaken as an adjunct to the mineralogical studies utilizing a method developed by Plant, Goode & Herrington (1976).

The results are given in table 2 and demonstrate the increase in U/Th ratios from the Dominion to the Vaal reefs in the Witwatersrand basin. Freddies Reef, East Geduld, and Daggafontein are somewhat higher and similar to one another, whereas samples from West Driefontein, dominated by carbonaceous matter, have the highest ratios. Twenty-four additional elements obtained by this method on the same sample are presented for comparison with uranium and thorium. This gradational variation in the U/Th ratio is an approximate measure of the depositional environment. The high-energy environment has a low ratio and the low-energy environment a high ratio with continuous variation between the two.

Bimodal nature of the uranium mineralization

The occurrence of allogenic grains of uraninite in the Dominion Reef (Taylor, Bowie & Horne 1962) and the Witwatersrand (Liebenberg 1955; Grandstaff 1975) is well established. This phase occurs in the Dominion Reef in association with resistate phases such as garnet, monazite, cassiterite, zircon, allogenic sulphides, rare authigenic sulphides and gold. The similarity of this assemblage with modern gravels on banks in the Indus is notable, although uraninite in the Indus is at present sub-economic (Miller 1963). In the Witwatersrand System the characteristically lower content of allogenic uraninite and rounded resistate phase, the relatively greater importance of concretionary pyrite and the appearance of carbonaceous matter as an important accessory or even dominant phase, represent a markedly different style of mineralization.

The general similarity of the median values of the UO_2/ThO_2 ratios between 14 and 20 for allogenic uraninite from the Indus Valley, Dominion Reef and Witwatersrand is most significant. However, the pitchblende associated with granular carbonaceous material in the Witwatersrand has a much higher median ratio of about 32 and this is a distinct and separate phase of mineralization differing from the allogenic uraninite texturally, compositionally, and in its close association with carbonaceous matter and gold.

The fission track studies have clearly indicated an association of uranium in Witwatersrand sediment with clay minerals occurring individually or intergrown with, or overgrowing, pyrite, and in many cases this association has the appearance of a primary, essentially syngenetic, relationship unaffected by appreciable uranium remobilization.

Evidence of this type from Witwatersrand sediments provides support for the existence of some uranium in solution in the Basin during sedimentation and diagenesis as discussed by Pretorius (1975). The uranium would be highly mobile as the soluble uranyl ion, UO_2^{2+}, which would subsequently be absorbed, reduced, and precipitated by organic-rich muds probably aided by and associated with the simultaneous reduction of sulphate by bacteria as proposed by Trudinger (1971):

$$SO_4^{2-} + 8e + 10H^+ \rightarrow H_2S + 4H_2O.$$

The hydrogen sulphide formed would subsequently react with other metals in solution such as iron and lead to form the authigenic intergrowths of pyrite and galena with clay minerals, gold and uranium observed in the sediments.

TABLE 2. NEUTRON ACTIVATION ANALYSIS (IN PARTS/10^6 EXCEPT WHERE STATED)

sample location	rock sample	Na	K	Sc	Cr	Fe%	Co	Zn	As	Rb	Ag	Cd	Sb	Cs
Dominion Reefs	5A 2006/2133	2.19%	< 2000	38	< 400	10.2	570	< 300	3800	< 100	< 40	< 100	28	< 5
	BR8N2(B) 2004/2134	< 200	6600	24	249	7.31	260	< 300	340	< 200	< 35	< 100	< 6	< 5
	BR6N4(A) 2018/2135	< 200	< 2000	30	374	4.96	425	< 300	3100	< 200	< 40	< 100	< 10	< 6
	BR7N1(B) 1998/2136	< 1000	< 2000	32	297	7.63	420	< 300	3600	< 200	< 40	< 100	19	< 10
Vaal Reefs	UR21A 2055/2121	< 800	< 2000	10	1400	6.56	260	344	605	< 100	< 20	< 100	25	< 5
	UR3 2034/2122	< 1000	< 2000	13	450	2.80	216	< 350	1200	< 200	< 40	< 100	53	< 6
	UR5 2039/2123	980	< 2000	7	890	4.89	229	< 160	670	< 200	< 40	< 100	27	7
	UR16 2049/2124	990	< 2000	8	315	1.65	120	< 160	370	< 100	< 30	< 100	21	5
Freddies Reef	FW4 2105/2137	52	< 2000	4.2	850	1.77	108	440	430	< 100	< 15	< 100	6	< 5
	FW2 2103/2138	66	< 2000	46	760	3.17	123	354	620	< 80	22	< 100	10	< 5
East Geduld	EG4 2064/2139	330	5900	6.7	2300	5.09	200	366	640	< 100	< 15	< 100	15	< 5
	EG18 2078/2140	190	930	4.6	560	3.63	117	295	140	< 100	< 40	< 100	< 5	< 5
Daggafontein	26 1995/2128	94	< 2000	6	152	6.76	312	239	336	< 100	24	< 100	< 5	< 3
	27 1996/2129	256	< 2000	18	1200	7.67	219	< 800	296	< 100	< 40	< 100	< 5	< 3
	KE4/7 1975/2130	220	< 2000	3	115	0.21	21	220	29	< 50	< 15	< 100	< 5	< 3
	K6F12/11 1979/2131	86	< 2000	8	244	1.19	43	818	134	< 100	< 15	< 100	< 5	< 3
	KG6/10 1978/2132	520	2200	11	650	2.79	55	< 100	120	< 70	< 15	< 100	6	< 3
West Driefontein	8A 1959/2125	387	< 2000	7.5	1040	4.93	140	360	450	< 100	46	< 100	9	< 3
	4B 1950/2126	204	< 2000	4	235	4.34	59	264	46	< 50	39	< 100	< 5	< 3
	5 1951/2127	< 400	< 2000	4	84	2.38	14	463	60	< 150	130	< 100	7	< 3

TABLE 2 (*cont.*)

sample location	rock sample	Ba	La	Ce	Nd	Sm	Eu	Tb	Lu	Hf	Ta	Au	Th	U	U/Th
Dominion Reefs	5A														
	2006/2133	< 500	1.3%	1200	1000	445	< 2	20	14	< 10	410	3	809	3900	4.8
	BR8N2(B)														
	2004/2134	< 1000	906	1200	850	285	12	16	10	15	240	9	620	2300	3.7
	BR6N4(A)														
	2018/2135	< 1000	1400	2200	910	335	12	17	11	19	450	2	753	2300	3.1
	BR7N1(B)														
	1998/2136	< 1000	1100	1800	1270	600	20	15	18	18	450	5	970	5400	5.6
Vaal Reefs	UR21A														
	2055/2121	< 1000	260	700	1500	450	20	8	13	22	8	154	477	4500	9.4
	UR3														
	2034/2122	< 1000	475	900	2800	850	37	24	22	30	< 100	218	821	8400	10.2
	UR5														
	2039/2123	< 1000	248	350	860	200	17	6	6	36	7	69	298	2100	7.1
	UR16														
	2049/2124	< 1000	172	500	940	250	15	6	8	11	< 5	214	273	2700	9.9
Freddies Reef	FW4														
	2105/2137	< 500	59	260	170	60	4.7	< 5	< 3	18	30	90	52	685	13.2
	FW2														
	2103/2138	< 500	68	135	195	65	5.3	< 5	< 3	< 20	30	115	80	765	9.6
East Geduld	EG4														
	2064/2139	< 500	41	< 200	280	< 10	3.6	5	< 3	17	6	118	40	510	12.8
	EG18														
	2078/2140	< 500	57	80	73	12	1.2	2	< 3	11	4	1.5	20	75	3.8
Daggafontein	26														
	1995/2128	< 1000	44	< 100	227	75	1.5	< 2	< 1	4	15	173	71	895	12.6
	27														
	1996/2129	< 1000	42	< 10	400	160	8	3	< 3	8	20	132	102	2000	19.6
	KE4/7														
	1975/2130	< 1000	20	22	9	6	1	< 2	< 1	< 2	< 5	0.4	< 5	43	—
	K6F12/11														
	1979/2131	< 1000	16	45	112	30	1.5	< 2	< 1	2	2	28	< 10	337	—
	KG6/10														
	1978/2132	< 300	22	55	43	20	2	< 2	< 1	2	30	11	15	180	12.0
West Driefontein	8A														
	1959/2125	< 1000	47	< 300	88	40	3	< 2	< 5	19	50	428	40	460	11.5
	4B														
	1950/2126	< 1000	25	< 10	340	100	6	3	< 3	7	< 5	221	75	1400	18.7
	5														
	1951/2127	< 1000	69	< 30	454	140	7	16	4	< 5	< 5	444	99	1500	15.2

The most likely modes of introduction of uranium, gold and sulphate in solution are the complex fault system of the Witwatersrand basin and dissolution of coexisting detrital minerals. Some of the sulphate would have been precipitated in close proximity to hot springs at the margin of the Basin, but some gold and uranium would have remained in solution, perhaps with the aid of metal-organic complexes (Vine, Swanson & Bell 1958; Ling Ong & Swanson 1974; Boyle, Alexander & Aslin 1975). The gold and uranium in solution would have been carried out into the Basin to be precipitated together on the distal portions of the alluvial fans by the action of decaying organic matter.

This process accounts for the observed primary distribution of uranium and gold other than the purely detrital material, and explains the separation of uranium and thorium in the

progression from the higher energy Dominion Reef to the lower energy Witwatersrand environment. Though relatively unimportant in the higher energy banket type of mineralization, deposition from solution through the agency of organic matter would seem to be responsible for major economic concentrations of both uranium and gold over large areas in the Witwatersrand Basin in the lower energy Carbon Leader type of mineralization.

Conclusions

The overall control of the uranium mineralization in the Witwatersrand and Dominion Reef Systems is the presence of a depositional basin overlying an Archaean craton in which very early differentiation on the model proposed by Fyfe (1970, 1973) and amplified by Moorbath (1975) enriched the upper crust in oxyphile metals including uranium. This process has been considered by Bowie (1970) as a fundamental control in the delineation of metallogenic provinces and hence in the distribution on a global scale of economic concentrations of uranium.

In this Basin, uranium was deposited in two ways, as detrital allogenic uraninite and by precipitation from solution. The detrital components were concentrated in the higher energy conglomerate environment of the Dominion Reef and proximal parts of the Witwatersrand basin. The solution components including uranium and gold were precipitated under reducing conditions through the agency of decaying organic matter in the lower energy or distal regions of the Basin, giving rise through diagenesis and metamorphism to such uraniferous horizons as the Carbon Leader of the West Wits, which are not directly related to known palaeogeographical channels. It can now be clearly demonstrated that relatively small amounts of thorium increases the resistance to attrition and oxidation to the extent that a thorian uraninite with 1 % or more thorium oxide can survive as river detritus under present-day atmospheric conditions. All of the uraninite grains from the Witwatersrand Basin considered to be of detrital origin contain 1 % thorium oxide or more, hence it is unnecessary to postulate a reducing atmosphere, indeed the retention of sulphate and uranyl ions in solution would seem to require the existence of an oxidizing atmosphere in the model proposed here for the deposition of uranium from solution.

This conclusion therefore suggests that the occurrence of pebble conglomerates with detrital uraninite and pitchblende deposited from solution may have a more widespread occurrence throughout geological time than hitherto suspected, provided the necessary geological criteria for their formation are met.

The writers wish to acknowledge the assistance of I. R. Basham and D. A. Briggs in preparing heavy mineral concentrates from the alluvium samples from Hazro, Indus river. B. R. Skilton and J. A. T. Smellie prepared polished thin sections and M. J. Cope prepared Lexan prints. D. Atkin provided X-ray diffraction identification. In particular we wish to acknowledge helpful discussions with S. H. U. Bowie, A. G. Darnley and J. E. T. Horne. We are indebted to A. G. Darnley and J. M. Miller for the Indus river samples and to S. H. U. Bowie, A. G. Darnley and H. C. M. Whiteside for samples from the Dominion Reef and Witwatersrand sediments. C. Goode and J. Herrington of the Herald Reactor Group, A. W. R. E., Aldermaston, are thanked for the provision of whole-rock instrumental neutron activation analyses and for irradiation of sectioned material for induced fission-track analysis. Jane Plant is thanked

for helpful discussions on solution chemistry, and R. J. Howarth for advice on statistical methods. This work forms part of the research programme of the Institute of Geological Sciences and is published with the approval of the Director.

References (Simpson & Bowles)

Bourret, W. 1973 *First uranium report – Witwatersrand, South Africa.* Utah International, Inc. San Francisco, 61p.

Bowie, S. H. U. 1970 Some geological concepts for consideration in the search for uranium provinces and major uranium deposits. In *Uranium exploration geology* (Proceedings of a Panel, Vienna 1970), IAEA, Vienna, 285–300.

Bowie, S. H. U., Simpson, P. R. & Atkin, D. A. 1975 Reflectance measurements in monochromatic light on the Bowie–Taylor suite of 103 ore minerals. *Fortschr. Miner.* **52**, 567–582.

Bowie, S. H. U., Simpson, P. R. & Rice, C. M. 1973 Application of fission-track and neutron activation methods to geochemical exploration. In *Geochemical Exploration* 1972, pp. 359–372. Inst. Min. Metal. London.

Bowles, J. F. W. 1975 An automatic data-handling system for quantitative X-ray microprobe analysis. *Rep. Inst. Geol. Sci.* No. 75/9. 14 pp.

Bowles, J. F. W. (in preparation). Quantitative energy dispersive analysis of ore minerals.

Boyle, R. W., Alexander, W. M. & Aslin, G. E. M. 1975 Some observations on the solubility of gold. *Geol. Surv. Can. Pap.* **75–24**, 6 pp.

Claringbull, G. F. & Hey, M. H. 1953 A re-examination of churchite. *Mineral. Mag.* **30**, 211–217.

Coetzee, F. 1965 Distribution and grain-size of gold, uraninite, pyrite and certain other heavy minerals in gold-bearing reefs of the Witwatersrand Basin. *Trans. geol. Soc. S. Afr.* **68**, 61–88.

Cooper, R. A. 1923 Mineral constituents of Rand concentrates. *Chem. met. miner. Soc. S. Afr.* **24**, 90–95.

Darnley, A. G. 1962 Detrital uraninite from the Hunza River, Kashmir, Age Determination Rep. No. 22. *Geol. Surv. G.B. Atomic Energy Division* (unpublished).

Davidson, C. F. & Bowie, S. H. U. 1951 On thucholite and related hydrocarbon-uraninite complexes. *Bull. Geol. Surv. G.B.* **3**, 1–18.

Drake, M. J. & Weill, D. F. 1972 New rare earth element standards for electron microprobe analysis. *Chem. Geol.* **10**, 179–181.

Feather, C. E. & Koen, G. M. 1975 The mineralogy of the Witwatersrand reefs. *Miner. Sci. Eng.* **7**, 189–224.

Frondel, C. 1958 Systematic mineralogy of uranium and thorium. *Bull U.S. Geol. Surv.* 1064.

Fyfe, W. S. 1970 Some thoughts on granitic magmas. In *Mechanism of igneous intrusion* (eds G. Newall & N. Rast). *Geol. J.* Special Issue No. **2**, 201–216.

Fyfe, W. S. 1973 The granulite facies, partial melting and the archaean crust. *Phil. Trans. R. Soc. Lond.* A **273**, 457–462.

Grandstaff, D. W. 1975 Microprobe analyses of uranium and thorium in uraninite from the Witwatersrand, South Africa, and Blind River, Ontario, Canada. *Trans. geol. Soc. S. Afr.* **77**, 291–294.

Graton, L. C. 1930 Hydrothermal origin of the Rand gold deposits: part I – testimony of the conglomerates. *Econ. Geol.* **25**, supp. to No. 3, 185 pp.

Hallbauer, D. K. & Van Warmelo, K. T. 1974 Fossilized plants in thucholite from Precambrian rocks of the Witwatersrand, South Africa. *Precambrian Res.* **1**, 199–212.

Hallbauer, D. K., Jahns, H. M. & Beltmann, H. A. 1975 Morphological and anatomical observations on some Precambrian plants from the Witwatersrand, South Africa. *Res. Rep.* **49/75**, *Chamber of Mines of S. Afr.* 22 pp.

Hallbauer, D. K. 1975 The plant origin of the Witwatersrand carbon. *Miner. Sci. Eng.* **7**, 111–131.

Henrich, F. 1935 A mineral occurring in Germany with rare earths as essential constituents. *J. Prakt. Chem.* **142**, 1–5.

Jefford, G. 1962 Xenotime from Rayfield, N. Nigeria. *Am. Miner.* **47**, 1467–1473.

Köppel, V. H. & Saager, R. 1974 Lead isotope evidence on the detrital origin of Witwatersrand pyrites and its bearing on the provenance of the Witwatersrand gold. *Econ. Geol.* **69**, 318–331.

Kleeman, J. D. & Lovering, J. F. 1967 Uranium distribution studies by fission track registration in Lexan plastic prints. *Atomic Energy Aust.* **10**, 3–8.

Liebenberg, W. R. 1955 The occurrence and origin of gold and radioactive minerals in the Witwatersrand System, the Dominion Reef, the Ventersdorp Contact Reef and the Black Reef. *Trans. geol. Soc. S. Afr.* **58**, 101–223.

Ling Ong, H. & Swanson, V. W. 1974 Natural organic acids in the transportation deposition and concentration of gold. *Colorado Sch. Mines Q.* **69**, 395–425.

Mason, P. K., Frost, M. T. & Reed, S. J. B. 1969 B.M.–I.C.–N.P.L. Computer programs for calculating corrections in quantitative X-ray microanalysis. National Physical Laboratory I.M.S. Rep. No. 2 (unpublished).

Miller, J. M. 1963 Uraninite-bearing placer deposits in the Indus alluvium near Hazro, Pakistan. Rep. No. 254 *Geol. Surv. G.B. Atomic Energy Division* (unpublished).

Milton, C., Murata, K. J. & Knechtel, M. M. 1944 Weinschenkite, Yttrium phosphate dihydrate, from Virginia. *Am. Miner.* **29**, 92–107.

Moorbath, S. 1975 The geological significance of Early Precambrian Rocks. *Proc. geol. Ass.* **86**(3), 259–279.

Plant, J., Goode, C. & Herrington, T. 1976 An instrumental neutron activation method for multi-element mapping. *J. geochem. Explor.* **6** (3), 299–319.

Pokrovskiy, P. V., Tormosova, G. F. & Kolenko, L. I. 1965 Weinschenkite from the Central Urals. *Dokl. Earth Sci. Sect.* **162**, 133–136. Transl. from *Dokl. Akad. Nauk SSSR* **162**, 173–175.

Pretorius, D. A. 1975 The depositional environment of the Witwatersrand gold fields. A chronological review of speculations and observations. *Miner. Sci. Eng.* **7**, 18–47.

Price, P. B. & Walker, R. M. 1963 A simple method of measuring low uranium concentrations in natural crystals. *Appl. Phys. Lett.* **2**, 23–5.

Ramdohr, P. 1958 New observations on the ores of the Witwatersrand in South Africa and their genetic significance. *Trans. geol. Soc. S. Afr.* (Annexure) **61**, 1–50.

Robertson, D. S. 1974 Basal Proterozoic units as fossil time markers and their use in uranium prospection. In *Formation of uranium ore deposits*, pp. 495–512. Vienna: IAEA.

Saager, R. & Mihálik, P. 1967 Two varieties of pyrite from the Basal Reef of the Witwatersrand System. *Econ. Geol.* **62**, 719–731.

Saager, R. 1970 Structures in pyrite from the Basal Reef in the Orange Free State Gold-field. *Trans. geol. Soc. S. Afr.* **73**, 31–46.

Taylor, K., Bowie, S. H. U .& Horne, J. E. T. 1962 Radioactive minerals in the Dominion Reef. *Mineral. Mag.* **107**, 329–332.

Tourtelot, H. A. 1968 The hydraulic equivalance of grains of quartz and heavier minerals and implications for study of placers. *U.S. geol. Surv. Prof. Pap.* 594F.

Trudinger, P. A. 1971 Microbes, metals and minerals. *Miner. Sci. Eng.* **4**, 13–25.

Viljoen, R. P. 1963 Petrographic and mineragraphic aspects of the Main Reef and Main Reef Leader on the Main-Bird Series, Witwatersrand System. Unpublished M.Sc. Thesis, University of the Witwatersrand, Johannesburg.

Vine, J. D., Swanson, V. E. & Bell, K. G. 1958 The role of humic acids in the geochemistry of uranium. *Proc. Second U.N. Int. Conf. on Peaceful uses of Atomic Energy* **2**, 187–191.